2014

Volume Swing Frequency Response Method For Determining Mass Transfer Mechanisms in Microporous Adsorbents

Mohammad Iftekhar Hossain
University of South Carolina - Columbia

VOLUME SWING FREQUENCY RESPONSE METHOD FOR DETERMINING MASS TRANSFER MECHANISMS IN MICROPOROUS ADSORBENTS

by

Mohammad Iftekhar Hossain

Bachelor of Science
Bangladesh University of Engineering and Technology, 2004

Master of Engineering
National University of Singapore, 2008

Submitted in Partial Fulfillment of the Requirements

For the Degree of Doctor of Philosophy in

Chemical Engineering

College of Engineering and Computing

University of South Carolina

2014

Accepted by:

James Ritter, Major Professor

Armin Ebner, Committee Member

Vincent Van Brunt, Committee Member

Jamil Khan, Committee Member

John Weidner, Committee Member

Lacy Ford, Vice Provost and Dean of Graduate Studies

DEDICATION

To my parents, for all the sacrifices, they made and to all the martyrs who sacrificed their lives during the Independence war of Bangladesh in 1971.

ACKNOWLEDGEMENTS

This is the most significant accomplishment in my career so far and it would be impossible without the people who believed in me and supported me from their respective position. I would like to take this opportunity to express my sincere gratitude towards them.

First, I would like to express my deepest appreciation to my supervisor, Dr. James A. Ritter for giving me the opportunity to work with him as well as for his excellent guidance and continued support throughout my graduate student life at University of South Carolina.

I would particularly like to thank my co-advisor Dr. Armin D. Ebner for his resourceful suggestions, comments and invaluable ideas that help me to explore new areas of thoughts as well as to improve my problem solving skills. A major portion of the ideas in my research works is a consequence of our regular detailed and in-depth discussions related to the field of adsorption and adsorption based separation.

I am grateful to all my committee members Dr. Vincent Van Brunt, Dr. Jamil Khan and Dr. John Weidner for their time, support and guidance during my research, and for being a part of my committee.

It was a pleasure to work with all highly motivated colleagues in Ritter's research group. Special thanks to Dr. Marjorie Nicholson for all her help in carrying out my experiments and Charles Holland for building the volume swing frequency response

system for my research works. I would also like to acknowledge all previous and present research group mates, Dr. Shubhra Bhadra, Dr. Amal Mehortra, Dr. Hai Du, Dr. Jan Mangual, Dr. Fan Wu, Lutfi Erden, Hanife Erden, Anahita Abdollahi, MD. Atikur Rahman, Nima Mohammadi for all their support and for maintaining a healthy, enjoyable and pleasant working environment.

I am deeply indebted to all my friends from Bangladesh Student Association in University of South Carolina for their support and love. Special thanks to my friend Dr. Iftheker Ahmed Khan for being an awesome friend and guide and for helping me cope with the rigors of graduate student life.

Especially, I want to express my deep gratitude and love for my parents and siblings, who wholeheartedly supported me in my work with their blessing and love.

ABSTRACT

Because of their numerous important applications in industrial catalytic, separation, and purification processes, miroporous materials have attracted considerable attention. Understanding the dynamic behavior of various gases in these porous materials is a critical step in designing, developing and effective operation of such kind of industrial processes. Frequency response (FR) methods have proven to be one of the best recently developed techniques that have been widely used to investigate kinetics behavior of various gas-solid systems due to their ability to discriminate among different rate limiting mechanisms. The current work has been focusing on the development of a volume swing frequency response system and demonstration of the robustness and applicability of the newly developed system in identifying the mass transfer mechanisms of various adsorbate-adsorbent systems effectively.

A new volume swing frequency response system along with a new approach to analyze the response curve using frequency response simulator is developed. The new system is fully automated and has the ability to characterize more thoroughly over wide frequency spectra thus provide ability to identify both slow mass transfer resistances and fast mass transfer resistances that do not visible at lower frequencies. The strength and the robustness of the developed frequency response analysis has been successfully demonstrated for study the adsorption kinetics of CO_2 and N_2 in commercial 13X zeolite pellets and O_2, N_2 and Ar in CMS materials. In this work, the newly developed frequency

response system and new analytical approach is discussed in details. The experimental procedure and the method of analysis have been demonstrated for two commercially available adsorbent materials for various gases. The new system is able to identify the key mechanisms for CO_2 and N_2 in13X zeolite and for O_2, N_2 and Ar in CMS adsorbent and thus illustrates the robustness and the strength of this newly developed tools in identifying the kinetics mechanisms of gases in microporous materials. Additionally, a new and modified expression for the estimation of cycle time dependent LDF mass transfer coefficient have been proposed for diffusion limited mass transfer processes which could be used for both slow and rapid cycling processes.

TABLE OF CONTENTS

LIST OF TABLES

LIST OF FIGURES

LIST OF SYMBOLS

A	area for heat transfer, m^2
b	affinity constant in Toth isotherm model, kPa^{-1}
B	energy term of affinity constant in Toth isotherm model, K
b_o	pre exponential factor for affinity constant in Toth isotherm model, kPa^{-1}
Cp_a	specific heat of adsorbed phase, kJ/K/mol
Cp_g	specific heat of gas phase, kJ/K/mol
Cp_s	specific heat of the adsorbent, kJ/K/kg
$\overline{C}_p$	volume average gas phase concentration over the pellet volume, mol/m^3
D	diffusivity, m^2/s
$D_{M,g}$	Macropore gas diffusivity, m^2/s
$D_{m,s}$	Micropore surface diffusivity, m^2/s
$D_{M,s}$	Macropore surface diffusivity, m^2/s
D_p	macropore diffusivity, m^2/s
D_s	surface diffusivity, m^2/s

E_a	activation energy for mass transfer coefficient, kJ/mol
f	frequency, Hz
h	heat transfer coefficient, $kJ/m^2/K/s$
I	Intensity of the response curve
k	mass transfer coefficient, s^{-1}
k'	Glueckauf LDF mass transfer coefficient. s^{-1}
k''	LDF mass transfer coefficient estimated using expression given by Alpay and Scott. s^{-1}
k	extracted LDF mass transfer coefficient, s^{-1}
k_{LDF}	linear driving force mass transfer coefficient, s^{-1}
k_m	parameter for mouth resistance, s^{-1}
k_o	pre-exponential term in Erying plot for mass transfer coefficient, s^{-1}
m/m_a	mass of adsorbent, kg
n	parameter for Toth isotherm model
P	pressure inside macropore, kPa
P_b	system pressure, kPa
P_d	differential pressure, kPa
$P_{d,o}$	offset for differential pressure , kPa

P_o	partial pressure of the adsorbate, kPa
$P_{o,E}$	the equilibrium absolute pressure, , kPa
$P_{o,EX}$	equilibrium absolute pressure for Helium run, , kPa
$P_{o,SS}$	equilibrium absolute pressure, , kPa
q	adsorbed phase concentration or loading, mol/kg
q^*	equilibrium loading, mol/kg
q^*_o	initial equilibrium loading , mol/kg
q_i	initial loading of the particle, mol/kg
q_s	saturation capacity of gas in Toth isotherm model, mol/kg
$\bar{q}$	volume average loading over crystal, mol/kg
$\bar{\bar{q}}$	volume average loading over the pellet volume, mol/kg
$\overline{Q}$	total loading including the gas phase in macropore, mol/kg
r	distance from the center of the particle, m
R/R_g	universal gas constant, kJ/mol/K
R	radius of spherical particle, m
R_c	radius of crystal, m
R_p	radius of pellet, m

T	temperature, K
t	time, s
t_c	half cycle time, s
T_o/T_w	temperature of the wall, K
V_b	system volume, m^3
V_{b0}	volume of the system phase at equilibrium, m^3
V_E	empty volume, m^3
V_{EX}	excluded volume, m^3
V_{EXT}	part of the working volume external to the volume of the materials, m^3
V_I	volume of the inert materials, m^3
V_P	pellet volume of the adsorbent, m^3
V_{SS}	volume of standard stainless steel spheres, m^3
Z_E	dimensionless expression defined by equation 2.11
Z_{EX}	dimensionless expression defined by equation 2.8
$a(q)$	function of loading depends of type of diffusion and determined from isotherm
$b(q)$	function of loading depends of type of diffusion and determined from isotherm

$\phi(\sqrt{\theta_c})$	Fermi Dirac function defined by equation (5.28)
$\psi(\sqrt{\theta_c})$	correction factor as a fuction of dimensionless half cycle time, evaluated by equation (5.29)
$\vartheta(q)$	function representing the loading dependency of diffusivity depends of type of diffusion and evaluate by ratio $b(q)/a(q)$
ΔH_a	heat of adsorption, KJ/mol
ΔP	amplitude of the perturbation of Pressure, kPa
ΔP_d	amplitude of the differential pressure response, kPa
$\Delta P_{d,E}$	amplitude of the differential pressure for the empty run, kPa
$\Delta P_{d,EX}$	amplitude of the differential pressure for the Helium run, kPa
$\Delta P_{d,SS}$	amplitude of the differential pressure for the run with the stainless steel beads, kPa
ΔV	amplitude of the change of volume, m^3
$\Delta\delta$	amplitude of the shaft displacement, m
α	fraction of adsorption sites participating in surface diffusion at the macropore (chapter 5)
α	fraction of loading adsorbed in macropore surface

γ	ratio between surface diffusion and gas diffusion in the macropore
δ	shaft displacement , m
δ_o	offset for shaft displacement , m
ε_b	bulk porosity
ε_p	pellet porosity
ξ_c	dimensionless radial distance of crystal
ξ_p	dimensionless radial distance of pellet
θ_c	dimensionless half cycle time defined by $D_c t_c/R^2$
κ	permeability of porous adsorbent, m^2
μ	kinetic viscosity of gas, Nm/s
ρ_b	bulk density, kg/m^3
ρ_p	pellet density, kg/m^3
ρ_S	skeletal density of the material, kg/m^3
φ	phase lag between shaft displacement and differential pressure response , rad
φ_P	phase angle for differential pressure response ,rad
φ_δ	phase angle for shaft displacement , rad

LIST OF ABBREVIATIONS

CMS ..... Carbon Molecular Sieve

FR ..... Frequency Response

LDF .....Linear Driving Force

LVDT .....Linear Variable Differential Transformer

PSA .....Pressure Swing Adsorption

PSFR .....Pressure Swing Frequency Response

TSA .....Thermal Swing Adsorption

VSA.....Vacuum Swing Adsorption

VSFR.....Vacuum Swing Frequency Response

ZLC .....Zero Length Column

CHAPTER 1

INTRODUCTION

1.1 Sorption Kinetics in Porous Adsorbents

Porous adsorbent materials are critically important for numerous industrial catalytic, separation, and purification operations. Porous adsorbents are employed in a variety of industrial and environmental applications including production of highly pure oxygen from air, recovery and purification of hydrogen, variety of drying processes, natural gas purification, capturing carbon dioxide from flue gases, etc[Ruthven, 1984; Sircar, 2006]. In latest few decades separation and purification of various commercially important component by adsorption based processes like PSA/VSA/TSA has become an alternative method due to its potential to provide economic solutions to energy intensive separation processes. With the advancement of commercialized adsorbent based separation processes, adsorption characteristics of various commercially important gases like oxygen, nitrogen, argon, methane, carbon dioxide etc in microporous solids has become a topic of considerable importance.

For porous adsorbent materials, the overall uptake and the performance of separation depends on the interplay of different controlling mechanisms within the particle (Rutherford and Do, 2000). The transport of adsorbate molecules in adsorbent particles from the bulk phase to the interior of adsorption sites are restricted by various resistances shown in figure 1.1. The external film resistance usually presents for the

multicomponent mixture adsorption and often very small under practical condition of operation. Major resistances of mass transfer are usually due to micropore resistance of adsorbent crystals or microparticles and the macropore resistance of the pellet. Four different mechanism have been suggested for transport of gases through the macropores that includes molecular diffusion, Knudsen diffusion, surface diffusion and advection or Poiseuille flow (Ruthven, 1984). Depending on the size of molecule, size of pore and fluid-wall interaction either single mechanism or combination of these mechanism could become the governing macropore transport mechanism. Molecular diffusion occurs due to the molecular interaction of gases and become dominant when the mean free path of the gas is small relative to pore diameter. When the mean free path approaches to the pore diameter, interaction between pore wall and gas molecules become significant and Knudsen diffusion start to become dominant. There could be additional contribution of flux from transport through the adsorbed layer on the macropore surface usually termed as surface diffusion. If there is a significant gradient of pressure across the porous particle there will be flow through the macropore. This kind of flow is termed as Poiseuille flow or advection. In micropore, the adsorbed face diffusion is the main controlling mechanism but sometimes restriction in micropore mouth or entrance could play significant role to govern the transport mechanism. Though for the most adsorbent materials the transport is controlled by the micropore or macropore diffusion processes, the dominating mechanism of mass transfer varies from system to system. Also the thermal effect caused by the heat of adsorption may further contribute to the dynamic behavior (Karger and Ruthven, 1992; Wang and LeVan, 2010). Understanding the mass transfer characteristics of the commercially important gases in such porous adsorbents is

of fundamental interest of researchers due to its practically significance for improved design and efficient operation of gas separation processes.

A number of different experimental methods has been used for both pure and multicomponent gas adsorption kinetics (Sircar, 2007). That includes gravimetric analysis, volumetric analysis, combined gravimetric-volumetric analysis, break through curve analysis along with some recently developed methods like frequency response techniques (LeVan et al, 2003; Do et al, 2000; Yasuda, 1976), zero length column techniques (Brandini, 1998; Ruthven et al, 1998, 2003), total desorption method (Do et al 1994,1996; Farooq et al, 2003) etc. Sircar (2006, 2007) provided a compact review on various experimental techniques to study the kinetic of gas adsorption-desorption processes. The description of all these techniques is beyond the scope of this dissertation. Due to the relevancy with this work only frequency response technique has been discussed briefly in following section.

1.2 Concept of Frequency Response Method

Frequency Response (FR) method was earlier developed and applied in the 1960s by Polinski and Naphtali (1963) and later received more attention in last couple of decade to study the mass transfer kinetics in adsorbents (Jordi and Do, 1993; Yasuda et al., 1984,2002; Sun et al., 1994; Reyes et al., 1994,1997; LeVan et al., 2003,2008).

The basic principle of FR methods is that a system in equilibrium subject to a periodic perturbation produces a periodic response with same frequency as the input but with different amplitude and a phase lag with respect to the input(figure 1.2) (Coughanowr and Koppel, 1965; Stephanopoulos, 1984). The amplitude and the phase

lag are directly related to the physical characteristics of the system and time scale of the dynamics processes occurring within the system and thus uniquely reflects on system thermodynamic and kinetic characteristics. The system could be an open system or a closed system. Usually in most closed system FR experiment is conducted by a sinusoidal variation in system volume and recording of the pressure response and termed as volume swing frequency response technique. The open system or flow through system is usually either pressure-swing or concentration-swing frequency response techniques. In pressure swing technique, system pressure is perturbed sinusoidally and the response in the flow rate at outlet is measured and in concentration swing technique, the composition of the inlet stream with constant total molar flow rate is perturbed and response in the outlet stream composition is measured. Response for frequency spectrum over wide range of frequencies then can analyze to determine mechanism associated with kinetic processes in adsorbent as well as to measure the corresponding mass transfer parameters. The frequency response (FR) method is one of the best macroscopic techniques. Because of its potential for discriminating between different rate limiting mechanisms, the FR method has been widely used to investigate the kinetic behavior of gas-solid systems.

1.3 Application of FR Techniques in Study of Dynamic Processes

Napthali and Polinski (1963) were the first to use FR methods to characterize the adsorption processes in porous materials by studying the rate of hydrogen adsorption on a supported Ni catalyst and they were able to identify the presence of different types of (slow and fast) adsorption sites on the surface. Later in 1970, Evnochides and Henley demonstrated the use of FR method to measure both the capacities and dynamics by

measuring the solubility and diffusivity of ethane in polyethylene films. Work of Yasuda and co-workers(1976, 1985, 1991) on the theoretical development of FR method along with the application of FR method for investigating the kinetics behavior of adsorption in zeolites (1982, 1985) significantly enhance the efficacy of the FR techniques in the study of adsorption and diffusion processes in porous media. Frequency response method also used by several other research groups to investigate the mass transfer characteristics of porous adsorbent and catalytic materials. Rees and Shen have studied the diffusion of gases within zeolites (1991), Rees and co-workers (2000) used a batch system FR experiment with square wave volume perturbation to study hydrocarbon adsorption on silicate materials. Jordi and Do (1993, 1994) extensively studied the sorption kinetics of gases on bidispersed adsorbents by developing a theoretical model of gas sorption in a batch system subjected to a small periodic volume perturbation. This technique was also applied to sorption kinetics of methane, ethane, and propane on activated carbon systems (Do et al, 2000).

Along with the batch system, there have been other applications in flow through system involving concentration perturbations. Recently LeVan and co-workers have developed the flow through pressure swing and concentration swing frequency response methods to investigate mass transfer mechanism of gases on various adsorbent including CMS, silica gel, activated carbon (2003, 2005, 2007, 2008, 2010). They have developed theoretical response curve representing various mass transfer mechanism for both volume swing (VSFR) and pressure swing (PSFR) frequency response system with small perturbation and by comparing the experimental response from both VSFR and PSFR system with the theoretical response they have tried to understand the mass transfer

behavior of a various gases including Nitrogen and Oxygen. Some recent applications of different frequency response techniques to study the transport kinetics of gases on porous adsorbent are tabulated in table 1.1.

1.4 Dissertation Overview and Organization

The ultimate goal of this work is to develop a volume swing frequency response apparatus and analytical technique as well as implement that technique to understand the mass transfer mechanism of various gases on microporous adsorbents. As, discussed before there are a number of available techniques for kinetic study, but for this project frequency response method has been selected primarily for its ability to distinguish different transfer mechanisms. Moreover, volume swing frequency response has been selected due to its ability to measure FR spectra over wide range of frequencies including both low and high frequencies that is desired in order to thoroughly and accurately analyze the dynamics of both slow and fast mass transfer controlling systems. This dissertation strives to introduce the newly developed and commissioned volume swing frequency response apparatus in USC, discuss and present experimental procedure, analytical techniques, results obtained by implementing this new tools in study of the mass transfer characteristics of different gases on industrially important and commercial microporous adsorbent materials like CMS and 13X zeolite pellets. During the course of study, a modified correlation for LDF mass transfer coefficient in diffusion limited processes is established which is also included in this dissertation.

Chapter 2 provides a detailed description of the newly developed volume swing frequency response apparatus including the its instrumentation and controlling features. It

also includes the description of how to run the frequency response experiment, procedure for characterization of the system, extraction of response curves from experimental raw data, description of the frequency response simulator and analytical procedure to use the developed tools to study the kinetics of certain adsorbent-adsorbate system.

Chapter 3 illustrate the use of the newly develop frequency response system to study the mass transfer mechanism of CO_2 and N_2 in 13X zeolite and also show that the Frequency Response (FR) analysis is a robust technique that unequivocally identifies the mass transfer mechanisms in adsorbents. Experiments have been carried out for different pressure and temperatures condition and then three mass transfer models have been investigated by using the simulator to fit the experimental response curves and eventually found that the mass transfer processes in 13X zeolite for both CO_2 and N_2 are govern by nonisothermal macropore diffusion mechanism.

Chapter 4 also illustrates robustness and the strength of the developed Frequency Response (FR) analysis tool with another set of studies. In this chapter adsorption kinetics of industrially important gases like O_2 N_2 and Ar in CMS material have been studied.

In chapter 5, a generalized graphical method were presented along with a new modified analytical expression to estimate LDF mass transfer coefficient that could be used for both macropore or micropore diffusion limited process for a wide range of cycle time form very slow to very fast cycling processes.

1.5 Tables

Table 1.1 Recent applications of frequency response technique in study of adsorption kinetics of gaess in microporous adsorbents.

Researchers	Applications
Yasuda et al 1982, 1985	Adsorption kinetics of gases in zeolites
Rees and Shen, 1991	Diffusion of gases in zeolites
Rees et al, 2000	Hydrocarbon adsorption in silicate materials
Onyestyák et al., 1995	Diffusion of CO2 in commercial 5A powders and pellets
Do et al., 2000	Adsorption kinetics of methane, ethane, propane on activated carbon
LeVan and co-workers, 2003, 2005, 2007, 2008	Mass transfer mechanisms of gases on various adsorbents including silica gel, activated carbon, etc
Wang and LeVan, 2010	Mass transfer mechanism of O2, N2, CH4 and CO2 on CMS. Theoretical analysis of heat effect on response curve
Giesy et al., 2012	Kinetics of CO2 in 13X using combined pressure swing and volume swing frequency response techniques

1.6 Figures

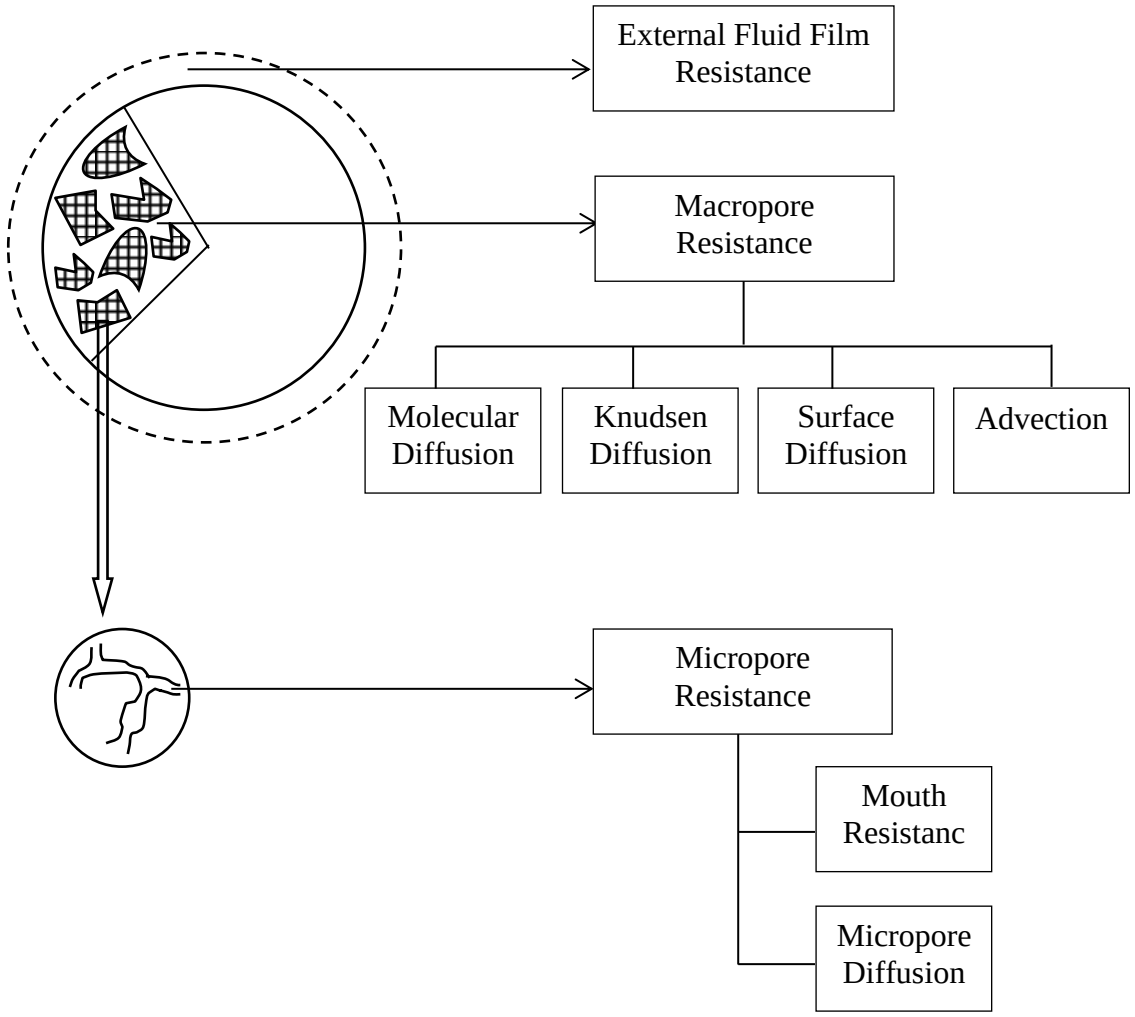

Figure 1.1 Schematic diagram showing various resistance to transport of adsorbate gas in microporous adsorbents

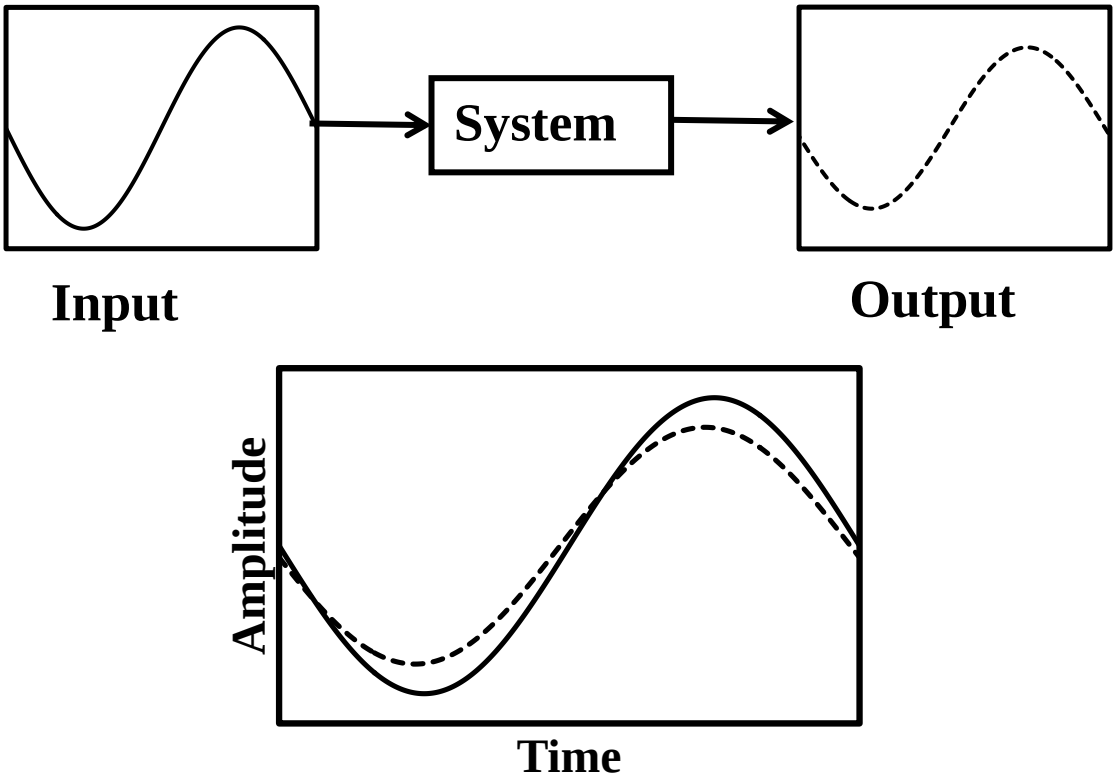

Figure 1.2 Fundamental concept of frequency response analysis. System subject to sinusoidal perturbation produces sinusoidal response with different amplitude and phase angle reflecting the thermodynamic and kinetic characteristics of the system.

CHAPTER 2

VOLUME SWING FREQUENCY RESPONSE APPARATUS FOR DETERMINING THE MASS TRANSFER MECHANISM IN MICRPOROUS ADSORBENTS

2.1 Introduction

Because of their practical applicability in industrially important catalysis or selective adsorbents for separation processes, identifying the controlling mass transfer mechanisms for various industrial valuable gases in microporous materials like zeolites or carbon molecular sieves has attracted considerable attention of the researchers around the globe. A variety of different experimental techniques applied to study the kinetics of gases in porous materials that includes both gravimetric and volumetric methods and also both transient and steady state measurements. In recent couple of decades, frequency response method have become an very effective tools with ability to correctly identify the governing mass transfer mechanism and measuring the corresponding mass transfer parameters. In this work a newly constructed volumetric FR system has been introduced for study the mass transfer characteristics of gases in adsorbents. The FR apparatus has the ability to characterize more thoroughly over wide frequency spectra starting from 10^{-5} Hz to 10 Hz thus provide ability to identify slow mass transfer resistances as well as fast mass transfer resistances that do not visible at lower frequencies. The system is automated and could be operate, monitor and record experimental data by a LabVIEW program running on a PC. A standard operating procedure has been developed to conduct

the FR experiments along with a technique to convert the experimental raw data into analyzable frequency response functions. This chapter provides a detailed description of the newly developed frequency response system in USC as well as explains every steps of the experiment and the analysis of the experimental data in details.

2.2 Volumetric Frequency Response Apparatus

The schematic of the automated batch volume swing FR system is shown in Figure 2.1. The system, which uses total volume as input and pressure as output, has been constructed to operate at frequencies between 5×10^{-5} and 10 Hz, temperatures up to 80 ^{o}C, and vacuum pressures down to 0.2 atm. The system comprises of three different volume zones: a) the working volume in dark gray b) the reference volume in light gray, and c) the external volume in white connecting the system with the vacuum or gas feeds. Except for the immersed components, all parts of containing the working and reference volumes are thermally insulated to reduce any thermal influence from the laboratory. The working volume includes a sample container to analyze between 10 and 100 g of sample and a metal bellows that contracts and expands via a shaft for volume modulation. During a run the sample container is immersed in a temperature controlled water jacketed bath that is connected to a chiller. During sample activation, the bath is removed and the container is heated via aluminum concentric sleeves and rigid electric band heaters. A closed sheath thermocouple is immersed in the sample for temperature determination. The shaft connected to the metal bellows is driven via an eccentric sheave for the working volume to vary sinusoidally. The position of the bellows is determined by a linear variable differential transformer (LVDT) along with a linear encoder and an

angular encoder (US digital), which measures the input volume perturbation. A pressure transducer (MKS instruments Inc, USA). The Reference volume includes a two-liter ballast that is immersed within the bath of the chiller for temperature, and thus pressure, stabilization. The equilibrium pressure and the changes of pressure are respectively followed by An MKS pressure transducer located at the reference volume and a differential pressure transducer (Omegadyne, Inc) located between the reference and working volumes. Connectivity between the different zones is controlled via solenoid valves V1 through V4. Data acquisition from the LDVT, pressures transducers and thermocouple is accomplished via a LabVIEW program running on a Dell PC-AT 320. Microsoft excel program is used to determine actual frequency, phase lags, amplitude of input and output variables, and characteristic response functions from pressure-volume experimental data.

2.3 Experimental Section

2.3.1 Sample Activation and Preparation

After the sample has been located within the sample container, typically between two layers of glass beads that fill up the container (Figure 2.2), the system is evacuated by keeping valves V1, V2 and V4 open while valve V3 remains closed (Figure 2.1). The sample container will not be immersed in the water jacketed bath. Instead it will be heated with the aluminum sleeves and the electric band heaters to any desired goal temperature. This is typically carried out for a period of hours or days at the target temperature until the pressure at the vacuum pump is less than 1.5×10^{-5} torr (Granville-Phillip 350 Ionization Gauge), which suggests satisfactory sample regeneration. Then,

the system is let cool, the heaters and sleeves are removed and the container is fully immersed in the water jacketed bath which is set at the target temperature. Valve V4 is then closed and then the working gas is allowed in via valve V3 to pressurize the system to the target pressure. A needle valve is used (not shown) to control the flow of the working gas into the system. Once at a relatively stable target pressure, the shaft is moved to position where the bellows is at the mid-point. Valve V2 is then closed and the system is let equilibrate for another several hours or days. Once at equilibrium, valve V1 connecting the reference and working volumes is closed, the differential pressure ΔP between the two is at zero and the system is ready for a sample run.

In case of a new run with the same working gas, no activation is needed. Instead, the sample container is maintained inside the water jacketed bath, then valves V1 and V2 are opened and, depending on the new target temperature and pressure, gas is vacuum removed from or fed into the system via valves V4 and V3, respectively. Once at a relatively stable target pressure, the shaft is again moved to position to bring the bellows to mid-point. Valve V2 is then closed and the system is ready for a sample run after system equilibrium is reached.

Finally, In the case of a run with either an empty sample container, a container with calibration stainless steel beads or a container with glass beads only, the whole process of system evacuation, gas filling and equilibration is carried with the sample container always immersed in the water jacketed bath.

2.3.2 Sample Run and Responses

Once the system is ready to start at equilibrium, the sample to subjected to volume modulation at a predefined set of frequencies between 5.0×10^{-5} and 10 Hz. Ten cycles are typically run at each particular frequency, before switching to the next. At the

end of the run, the collected values of the shaft displacement and the differential pressure from the LDVT and the differential pressure transducer, respectively, are analyzed and fitted at the periodic behavior using the following functions (Figure 2.3):

$$\delta = \delta_o + \Delta\delta \sin(2\pi ft + \varphi_\delta) \tag{2.1}$$

$$P_d = P_{d,o} + \Delta P_d \sin(2\pi ft + \varphi_P) \tag{2.2}$$

where f is the frequency, t is the time, δ and P_d are the shaft displacement and the differential pressure, respectively; δ_o and $P_{d,o}$ are the corresponding offsets, which at the periodic behavior are different from the zero value; φ_δ and φ_P, are the corresponding phase lags; and $\Delta\delta$ and ΔP_d are the corresponding amplitudes.

For each frequency the system can provide a response in the form of two variables. One of them is the phase lag response which is given by

$$\varphi = \varphi_P - \varphi_\delta \tag{2.3}$$

and the intensity response, which is conveniently expressed as:

$$I = \left(\frac{\Delta V}{V_{EXT}} \cdot \frac{P_o}{\Delta P_d} - 1 \right) \tag{2.4}$$

where Po is the absolute pressure at equilibrium, ΔV is the amplitude of the change of the working volume and V_{EXT} is the volume within the working volume external to the volume of the materials in the container (adsorbent, glass bead, etc). With V_E being the working volume when empty, then

$$V_{EXT} = V_E - V_P - V_I \tag{2.5}$$

where V_P is the pellet volume of the adsorbent and V_I is the volume of the inert materials in the container such as glass beads, both independently determined.

Equation (2.4) is meant to capture deviations to the ideal gas law due to the presence of an adsorbent. When the container is empty, or when is filled with a non-adsorbing material such as glass beads, or when running at such fast conditions where transport resistance for the adsorbate in and out the adsorbent is total, the value of I should be identical to the zero value. At any other condition I is a positive number, i.e., adsorption is taking place.

The amplitude of the change of the working volume ΔV and the empty volume V_E are determined by carrying out an empty container run and with standard stainless steel spheres of volume V_{SS} at any frequency, preferably low (Figure 2.4). From these runs,

$$\Delta V = \left(V_E - V_{SS}\right) \cdot \Delta P_{d,SS} / P_{o,SS} \tag{2.6}$$

$$V_E = V_{SS} / (1 - Z_E) \tag{2.7}$$

With

$$Z_E = P_{o,E} / P_{o,SS} \cdot \Delta P_{d,SS} / \Delta P_{d,E} \tag{2.8}$$

where $P_{o,E}$ and $\Delta P_{d,E}$ are respectively the equilibrium absolute pressure and the amplitude of the differential pressure for the empty run, and $P_{o,SS}$ and $\Delta P_{d,SS}$ are respectively the equilibrium absolute pressure and the amplitude of the differential pressure for the run with the stainless steel beads. Figure 2.5 shows a typical experimental response curve.

2.3.3 Other Properties

One other piece of information that frequency response can determine is the skeletal density of the material as well as the slope of the isotherm. The skeletal density ρ_S is evaluated via the excluded volume V_{EX} according to

$$\rho_S = m_a /(V_E - V_{EX} - V_I) \tag{2.9}$$

where m_a is the mass of adsorbent. V_{EX} is determined via a run with the sample under Helium and the run with stainless steel spheres using identical expressions to equations (2.6) and (2.8):

$$V_{EX} = V_{SS}/(1 - Z_{EX}) \tag{2.10}$$

With

$$Z_{EX} = P_{o,EX}/P_{o,SS} \cdot \Delta P_{d,SS}/\Delta P_{d,EX} \tag{2.11}$$

Where $P_{o,EX}$ and $\Delta P_{d,EX}$ are respectively the absolute pressure at equilibrium and the amplitude of the differential pressure for the run. The slope of the isotherm can be determined at the slowest frequencies as long as the sample is operating under local equilibrium:

$$\left.\frac{\partial q}{\partial P}\right|_{eq} = \frac{V_E}{m_a RT}\left(\frac{\Delta V}{V_E}\cdot\frac{P_o}{\Delta P_d} - 1\right) \tag{2.12a}$$

or from Eq. (4)

$$\left.\frac{\partial q}{\partial P}\right|_{eq} = \frac{V_E}{m_a RT}\left(\frac{V_{EXT}}{V_E}\cdot(I+1) - 1\right) \tag{2.12b}$$

2.4 Analytical tools and mathematical models

Yasuda (1976) showed a detailed theoretical treatment of frequency response data of volumetric frequency response apparatus in the form of in-phase and out-of-phase component of experimental response to analyze FR experimental results. However, Reyes and Iglesia (1994) showed that expressing FR data in the form of amplitude ratio and

phase lag response curves simplifies the analysis of simultaneous dynamic processes as well as help to identify controlling mechanism among multiple processes. Moreover, amplitude ratio curve allows estimation of isotherm slope from the low frequency plateau of response curve. In this work a simple function of amplitude ratio named as Intensity function and as defined in equation (2.4) is used to identify controlling mechanisms and evaluating corresponding rate parameters. The Intensity function takes a value of zero once the adsorbent behaves as an inert material (i.e., at high frequency).

Once the experimental results are available, a tool or methodology is needed to analyze the experimental response curve to extract kinetic information from it. A frequency response experiment simulator has been developed using first principle modeling by material and energy balance of the actual system. COMSOL Multiphysics (version 3.5a) along with Matlab has been used to develop the simulator that has the ability to simulate the FR experiments for desired adsorbate-adsorbent system at various conditions. The key features of the simulator are-

- It includes overall bed mass and energy balances
- It consists different isothermal/nonisothermal mass transfer models:
    - Macropore diffusion/advection model
    - Micropore diffusion model with or without mouth resistance
    - Bimodal distributed micoporous crystal with or without mouth resistance
    - LDF model
    - Combined macropore and micropore model, etc
- Aided by an optimization routine based on Davidon-Fletcher-Powell (DFP) algorithm to minimizing the error function defined as-

$$\sum \left(I_{\mathrm{mod}} - I_{\exp} \right)^2$$

2.4.1 Material and Energy Balances

A schematic representation of the batch frequency response system is shown in Figure 2.1, where system volume is perturbed periodically around the equilibrium value V_{b0}, and the system pressure P_b responds accordingly. Assuming that the entire system is at same pressure, the material balance over the entire volume is,

$$m\frac{\partial \overline{Q}}{\partial t}+\frac{\partial}{\partial t}\left(\frac{P_b V_b}{RT}\right)=0 \tag{2.13}$$

$$V_b = V_{b,o} + \Delta V \sin(2\pi f t) \tag{2.14}$$

$$\overline{Q} = \bar{\bar{q}} + \left(\varepsilon_p / \rho_p\right)\overline{C}_p \tag{2.15}$$

Energy balance is applied over the volume containing the adsorbent, assuming Temperature. T is only function of time; not of bed length or pellet radius,

$$\begin{aligned}&\frac{m}{\rho_p}\left[\frac{\varepsilon_b}{(1-\varepsilon_b)}+\varepsilon_p\right]\left[Cp_g\frac{P_b}{RT}\frac{\partial T}{\partial t}-\frac{\partial P_b}{\partial t}\right]+m\bar{q}Cp_a\frac{\partial T}{\partial t}\\&+mCp_s\frac{\partial T}{\partial t}+(-\Delta H_a)\frac{\partial \bar{\bar{q}}}{\partial t}=hA\left(T_{wall}-T\right)\end{aligned} \tag{2.16}$$

The quantities $\bar{\bar{q}}$ and $\overline{C}_p$ are the volume average loading and gas phase concentration respectively over the pellet volume and defined as,

$$\bar{\bar{q}} \equiv \frac{3}{R_p^2}\int_0^{R_p} \bar{q} r_p^2 dr_p \tag{2.17}$$

$$\overline{C}_p \equiv \frac{3}{R_p^2}\int_0^{R_p} C_p r_p^2 dr_p \tag{2.18}$$

Where C_p is the gas phase concentration inside pores and $\bar{q}$ is the volume average loading over crystals and expressed as,

$$\bar{q} \equiv \frac{3}{R_c^2} \int_0^{R_c} q r_c^2 dr_c \tag{2.19}$$

Depending on the kind of controlling mechanism $\bar{\bar{q}}$ and $\bar{q}$ can be correlated with the equilibrium loading in different manner which is explained in corresponding model description.

2.4.2 Macropore model

The macropore model used in this work includes advection, surface diffusion and macropore diffusion as mass transfer mechanisms. The advective flux is defined using Darcy's expression. A small fraction (a) of total capacity is attributed to the adsorption at macropore surface. The macropore mass balance equation is expressed in spherical coordinate in terms of dimensionless pellet radius with appropriate boundary and initial conditions,

$$\frac{\varepsilon_p}{RT}\frac{\partial P}{\partial t} - \frac{\varepsilon_p P}{RT^2}\frac{\partial T}{\partial t} + \rho_p \frac{\partial \bar{q}}{\partial t} = \frac{\varepsilon_p}{\xi_p^2}\frac{\partial}{\partial \xi_p}\left[\frac{\xi_p^2}{R_p^2}\left(\frac{\kappa}{\mu}\frac{P}{RT} + \frac{\alpha \rho_p D_s}{\varepsilon_p}\frac{\partial q^*}{\partial P}\bigg|_P + \frac{D_p}{RT}\right)\right] \tag{2.20}$$

Where, $\xi_p = \frac{r_p}{R_p}$

$$\frac{\partial P}{\partial \xi_p} = 0 \qquad \text{at} \qquad \xi_p = 0 \tag{2.21}$$

$$P = P_b \qquad \text{at} \qquad \xi_p = 1 \tag{2.22}$$

$$P = P_{b,0} \text{ and } T = T_0 \qquad \text{at} \qquad t = 0 \tag{2.23}$$

It is noteworthy that the same model is used for macropore advection controlled mechanism, surface diffusion controlled mechanism and macropore diffusion controlled mechanism. The only difference is that when the mass transfer is purely advective, the surface diffusion parameter D_s/R_p^2 and macropore diffusive parameter D_p/R_p^2 is set as zero and when the mass transfer is purely controlled by surface diffusion, the advective parameter κ and macropore diffusive parameter D_p/R_p^2 is set as zero and similarly when the mass transfer is purely diffusive, the advective parameter κ and surface diffusive parameter D_s/R_p^2 is set as zero. For macropore controlled models there is no resistance in micropore/ crystal hence, the quantity $\bar{q}$ is in equilibrium with local gas phase concentration in macropore and estimated as,

$$\bar{q}(r_p) = q^*(P(r_p), T) \tag{2.24}$$

2.4.3 Micropore diffusion model

In micropore diffusion model the loading dependency of micropore diffusion is expressed by Darken correction factor for diffusivity and the mass balance is written in terms of dimensionless microporous crystal radius. If there is a mouth resistance present in micropore crystal the only difference will be in the boundary conditions.

$$\frac{\partial q}{\partial t} = \frac{1}{\xi_c^2}\frac{\partial}{\partial \xi_c}\left(\xi_c^2 \frac{D_c}{R_c^2}\right)\frac{\partial q}{\partial \xi_c} \tag{2.25}$$

Where, $\xi_c = \dfrac{r_c}{R_c}$

$$\frac{\partial q}{\partial \xi_c} = 0 \qquad \text{at} \qquad \xi_c = 0 \tag{2.26}$$

$$q = q^{*}(\mathrm{P},\mathrm{T}) \quad \text{at} \quad \xi_c = 1 \tag{2.27}$$

$$q = q^{*}_{0} \quad \text{at} \quad t = 0 \tag{2.28}$$

If mouth resistance is present at the crystal entrance, the boundary condition is given as-

$$-3\frac{D_c}{R_c^2}\frac{\partial q}{\partial \xi_c} = k_m(q^{*}\text{-}q\big|_{\xi_c=1}) \quad \text{at} \quad \xi_c = 1 \tag{2.29}$$

with,

$$\frac{D_c}{R_c^2} = \frac{D_{co}}{R_c^2}\frac{1}{1-\left(\frac{q}{q_s}\right)^n} \tag{2.30}$$

2.4.4 Bimodal distributed micoporous crystal with or without mouth resistance

For various reasons there is possibility to have secondary crystal formation (cracks, etc) inside the pellet, which may introduce additional feature and may influence the mass transfer mechanism in the pellet. The existence of two transfer processes which occur independently can result in a bimodal form of frequency response curves. This can also be the result of a well-defined bimodal distribution of crystal sizes. In order to capture such effects a distributed micropors model has been developed where adsorption and diffusion through two different types of crystals are assumed to be occurred in parallel. The mass transfer in each crystal is governed by similar expression like the micropore diffusion model with diffusion parameters for each crystal as D_{c1}/R_{c1}^2 and D_{c2}/R_{c2}^2. The overall adsorption capacity is distributed between the two crystals.

2.4.5 LDF model

LDF model is a simplification of diffusion limited mass transfer to enhance the computational efficiency assuming that the average uptake rate is proportional to the driving force for adsorption and represented by-

$$\frac{\partial \bar{q}}{\partial t} = k_{LDF}(q^{*} - \bar{q}) \tag{2.31}$$

2.4.6 Combined macropore and micropore model

For bidisperse materials, diffusion resistances exist in series for the macropore and micropore regions and if the mouth resistance at micropore entrance is significant the micropore region is connected to the macropore region via this mouth resistance. A two dimensional model has been developed one dimension for micropore and second one for macropore. The governing equations and boundary conditions are similar for macropore model and micropore diffusion model.

2.5 Extraction of Mass Transfer Parameters

The procedure used to identify mass transfer mechanisms and measure corresponding mass transfer parameters is divided in to two parts. The first part is experimental parts that consist of characterization of system by measuring empty volume, external volume, inert volume, skeletal density of the materials, isotherms, etc. and conducting the frequency response experiments at different pressures and temperatures to get experimental response curves. In the second part, fitting those experimental curves using the developed tool using different mass transfer model to identify the governing mechanisms as well as extract the corresponding mass transfer parameters by minimizing

the error between the experimental intensity functions and that from the model at different frequencies and conditions. Only a single value of fitting parameters is optimized to predict the response curves at all the conditions. Thus running those experiments with different pressure conditions provide additional benefit to distinguish the controlling mechanism among other mechanisms as each model behaves differently as the pressure changed.

Depending on the choice of the model following fitting parameters are extracted by matching the theoretical response curve with the experimental response curve.

1) Macropore diffusion time constant, D_p/R_p^2
2) Surface diffusion time constant, D_s/ R_p^2
3) Parameter for advection, κ
4) Micropore diffusional time constant, D_c/R_c^2
5) Micropore mouth resistance, k_m
6) LDF mass transfer coefficient, k_{LDF}
7) Micropore diffusional time constant for crystal type 1 & 2 , D_{c1}/R_{c1}^2, D_{c2}/R_{c2}^2
8) Mass fraction of crystal types for bimodal distributed microporos material

To demonstrate the potential of the technique developed in USC, frequency response experiments have been conducted for two commercially available adsorbent pellets with different gases and the governing mass transfer mechanisms have been identified for each of the cases. The subsequent two chapters describe those two studies in details.

2.6 Conclusion

A newly constructed and commissioned automated volume swing FR system at USC has been introduced for study the mass transfer characteristics of gases in adsorbents. This new system can operate at frequencies between 5×10^{-5} and 10 Hz, temperatures up to 80 ^{o}C, and vacuum pressures down to 0.2 atm The FR apparatus has the ability to characterize more thoroughly over wide frequency spectra which is suitable for both slow and fast moving gas-adsorbent systems. A detailed description of the apparatus along with characterization technique of the system, experimental techniques and analysis of experimental data is included. Also a unique analytical tools and FR experiment simulator to extract the mass transfer information has also been introduced. It is not worthy that, representing the FR data in terms of a function of amplitude ratio and phase lag not only simplify the treatment of data but also enhance the understanding of multiple simultaneous dynamic processes. Additionally, it provides a fairly good estimation of the skeletal density of the materials and also the slope of the isotherm from the low frequency plateau of the response curve.

2.7 Figures

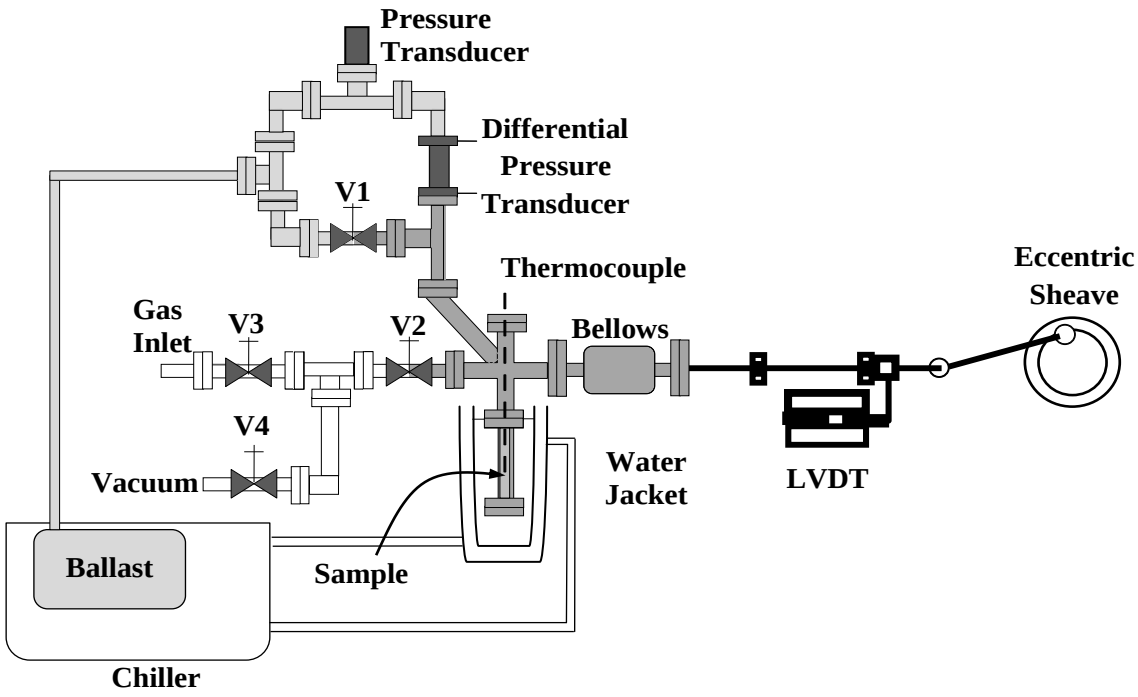

Figure 2.1 Schematic of Volume swing frequency response (FR) instrument developed in USC.

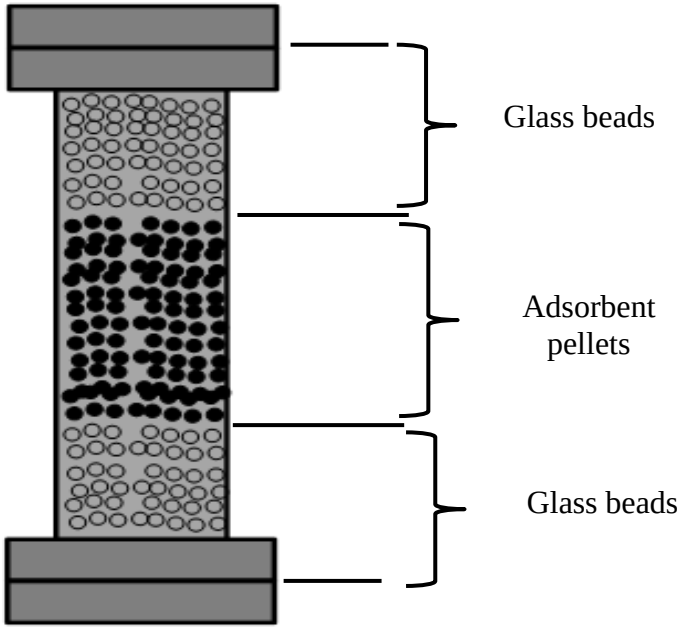

Figure 2.2 Usual packing technique of sample in sample container.

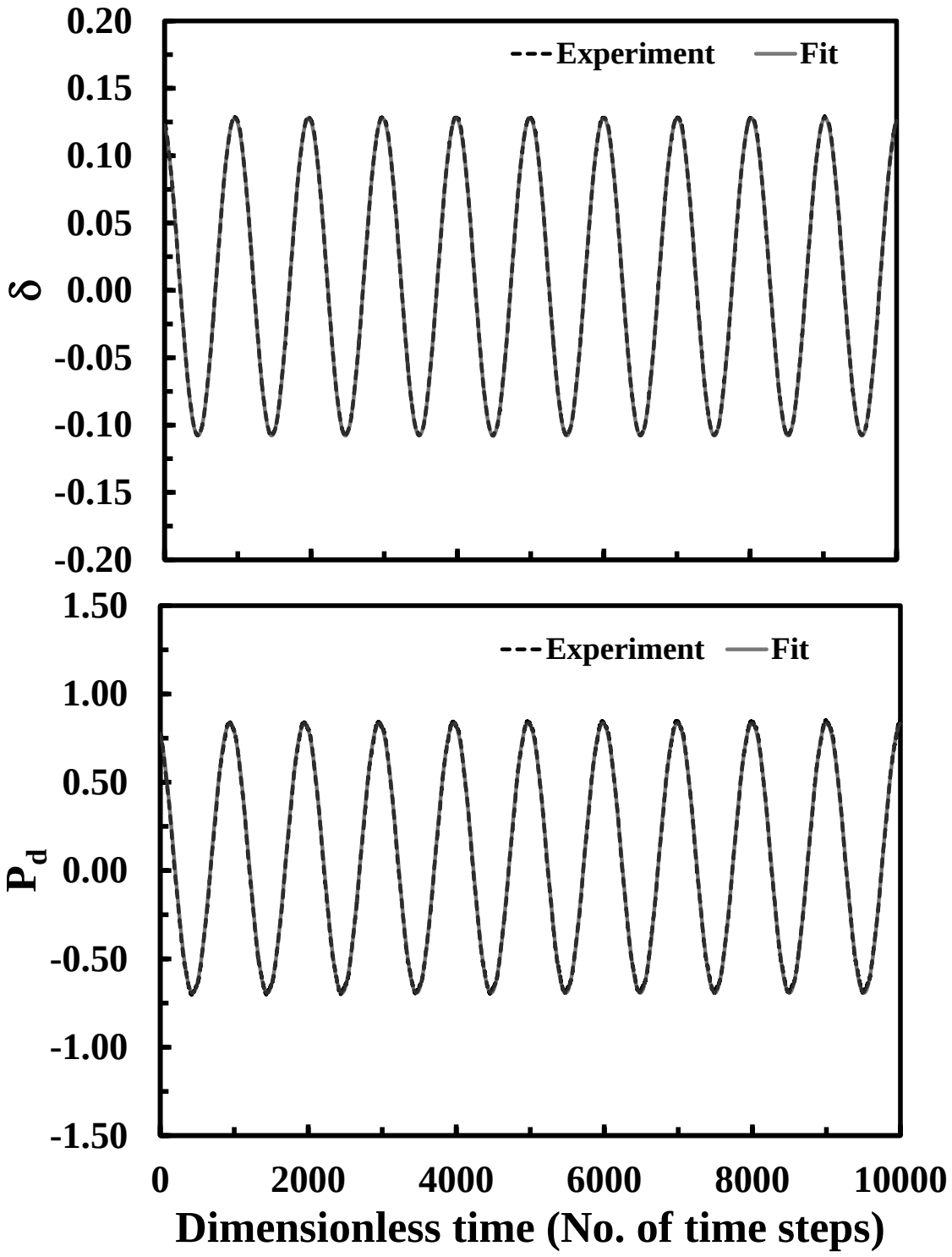

Figure 2.3 Functions used to fit periodic behavior from shaft displacement (top) and differential pressure transducer (bottom) to extract relevant experimental data.

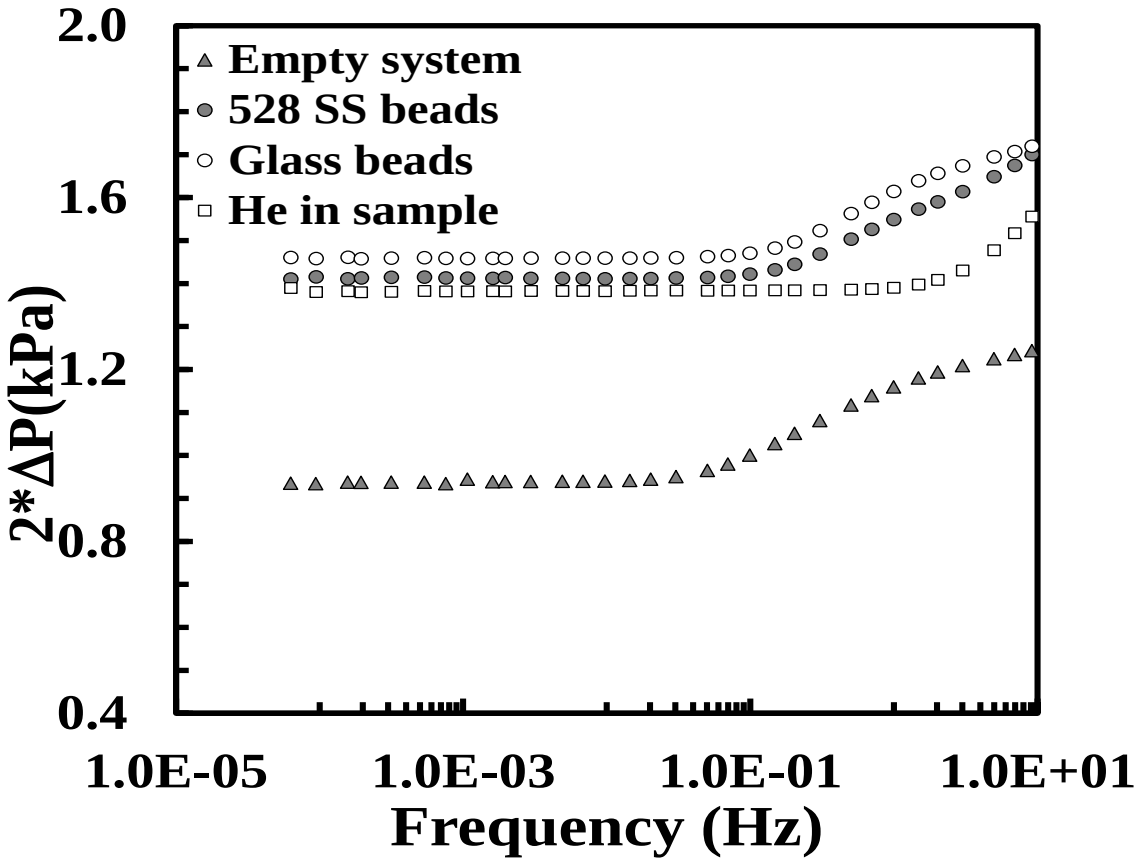

Figure 2.4 Typical response in differential pressure (ΔP) over the wide frequency range for runs with stainless steel beads, glass beads, empty system and run with He in sample.

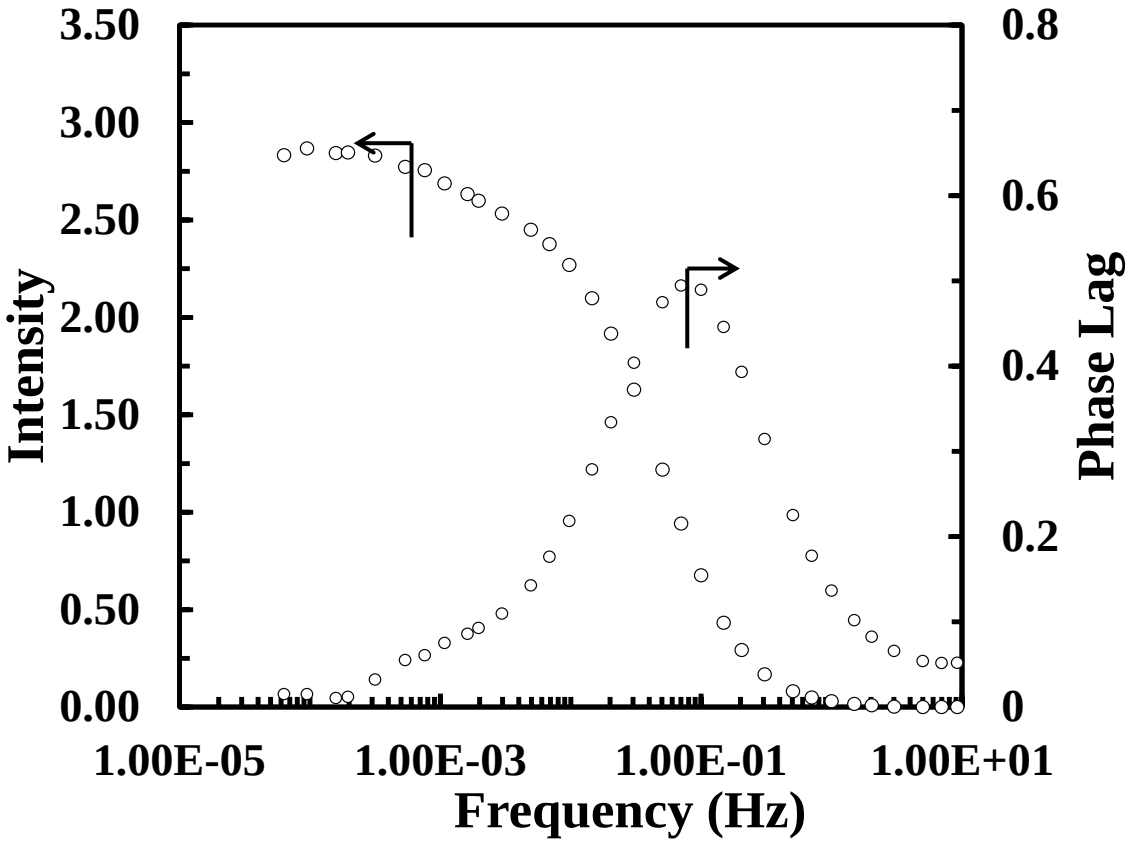

Figure 2.5 Typical experimental frequency response curves in terms of Intensity and Phase lag.

CHAPTER 3

DETERMINATION OF MASS TRANSFER PROCESSES OF CO_2 AND N_2 IN 13X ZEOLITE PELLET

Summary

CO_2 capture and sequestration has become a major research interest as CO_2 is the most anthropogenic greenhouse gas emitted from the combustion of fossil fuels especially in production of electric energy. PSA or VSA using porous adsorbents represents an efficient possible solution for CO_2 capture and 13X is considered to be most promising adsorbent commercially available for post combustion application. Despite its significant applicability very few studies have been conducted to understand the mass transfer behavior of CO_2 and N_2 (two major constituents of the flue gas) in 13X. The diffusion mechanism of an adsorbate into zeolite materials could be composed of either micropore or macropore or a combination of these diffusion mechanisms. The bidisperse structure of the zeolite pellets enhance the complexities of the mass transfer processes in zeolite materials. Understanding the mass transfer mechanism in zeolite becomes critical to design efficient adsorption based separation processes. In this work a newly constructed volumetric FR system is used to study the mass transfer characteristics of CO_2 and N_2 in 13X zeolite beads. Experimental frequency response spectra at different pressures and temperatures were fitted with three different nonisothermal mass transfer

models that includes macropore diffusion, micropore diffusion and macropore convection respectively and found that the macropore diffusion controlled model is the best to predict the experimental curves at all conditions thus confirm that the mass transport process of both CO_2 and N_2 in 13X zeolite is macropore diffusion controlled. The value of optimized diffusional time constant for the macropore diffusion, D_p/R_p^2 as determined by fitting the experimental response curves with that of the models is 3.32 s^{-1} for CO_2 and 5.1 s^{-1} for N_2. The value used for the heat transfer parameter hA is 0.17 J/K/s and 0.051 J/K/s respectively for CO_2 and N_2 experiments.

3.1 Introduction

Production and emission of carbon dioxide are strongly associated with combustions, energy generation and manufacturing. Most of it produced in the power generation through the combustion of fossil fuels. With the growing concern of global warming the demand of energy efficient and effective process for CO_2 capture and storage is also growing as CO_2 is the major part of the anthropogenic greenhouse gases. Over last two decades, technologies of CO_2 capture from fossil fuel combustion using adsorption processes has been widely studied and according to recent studies, pressure swing adsorption (PSA) using porous adsorbents shows promising development in providing energy efficient solution to CO_2 separation technology with the ability to fulfill the requirements for both environmental and energy goals (Xiao et al. 2008; Ebner and Ritter 2009, Kikkinides et al. 1993, Zhang and Webley, 2008). Several studied has identified 13X zeolite as one of the best commercially available adsorbents for carbon dioxide separation applications (Chue et. al. 1995; Siriwardane et al. 2003; Harlick and

Tezel, 2004). In order to design effective adsorption based processes like pressure swing or vacuum swing adsorption process, understanding the dynamic behavior of an adsorbent-gas system is of great importance.

In general, kinetics of adsorption desorption of a pure gas in zeolite could be controlled by a single mechanism like micropore diffusion, macropore diffusion, macropore convection, etc. or any combinations of these mechanisms. Addionally temperature changed in adsorbent caused by heat of adsorption may affect the dynamic behavior (Wang and LeVan, 2011; Kärger and Ruthven, 1992). It has been reported that, in faujasite –type zeolite like 13X with relatively large crystals due to more open lattice, mass transfer is expected to be fast (Ruthven and Lee, 1981). Nonetheless, the complex "bidispersed" structures of commercial zeolites consisting two porous domains; micropores in the individual crystal and macropore in intercrystaline voids arose difficulty in understanding the mass transfer characteristics of such adsorbents. It is therefore became a critical issue to find unequivocally which of the mass transfer mechanism exists in 13X zeolite for both CO_2 and N_2 sorption processes.

Comparatively very few data available in literature on kinetic measurements of CO_2 in 13X. Recently Hu et al. (2013) conducted kinetic experiments with zero length column (ZLC) system with results verified by transient uptake experiments in a commercial volumetric system (Quantachrome Autosorb) and confirmed evidence of macropore diffusion controlled process. Whereas, Silva et al. (2012) interpreted their ZLC experiments data for binderless beads of 13X zeolite at different temperatures and with different size of beads as the mass transfer process controlled by micropore diffusion. On the other hand, there is practically no such studies have been reported on

the mass transfer mechanism of N_2 in 13X. Although, Ruthven et al. (1993) and Sircar et al. (1999) have reported that the kinetics of N_2 adsorption into 13X is controlled by macropore diffusion.

Onyestyák et al. (1995), Onyestyák and Rees (1999), Onyestyák (2011) used frequency response techniques (FR) to measure the adsorption rate of CO_2 in commercial 13X beads and reported that the mass transfer is controlled by transport in macropore along with a heat transfer resistance. Giesy et al. (2012) also used a combined pressure swing and volume swing frequency response apparatus to identify the mass transfer mechanism of CO_2 in 13X beads. Experiments were conducted for different sizes and provide the evidence of macropore controlled diffusion process. Despite its unique ability, very few FR studies have been conducted to understand the mass transfer behavior of CO_2 in 13X. Clearly, it is necessary to explore the strength of the FR technique to understand unambiguously the nature of governing mass transfer mechanism for this system.

Frequency response (FR) methods have proven to be one of the best macroscopic techniques that have been widely used to investigate kinetics behavior of gas-solid systems (Yasuda (1976, 1984, 1991); Wang and LeVan (2005, 2007); Jordi and Do (1993)) due to their ability to discriminate among different rate limiting mechanisms. In FR studies, a system that is initially in equilibrium is subjected to a continuous perturbation, typically in the form of a sinusoidal function, of one physical variable, i.e., pressure, volume or concentration. The system then produces a periodic response with the same frequency as the input but that differs in amplitude and displays a phase lag that uniquely reflects on the thermodynamic and kinetic characteristics of the system. The

responses from a wide spectrum of frequencies at different pressures are analyzed to determine the parameters associated with the kinetic processes occurring in the adsorbent. The ability to process data at a wide frequency range at different pressures by FR provides this technique with a unique advantage that enables investigators to distinguish among mass transfer processes.

In this work, a newly constructed and commissioned volumetric FR system at USC is used to identify the governing mass transfer mechanism for adsorption of CO_2 and N_2 in 13X. A brief description of the apparatus is presented in corresponding section. The major advantage of this volumetric system over other frequency response system like flow through pressure swing or concentration swing system is its ability to measure response over a wide frequency spectra starting from 10^{-5} to near 10 Hz. This wide range is important specially for faster diffusing system like CO_2 in 13X in order to characterize the dynamics of the system thoroughly and accurately.

Frequency response experiments have been conducted at three different pressures (103, 185 and 744 Torr) at 25 ^oC for CO_2 and five different conditions for N_2 (200, 400 and 750 Torr at 25^oC and 40 and 55^oC at 400 Torr). The experimental response curves are then fitted with three nonisothermal mass transfer models namely, macropore diffusion, macropore advection and micropore diffusion model to identify the controlling mechanism of adsorption process as well as to estimate the corresponding mass transfer parameter. Investigating the response curves at different pressure along with a wide frequency range will help to explore the strength and robustness of FR method in identifying the controlling mechanism of the rate processes associated with the adsorption of CO_2 and N_2 in 13X pellet.

3.2 Volumetric Frequency Response Apparatus

The schematic of the automated batch volume swing FR system is shown in Figure 3.1. The system, which uses total volume as input and pressure as output, has been constructed to operate at frequencies between 5×10^{-5} and 10 Hz, temperatures up to 80 ^{o}C, and vacuum pressures down to 0.2 atm. The system comprises of three different volume zones: a) the working volume in dark gray b) the reference volume in light gray, and c) the external volume in white connecting the system with the vacuum or gas feeds. Except for the immersed components, all parts of containing the working and reference volumes are thermally insulated to reduce any thermal influence from the laboratory. The working volume includes a sample container to analyze between 10 and 100 g of sample and a metal bellows that contracts and expands via a shaft for volume modulation. During a run the sample container is immersed in a temperature controlled water jacketed bath that is connected to a chiller. During sample activation, the bath is removed and the container is heated via aluminum concentric sleeves and rigid electric band heaters. A closed sheath thermocouple is immersed in the sample for temperature determination. The shaft connected to the metal bellows is driven via an eccentric sheave for the working volume to vary sinusoidally. The position of the bellows is determined by a linear variable differential transformer (LVDT) along with a linear encoder and an angular encoder (US digital), which measures the input volume perturbation. A pressure transducer (MKS instruments Inc, USA). The Reference volume includes a two-liter ballast that is immersed within the bath of the chiller for temperature, and thus pressure, stabilization. The equilibrium pressure and the changes of pressure are respectively followed by An MKS pressure transducer located at the reference volume and a

differential pressure transducer (Omegadyne, Inc) located between the reference and working volumes. Connectivity between the different zones is controlled via solenoid valves V1 through V4. Data acquisition from the LDVT, pressures transducers and thermocouple is accomplished via a LabVIEW program running on a Dell PC-AT 320. Microsoft excel program is used to determine actual frequency, phase lags, amplitude of input and output variables, and characteristic response functions from pressure-volume experimental data.

3.3 Experiments

In this work, volumetric frequency response experiments have been conducted over a wide range of frequencies starting from 7×10^{-5} Hz to 9.25 Hz for 8-12 mesh 13X zeolite beads from Grace Davison with both CO_2 (Bone dry grade, Airgas) and N_2 (UHP300). The experimental conditions for CO_2 and that for N_2 are different.

For CO_2 frequency response experiments have been performed at three different pressures of 102 Torr, 185 Torr and 744 Torr at 25 ^{o}C. For this study, a system consisted of a 120 cc sample holder containing three layers: a top layer with 46.3 g of 3.0 mm glass beads, a center layer with 39.8 g of 13X beads and a bottom layer with 46.3 g of 3.0 mm glass beads had been used in volumetric frequency response apparatus (Figure 3.2). Whereas for N_2 five different conditions were used, at 200 Torr, 400 Torr and 750 Torr at 25 ^{o}C and also at 40oC and 50oC temperatures at 400 Torr. Similar as CO_2 experiments the sample holder contained three layers: a top layer with 32.3 g of 3.0 mm glass beads, a center layer with 9.9 g of 13X beads and a bottom layer with 129.3 g of 3.0 mm glass (Figure 3.2)

Prior to the experiments, sample activation was conducted. For activation the system is evacuated by keeping valves V1, V2 and V4 open while valve V3 remains closed (Figure 3.1). Aluminum sleeves and electric band heaters were used eventually reached at desired temperature, which is 350^{o}C for 13X. The activation had been carried for 40 hours or until the pressure at the vacuum pump (adixen DRYTEL, 1025) is less than 1.5×10^{-5} torr (Granville-Phillip 350 Ionization Gauge), which suggests satisfactory sample regeneration. Then, the system was let cool, the heaters and sleeves are removed and the container was fully immersed in the water jacketed bath which was set at desired temperature (25, 40 or 55 ^{o}C for this study). Valve V4 is then closed and then the working gas is allowed in via valve V3 to pressurize the system to the target pressure. A needle valve is used (not shown) to control the flow of the working gas into the system. Once at a relatively stable target pressure, the shaft is moved to position where the bellows is at the mid-point. Valve V2 is then closed and the system is let equilibrate for 24-48 hours. Once at equilibrium, valve V1 connecting the reference and working volumes is closed, the differential pressure ΔP between the two is at zero and the system is ready for a sample run.

Once the system is ready to start at equilibrium, the sample to subjected to volume modulation at a predefined set of frequencies between 7.0×10^{-5} and 9.25 Hz. Ten cycles are typically run at each particular frequency, before switching to the next. At the end of the run, the collected values of the shaft displacement and the differential pressure from the LDVT and the differential pressure transducer, respectively, are analyzed and fitted at the periodic behavior using the following functions:

$$\delta = \delta_o + \Delta\delta \sin(2\pi ft + \varphi_\delta) \tag{3.1}$$

$$P_d = P_{d,o} + \Delta P_d \sin(2\pi ft + \varphi_P) \tag{3.2}$$

where, f is the frequency, t is the time, δ and P_d are the shaft displacement and the differential pressure, respectively; δ_o and $P_{d,o}$ are the corresponding offsets, which at the periodic behavior are different from the zero value; φ_δ and φ_P, are the corresponding phase lags; and $\Delta\delta$ and ΔP_d are the corresponding amplitudes.

For each frequency the system can provide a response in the form of two variables. One of them is the phase lag response which is given by

$$\varphi = \varphi_P - \varphi_\delta \tag{3.3}$$

and the intensity response, which is conveniently expressed as:

$$I = \left(\frac{\Delta V}{V_{EXT}} \cdot \frac{P_o}{\Delta P_d} - 1 \right) \tag{3.4}$$

Where, P_o is the absolute pressure at equilibrium, ΔV is the amplitude of the change of the working volume and V_{EXT} is the volume within the working volume external to the volume of the materials in the container (adsorbent, glass bead, etc). This ensures that **I** to approach zero at highest frequencies

The isotherm of CO_2 and N_2 in 13X from the same lot was experimentally determined with a Micromeritics ASAP 2010 instrument. Figure 3.3 shows the isotherms of the CO_2 and N_2 in 13X at three different temperatures and fitted with Toth isotherm model. The heats of adsorption were estimated from the isotherm and for CO_2 the value of heat of adsorption is very close to the value reported in the literature (Dunne et al., 1996 ; Giesy et al., 2012). The system properties and isotherm parameters are given in table 1 and table 2 respectively. The details of the activation procedure, experiment and method of analysis of experimental data to determine intensity and phase lag as well as

the determination of skeletal density and slope from frequency response experiments are described in chapter 2.

3.4 Material and Energy Balances

A schematic representation of the batch frequency response system is shown in Figure 3.1, where system volume is perturbed periodically around the equilibrium value V_{b0}, and the system pressure P_b responds accordingly. Assuming that the entire system is at same pressure, the material balance over the entire volume is,

$$m\frac{\partial \overline{Q}}{\partial t}+\frac{\partial}{\partial t}\left(\frac{P_b V_b}{RT}\right)=0 \tag{3.5}$$

$$V_b = V_{b,o} + \Delta V \sin(2\pi f t) \tag{3.6}$$

$$\overline{Q} = \overline{\overline{q}} + \left(\varepsilon_p/\rho_p\right)\overline{C}_p \tag{3.7}$$

Energy balance is applied over the volume containing the adsorbent, assuming Temperature. T is only function of time; not of bed length or pellet radius

$$\begin{aligned}&\frac{m}{\rho_p}\left[\frac{\varepsilon_b}{(1-\varepsilon_b)}+\varepsilon_p\right]\left[Cp_g\frac{P_b}{RT}\frac{\partial T}{\partial t}-\frac{\partial P_b}{\partial t}\right]+m\bar{q}Cp_a\frac{\partial T}{\partial t}\\&+mCp_s\frac{\partial T}{\partial t}+(-\Delta H_a)\frac{\partial \overline{\overline{q}}}{\partial t}=hA\left(T_{wall}-T\right)\end{aligned} \tag{3.8}$$

The quantities $\overline{\overline{q}}$ and $\overline{C}_p$ are the volume average loading and gas phase concentration respectively over the pellet volume and defined as,

$$\overline{\overline{q}} \equiv \frac{3}{R_p^2}\int_0^{R_p}\bar{q}r_p^2 dr_p \tag{3.9}$$

$$\bar{C}_p \equiv \frac{3}{R_p^2} \int_0^{R_p} C_p r_p^2 dr_p \tag{3.10}$$

Where C_p is the gas phase concentration in side pore and $\bar{q}$ is the volume average loading over crystal and expressed as,

$$\bar{q} \equiv \frac{3}{R_c^2} \int_0^{R_c} \bar{q} r_c^2 dr_c \tag{3.11}$$

Depending on the kind of controlling mechanism $\bar{\bar{q}}$ and $\bar{q}$ can be correlated with the equilibrium loading in different manner which is explained in corresponding model description.

The macropore model used in this work includes both advection and macropore diffusion as mass transfer mechanisms. The convective flux is defined using Darcy's expression. The macropore mass balance equation is expressed in spherical coordinate in terms of dimensionless pellet radius with appropriate boundary and initial conditions,

$$\frac{\varepsilon_p}{RT}\frac{\partial P}{\partial t} - \frac{\varepsilon_p P}{RT^2}\frac{\partial T}{\partial t} + \rho_p \frac{\partial \bar{q}}{\partial t} = \frac{\varepsilon_p}{\xi_p^2}\frac{\partial}{\partial \xi_p}\left[\frac{\xi_p^2}{R_p^2}\left(\frac{\kappa}{\mu}\frac{P}{RT} + \frac{D_p}{RT}\right)\right] \tag{3.12}$$

Where, $\xi_p = \frac{r_p}{R_p}$

$$\frac{\partial P}{\partial \xi_p} = 0 \qquad \text{at} \qquad \xi_p = 0 \tag{3.13}$$

$$P = P_b \qquad \text{at} \qquad \xi_p = 1 \tag{3.14}$$

$$P = P_{b,0} \text{ and } T = T_0 \qquad \text{at} \qquad t = 0 \tag{3.15}$$

It is noteworthy that the same model is used for both macropore convection controlled mechanism and macropore diffusion controlled mechanism. The only difference is that when the mass transfer is purely advective, the diffusive parameter D_p/R_p^2 is set as zero and similarly when the mass transfer is purely diffusive, the advective parameter κ is set as zero. For macropore controlled models there is no resistance in micropore/ crystal hence, the quantity $\bar{q}$ is in equilibrium with local gas phase concentration in macropore and estimated as,

$$\bar{q}(r_p) = q^*(P(r_p), T) \tag{3.16}$$

And $\bar{\bar{q}}$ is obtained according to equation 3.9.

In micropore diffusion model the loading dependency of micropore diffusion is expressed by Darken correction factor for diffusivity and the mass balance is written in terms of dimensionless microporous crystal radius.

$$\frac{\partial q}{\partial t} = \frac{1}{\xi_c^2}\frac{\partial}{\partial \xi_c}\left(\xi_c^2 \frac{D_c}{R_c^2}\right)\frac{\partial q}{\partial \xi_c} \tag{3.17}$$

Where, $\xi_c = \frac{r_c}{R_c}$

$$\frac{\partial q}{\partial \xi_c} = 0 \qquad \text{at} \qquad \xi_c = 0 \tag{3.18}$$

$$q = q^*(P,T) \qquad \text{at} \qquad \xi_c = 1 \tag{3.19}$$

$$q = q_0^* \qquad \text{at} \qquad t = 0 \tag{3.20}$$

with,

$$\frac{D_c}{R_c^2} = \frac{D_{co}}{R_c^2} \frac{1}{1-\left(\frac{q}{q_s}\right)^n} \tag{3.21}$$

In case of micropore diffusion controlled model the quantity $\bar{q}$ is estimated using equation 3.11 and since there is no resistance in macropore, $\bar{\bar{q}}$ is equal to $\bar{q}$ and $\bar{C}_p$ is equal to $C_p=P_b/R/T$.

For all the models equilibrium loading is expressed by Toth isotherm:

$$q^* = \frac{bPq_s}{\left(1+(bP)^n\right)^{\frac{1}{n}}}; \quad b = b_0 e^{\left(\frac{B}{T}\right)} \tag{3.22}$$

3.5 Results and Discussion

The experimental response curves were obtained for the system as described in the experimental section. Table 3.1 includes the skeletal density as obtained by this approach along with the mass of adsorbent and glass beads and other relevant information on the systems used for CO_2 and N_2 experiments. Table 3.3 shows a comparison of the isotherm slope from FR method with the slopes of isotherm measured using ASAP 2010 for CO_2 reflecting quite a good agreement between these two methods.

Figure 3.4 shows the experimental response spectra in terms of intensity function and phase lag for CO_2 on the 13X zeolite beads at 25 ^oC at three different pressures. These responses show three distinct zones, A, B and C, each depicting the kinetics nature of the adsorption process.

Region **A** is identified by the initial plateau observed only at sufficiently low frequencies. The time of cycling the pressure is sufficiently slow compared to the time

constant of the diffusion process and mainly governed by the equilibrium. Thus the plateau indicates that the adsorbent is under isothermal local equilibrium conditions. This region is where the slope of the isotherm is determined.

Region **B** is represented by an intermediate plateau that reveals the existence of either an internal mass transfer resistance or a heat transfer limited local equilibrium process. The latter is the case for CO_2 on 13X, which is characterized by a relatively large heat of adsorption and fast mass transfer kinetics. It is important to note that temperature oscillations in this region (not shown) are not necessarily significant for the effect to be observed (~ 0.1 ^{o}C).

Region **C** is where the process is dominated by its own characteristic mass transfer limitation. Frequencies at this point are so fast that the sample no longer experiences heat effects and thus remains isothermal. This is the region where mass transfer mechanisms can be distinguished.

To identify the controlling mechanism of sorption process three different nonisothermal mass transfer models were used in this study. Figures 3.5, 3.6 and 3.7 show the intensity function and phase lag curves over the frequency spectra at all pressures fitted with nonisothermal macropore diffusion, nonisothermal micropore diffusion and nonisothermal macropore convection models respectively. All these models consist of a heat transfer parameter along with a mass transfer parameter. The same value of the parameter for heat transfer coefficient (hA=0.17 J/K/s) was used in all cases. Only the pertinent mass transfer parameter is optimized in each model to fit all three curves. The fitting parameters are D_p/R_p^2 for the Macropore Diffusion, κ for the Macropore

Advection, and D_{co}/R_c^2 for the Micropore Diffusion. The values of optimized mass transfer parameter are summarized in table 3.4.

All three models able to capture the experimental intensity curve in slowest frequency region (region **A**) where the processes were driven by local equilibrium. Although the temperature gradient along the bed and pellet is neglected, the models are able to qualitatively capture the shape of the curves in this frequency region and clearly depicted that the contribution of thermal resistance is also important in dynamic behavior of the system.

Although curves predicted by nonisothermal models sufficiently agreed with the experimental intensity curve, none of the models were able to capture the trends along the frequency spectra perfectly. This may be due to fact that in models, the bed is treated as a point which is too idealized to capture the overall dynamics behavior of the system. The assumption of no pressure drop along the bed and no temperature gradient along the bed or along the pellet might be not adequate to explain the system behavior fully. Despite that the model is able to describe response at high frequency (Region **C**) where the process is strictly isothermal.

The phase lag curves as predicted by the models are unable to capture the experimental phase lag curves fully. These disagreements between the experimental phase lag and that from the model is not fully understood at this point, but this could be due to phase lag associated with the inherent dynamics of the system. However, in figure 3.5, the location of the maxima in phase lag curves (connected by dotted line) for all three pressures as predicted by the macropore diffusion model exhibit fairly good agreement with the location of maxima for the experimental phase lag curves (connected by broken

line). Similarly in figure 3.6 and 3.7 the predictions of the loci of the maxima from other two competitive models (connected by dotted lines) are compared with loci of the maxima of the experimental phase lag curves.

Figure 3.8 shows how well each model correlates with the experimental data at all three pressures. The existence of macropore diffusion on the adsorption dynamics of the system was strongly established by the intensity curves predicted by the nonisothermal macropore diffusion model using a single D_p/R_p^2 value for all three pressures comparatively better than those predicted by nonisothermal micropore diffusion or nonisothermal macropore convection models. Moreover, pressure independence of macropore diffusion coefficients rejects the possibility of viscous flow mechanism for which diffusivity is a linear function of pressure. As it observed from the theoretical intensity curves the macropore convection model (κ = 1.02e-8 mm^2) and the micropore diffusion model (D_{co}/Rc^2 = 0.0043 s^{-1}) simply cannot represent the experimental trends, indicating unequivocally that these processes are not the controlling mechanism in this specific adsorption process. In addition, as described earlier the phase lag curves shown in figure 3.5, 3.6 and 3.7 the location of the maxima were also best predicted by the macropore model despie of some limitation to capture the phase lag curves properly. That also supports the existence of the macropore diffusion controlled mechanism in transport of pure CO_2 in 13X. Similar results have been reported by Giesy et al. (2012) using a combined pressure swing and volume swing frequency response apparatus. They confirmed the existence of macropore diffusion controlled mechanism by showing the strong dependence of dynamic response on particle size as the macropore diffusional time constant is a function of pellet size. For smaller particle some disagreement have been

reported between the model and the experiment, which might be resulted due to the fact that the mass transfer mechanism is shifting towards micropore/crystal diffusion limited or a combination of macropore and micropore diffusion controlled mechanism as the particle size decreases and the time constant for the macropore diffusion becomes comparable to that of the micropore/crystal diffusion.

Figure 3.9 shows the experimental response spectra in terms of intensity function and phase lag for N2 on the 13X zeolite beads at all five experimental conditions. Like the response of CO_2, these responses also show three distinct zones, A, B and C, each depicting the kinetics nature of the adsorption process. Though in this case, region B which reveals the existence of either an internal mass transfer resistance or a heat transfer limited local equilibrium process is not as significant as it is for the case of CO_2. This might be associated with the fact that the heat of adsorption for N2 on 13X (19.7 kJ/mol) is comparatively smaller than that of CO_2 on 13X.

Same three different nonisothermal mass transfer models were used to identify the controlling mechanism of sorption process of N_2 in 13X. Figures 3.10, 3.11 and 3.12 show the intensity function and phase lag curves over the frequency spectra at experimental conditions fitted with nonisothermal macropore diffusion, nonisothermal micropore diffusion and nonisothermal macropore convection models respectively. All these models consist of a heat transfer parameter along with a mass transfer parameter. The same value of the parameter for heat transfer coefficient (hA=0.051 J/K/s) was used in all cases. It is noteworthy that, the value for heat transfer parameter is associated with area available for heat transfer and the value is observed to be approximately proportional to the mass of adsorbent used for CO_2 experiments. Only the pertinent mass transfer

parameter is optimized in each model to fit all curves and values of optimized mass transfer parameter are summarized in table 3.5.

Similarly like CO_2 responses, all three models able to capture the experimental intensity curve in slowest frequency region (region A) where the processes were driven by local equilibrium. Like CO_2, for N_2 also both the intensity and the phase lag functions for all the conditions are best predicted by the nonisothermal macropore diffusion model. The location of the maxima in phase lag curves for all conditions as predicted by the macropore diffusion model exhibit fairly good agreement with the location of maxima for the experimental phase lag curves and show comparatively better agreement that other two models as shown in figure 3.10.

Figure 3.13 focuses on the zone C where the process is dominated by its own characteristic mass transfer limitation to show how well each model correlates with the experimental data at all five experimental conditions. The existence of macropore diffusion on the adsorption dynamics of the system was strongly established by the intensity curves predicted by the nonisothermal macropore diffusion model using a single $D_p/R_p^2(5.1\ s^{-1})$ value for all five conditions comparatively better than those predicted by nonisothermal micropore diffusion or nonisothermal macropore convection models. As it observed from the theoretical intensity curves the macropore convection model (κ = 1.25e-8 mm^2) and the micropore diffusion model (D_{co}/R_c^2 = 0.12 s^{-1}) simply cannot represent the experimental trends, indicating unequivocally that these processes are not the controlling mechanism in this specific adsorption process. In addition, as described earlier the phase lag curves shown in figure 3.10, 3.11 and 3.12 the location of the maxima were also best predicted by the macropore model despite of some limitation to

capture the phase lag curves properly. That also supports the existence of the macropore diffusion controlled mechanism in transport of pure N_2 in 13X. So, far no frequency response studies have been conducted for N_2 adsorption process in 13X. However, Ruthven et al. (1993) and Sircar et al. (1999) have reported that the kinetics of N_2 adsorption into 13X is controlled by macropore diffusion and Dantas et al. (2011) has found that the kinetics of N_2 is faster than CO_2 in 13X which also supports the findings of this study.

3.6 Conclusions

A newly constructed and commissioned volumetric FR system at USC has been introduced for study the mass transfer characteristics of gases in adsorbents. The FR apparatus has the ability to characterize more thoroughly over wide frequency spectra, which is suitable for both slow and fast moving gas-adsorbent systems. Moreover, representing the FR data in terms of a function of amplitude ratio and phase lag not only simplify the treatment of data but also enhance the understanding of multiple simultaneous dynamic processes. Additionally, it provides a fairly good estimation of the slope of the isotherm from the low frequency plateau of the response curve.

The ability and the robustness of the new FR system in identifying the controlling mass transfer resistance were demonstrated on CO_2 and N_2 in 13X system. The sorption kinetics of both pure CO_2 and pure N_2 on 13X zeolite beads were well described by nonisothermal macropore diffusion model. Macropore diffusion model is confirmed by conducting experiments at different pressures and temperature that aided to discriminate more clearly among different models. The equilibrium results (slope of the isotherm at

low frequency plateau) from the new apparatus were in good agreement with those obtained from the commercial ASAP 2010 system. However, there are certain issues that have not been clearly investigate and understand in this work which clearly, shows that more investigation along with further refinements of the models specially the heat transfer model for the interpretation of the volumetric system more adequately is needed to better characterize such faster transport mechanism like CO_2/N_2-13X system. Despite of few disagreements between the model and experiment, it has been showed that only nonisothermal macropore model were able to predict the experimental results quantitatively for all conditions and thus unequivocally concluded that the sorption of CO_2 and N_2 in 13X is macropore diffusion controlled.

3.7 Tables

Table 3.1 Properties of the system used in frequencies response study for CO_2 and N_2

	Parameters	**Value**	**Unit**
Properties of Adsorbents	Skeletal Density	2.42	g/ cm^3
	Pellet Density	1.12	g/ cm^3
	Bulk Density	0.710	g/ cm^3
	Heat Capacity	1.3	kJ/kg/K
Properties of Glass beads	Pellet density	2.52	g/ cm^3
	Bulk Density	1.49	g/ cm^3
System Properties	Total Empty Volume	236.68	cm^3
	Heat Capacity of Gas Phase	0.0295	kJ/mol/K
	Stroke Half Volume (ΔV)	1.1	cm^3
CO_2 Experiments	Mass of Glassbeads	92.6	g
	Mass of Adsorbent (13X)	39.8	g
	CO_2 Heat of Adsorption*	37.1 (102 Torr) 36.6 (185 Torr) 36.0 (744 Torr)	kJ/mol
N_2 Experiments	Mass of Glassbeads	161.6	g
	Mass of Adsorbent (13X)	9.9	g
	N_2 Heat of Adsorption*	19.7	kJ/mol

***Determined from experimental isotherm data obtained for CO_2 and N_2 on 13X at three temperatures.**

Table 3.2 Toth isotherm parameters for CO_2 and N_2 in 13X

Toth Parameter	**CO_2**	**N_2**	**Unit**
q_s	6.833	5.925	mol/kg
bo	3.204e-7	2.387e-7	kPa^{-1}
B	4806.57	2375.40	K
n	0.35	0.64	…

Table 3.3 Slope of the isotherm as determined from FR experiments for CO_2

Pressure **(Torr)**	***dq/dP**** **(isotherm)**	***dq/dP**** **(FR)**	**% Difference**
744	5.68	4.94	13
185	28.05	25.24	10
102	53.19	53.19	0

***Slope of the isotherm, dq/dP (mmol/kg/kPa).**

Table 3.4 Value of optimized fitting parameters for different models for CO_2

Models	Model parameter
Macrpore diffusion	$\mathbf{D_p/R_p^2 = 3.32\ s^{-1}}$
Macropore convection	$\mathbf{\kappa = 1.02e\text{-}8\ mm^2}$
Micropore diffusion	$\mathbf{D_{co}/R_c^2 = 0.0043\ s^{-1}}$

Table 3.5 Value of optimized fitting parameters for different models for N_2

Models	Model parameter
Macrpore diffusion	$\mathbf{D_p/R_p^2 = 5.1\ s^{-1}}$
Macropore convection	$\mathbf{\kappa = 1.25e\text{-}8\ mm^2}$
Micropore diffusion	$\mathbf{D_{co}/R_c^2 = 0.12\ s^{-1}}$

3.8 Figures

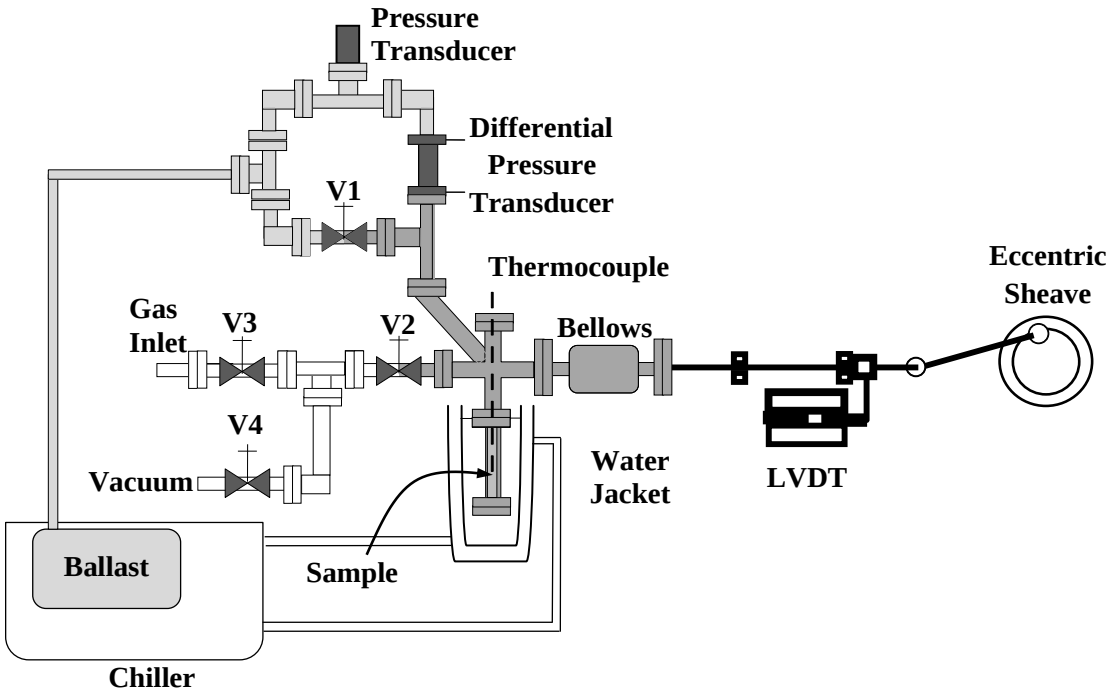

Figure 3.1 Schematic of volume swing frequency response (FR) instrument used for the kinetic study of CO_2 and N_2 in 13x zeolite.

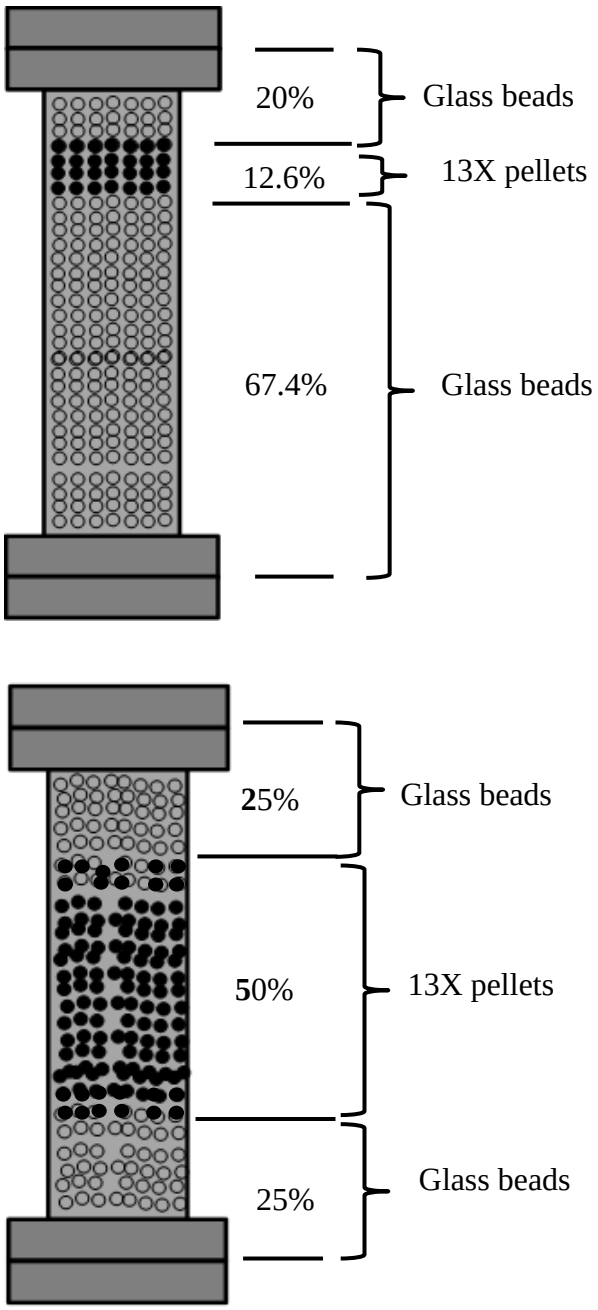

Figure 3.2 Packing of 13X pellets and glass beads in sample container for frequency response experiments with CO_2 (top) and N_2 (bottom).

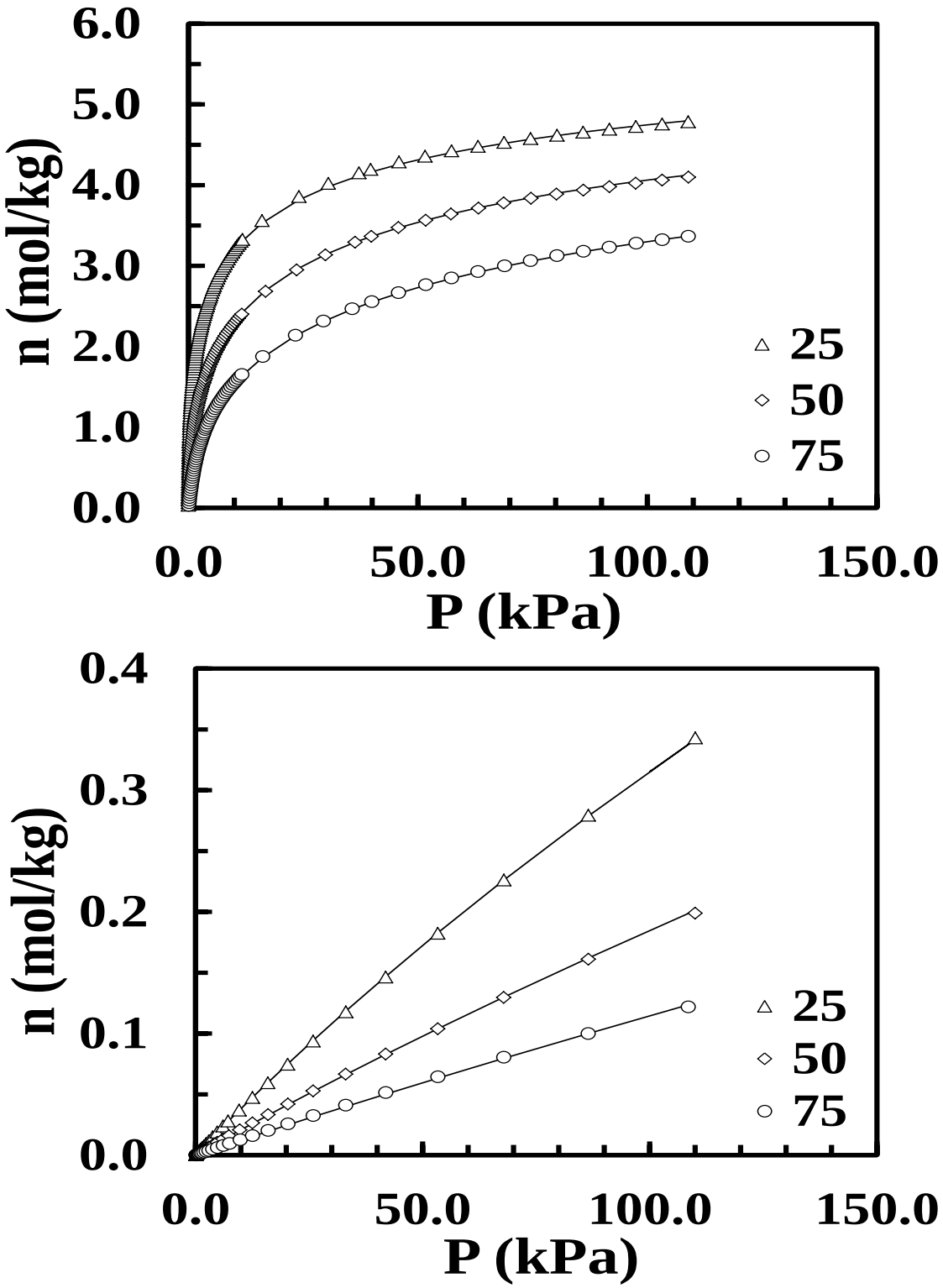

Figure 3.3 Isotherm of CO_2 (top) and N_2 (bottom) on 13X beads measured with Micromeritics ASAP 2010 and fitted with Toth model

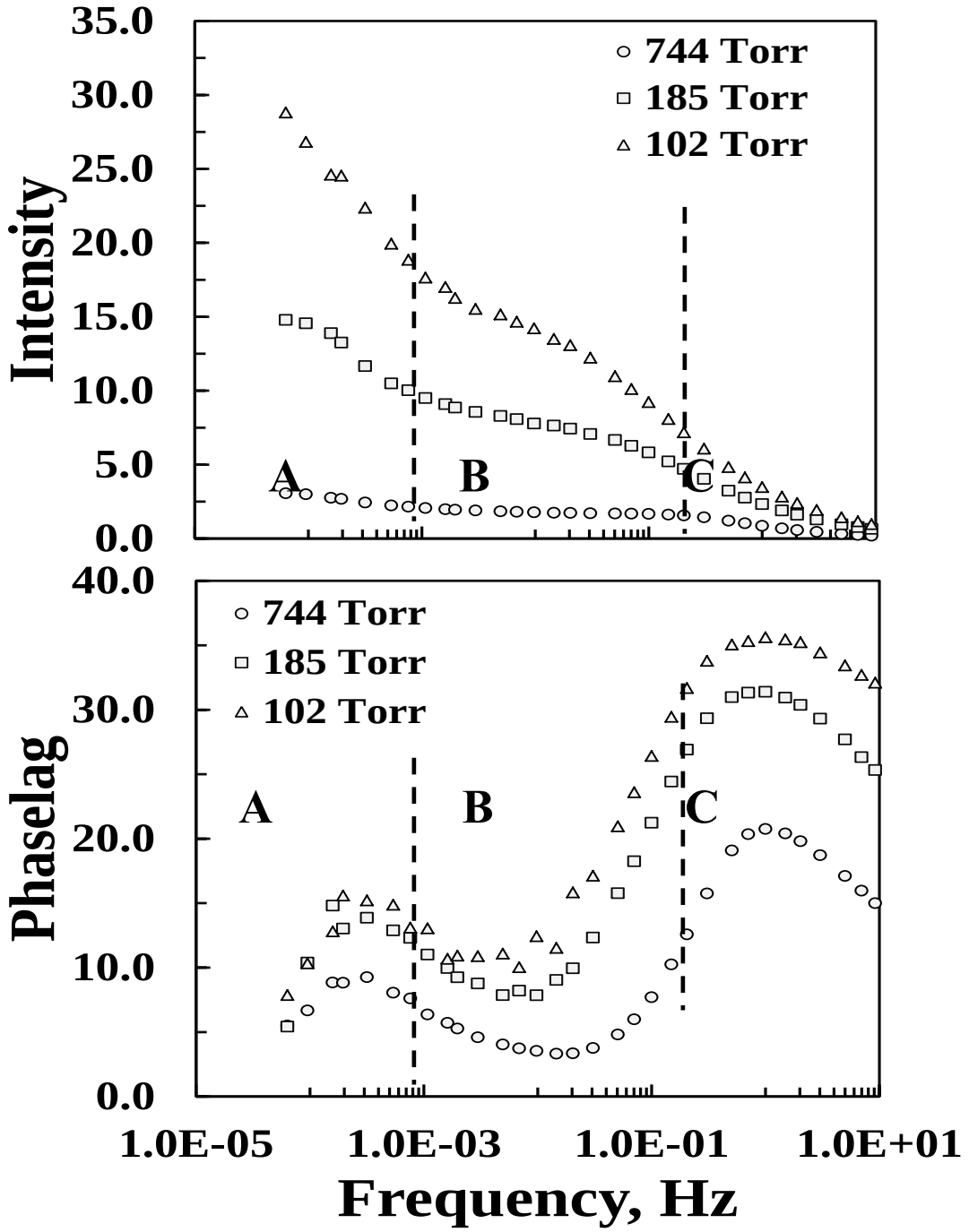

Figure 3.4 Experimental Intensity (top) and Phase Lag (bottom) functions of CO_2 on 13X at 25 ^{o}C at three pressures (102, 185 and 744 Torr) showing three distinct zones, A, B and C, each depicting the kinetic nature of the adsorption process

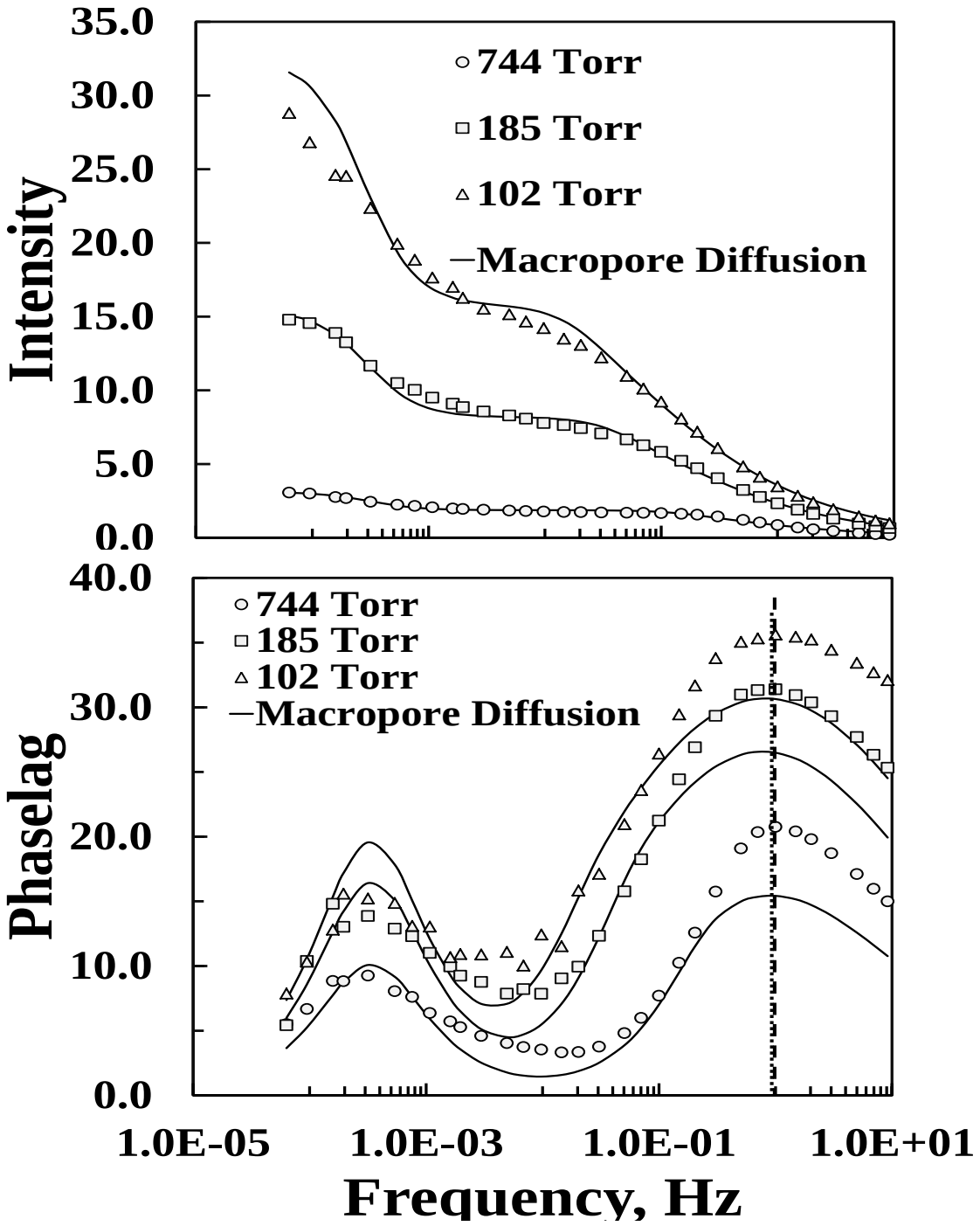

Figure 3.5 Intensity (top) and Phase lag (bottom) curves of CO_2 on 13X beads at 25 ^{o}C at three pressures (102, 185 and 744 Torr) compared with nonisothermal macropore diffusion model with D_p/R_p^2= 3.32 1/s and hA=0.17 J/K/s. The loci of the maxima for the experimental phase lag curves are connected by broken line and that from the model are connected by dotted line exhibit fairly good agreement.

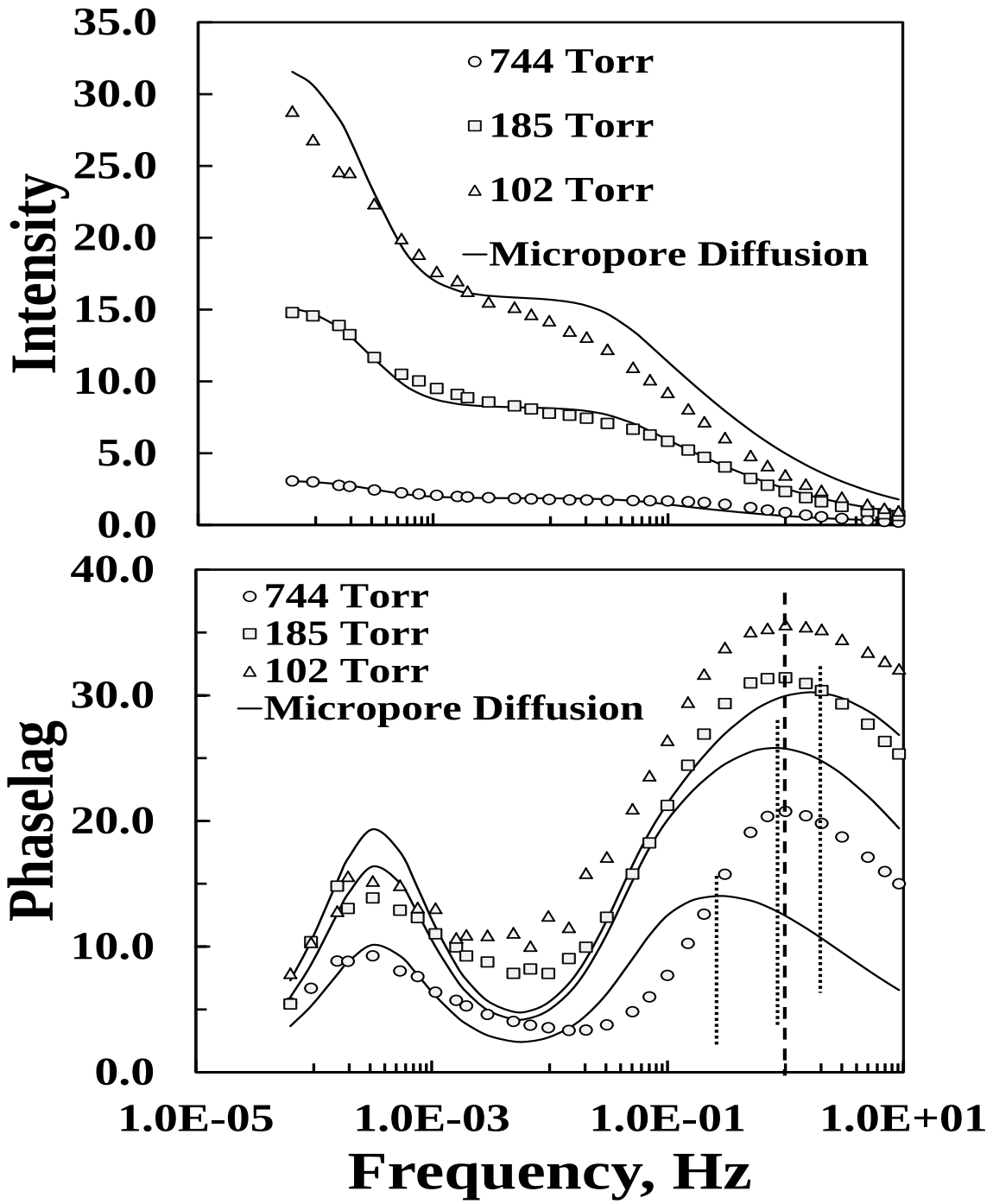

Figure 3.6 Intensity (top) and Phase lag (bottom) curves of CO_2 on 13X beads at 25 ^{o}C at three pressures (102, 185 and 744 Torr) compared with nonisothermal micropore diffusion model with D_{co}/R_c^2= 0.0043 1/s and hA=0.17 J/K/s. The loci of the maxima from the model are connected by dotted line are deviated from the loci of the maxima for the experimental curves (broken line).

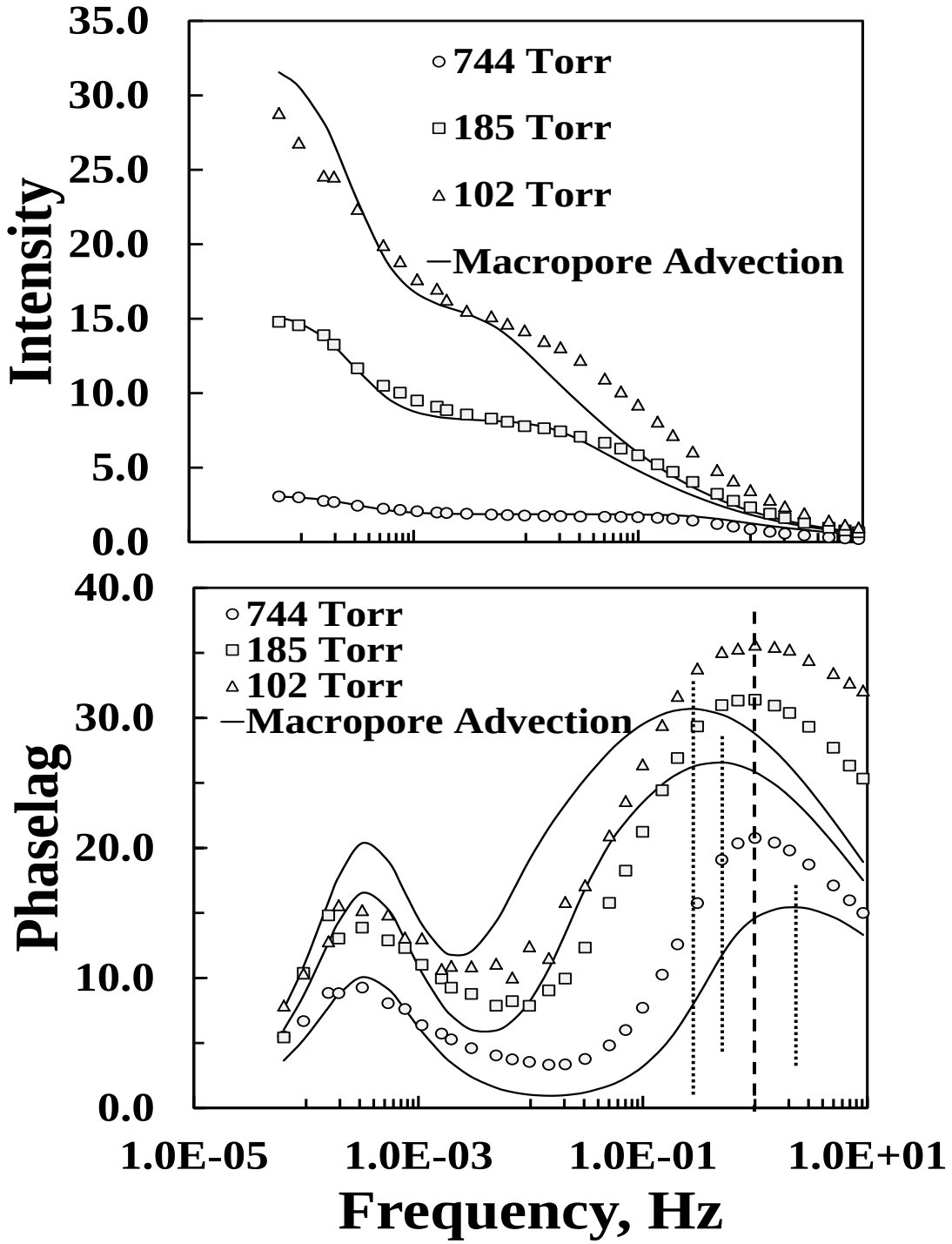

Figure 3.7 Intensity (top) and Phase lag (bottom) curves of CO_2 on 13X beads at 25 ^{o}C at three pressures (102, 185 and 744 Torr) compared with nonisothermal macropore advection model with permeability κ = 1.02e-8 mm^2 and hA=0.17 J/K/s. The loci of the maxima from the model are connected by dotted line are deviated from the loci of the maxima for the experimental curves (broken line).

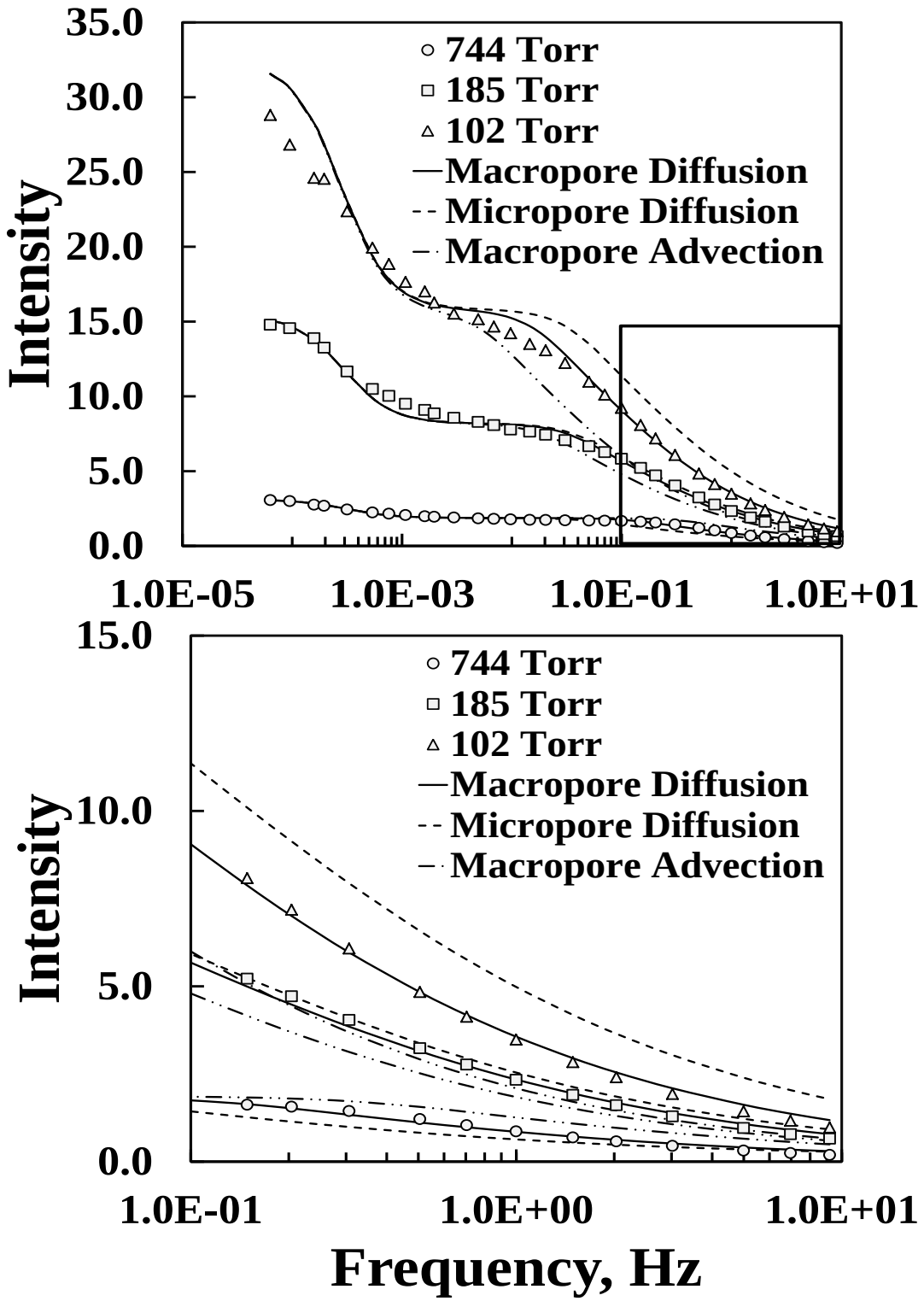

Figure 3.8 Comparison of fittings of three different mass transfer mechanisms with experimental intensity curve at 25^{o}C and three pressure conditions to identify the governing mass transfer mechanism for the sorption process of CO_2 in 13X (a and b). The best results observed with macropore diffusion model as compared to other two models.

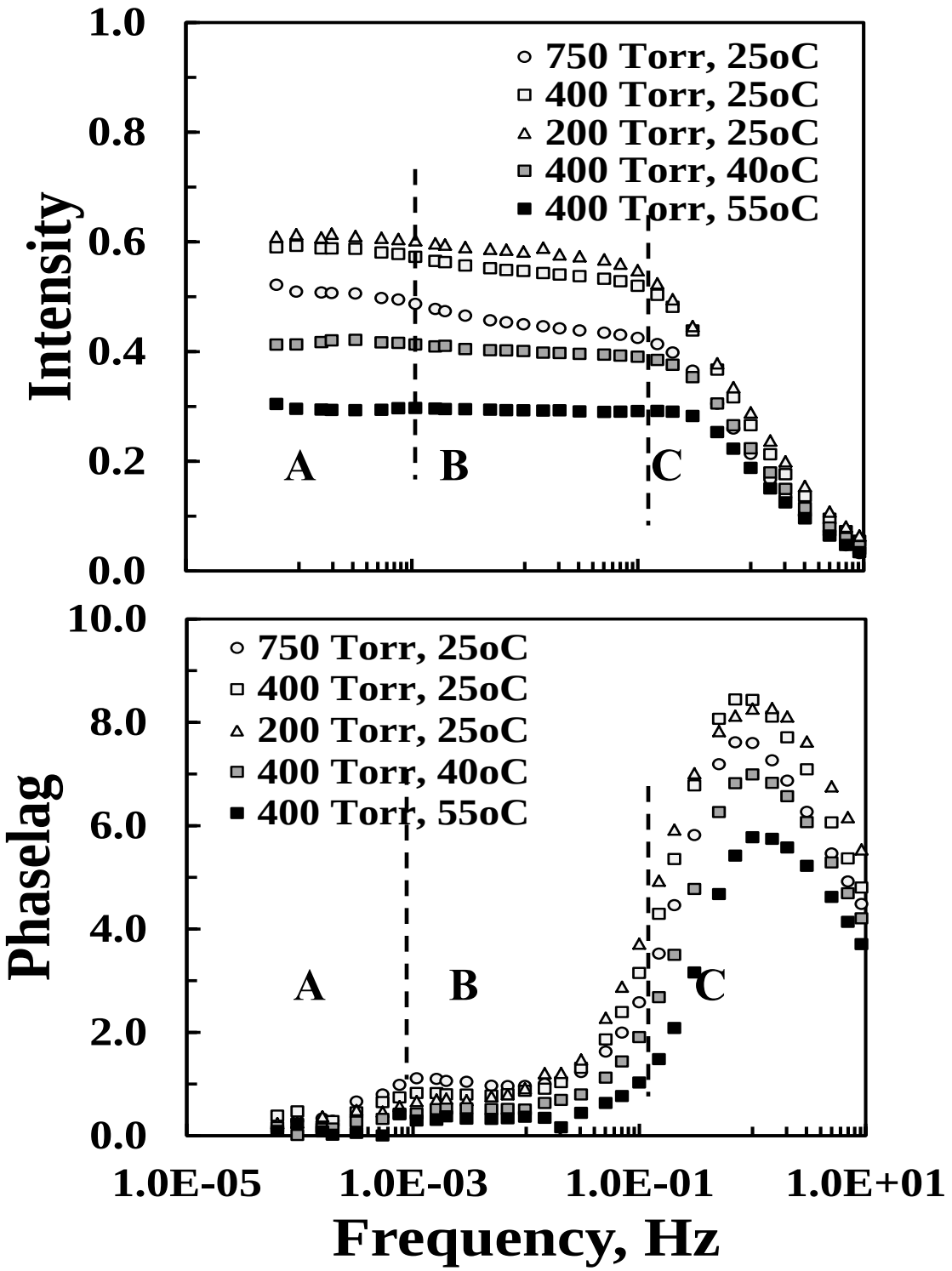

Figure 3.9 Experimental Intensity (top) and Phase Lag (bottom) functions of N_2 on 13X at five different experimental conditions showing three distinct zones, A, B and C, each depicting the kinetic nature of the adsorption process.

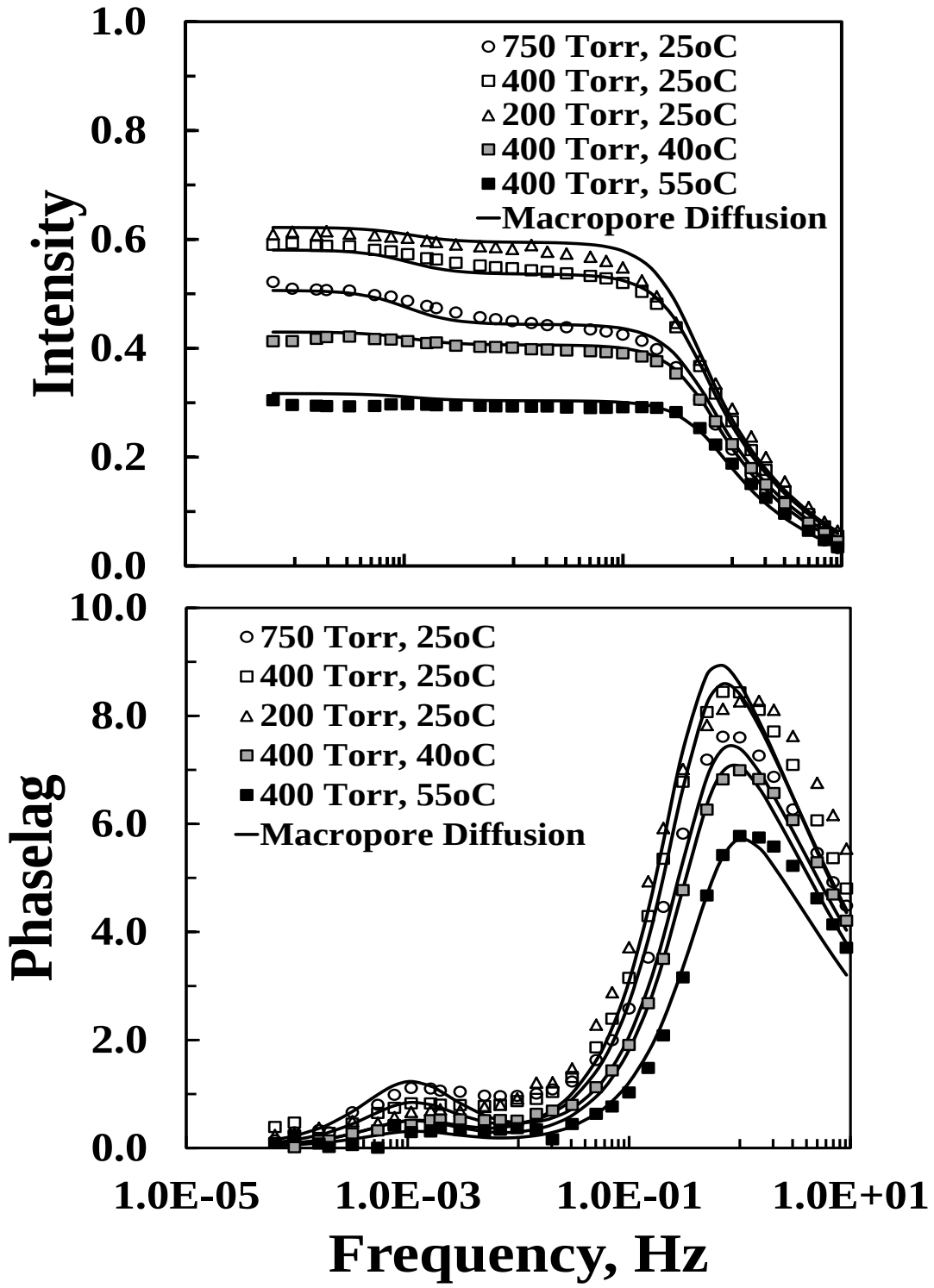

Figure 3.10 Intensity (top) and Phase lag (bottom) curves of N_2 on 13X beads at diffrerent conditions compared with nonisothermal macropore diffusion model with D_{co}/R_c^2= 0.12 1/s and hA=0.051 J/K/s.

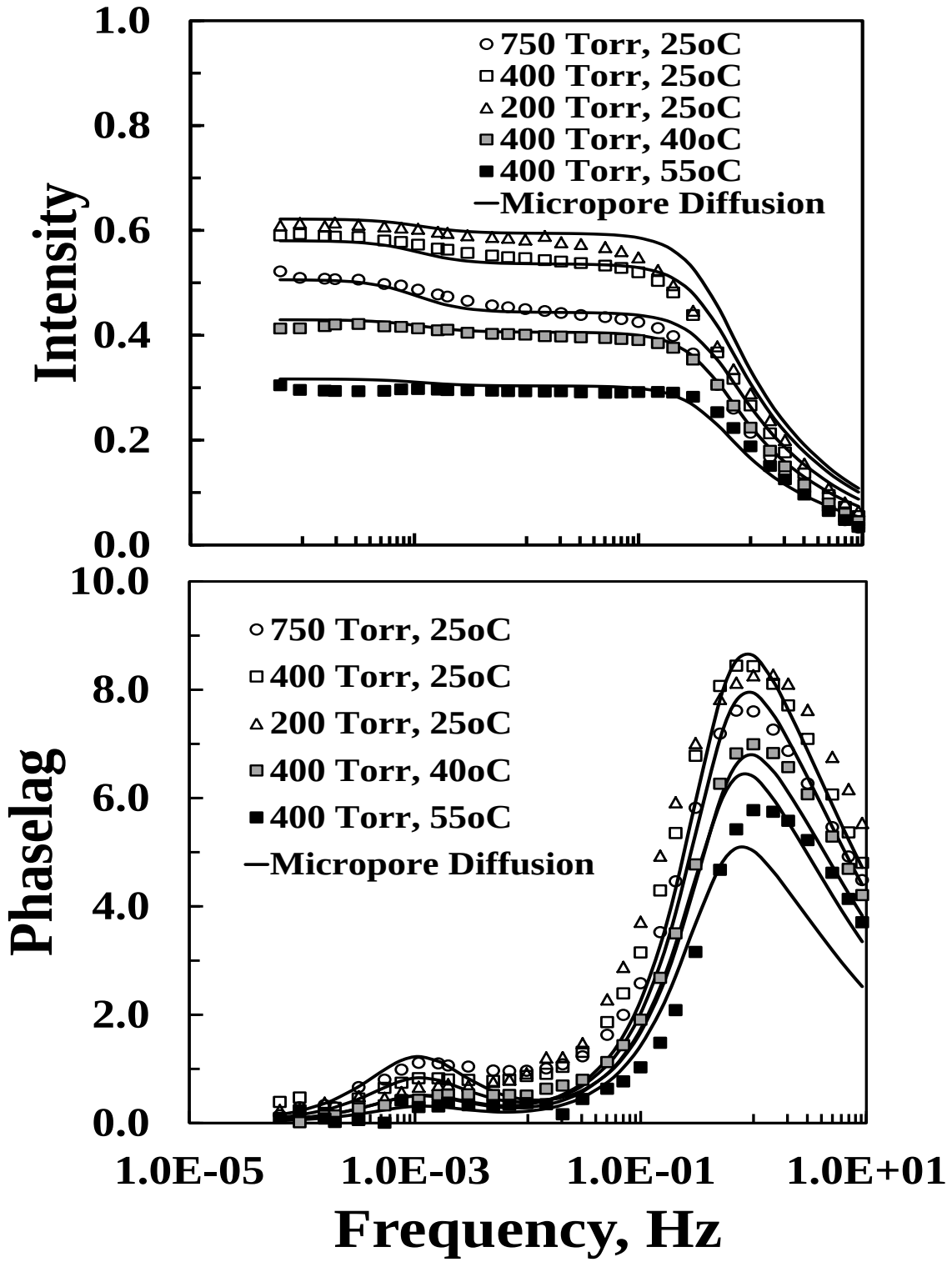

Figure 3.11 Intensity (top) and Phase lag (bottom) curves of N_2 on 13X beads at diffrerent conditions compared with nonisothermal macropore diffusion model with D_p/R_p^2= 5.1 1/s and hA=0.051 J/K/s.

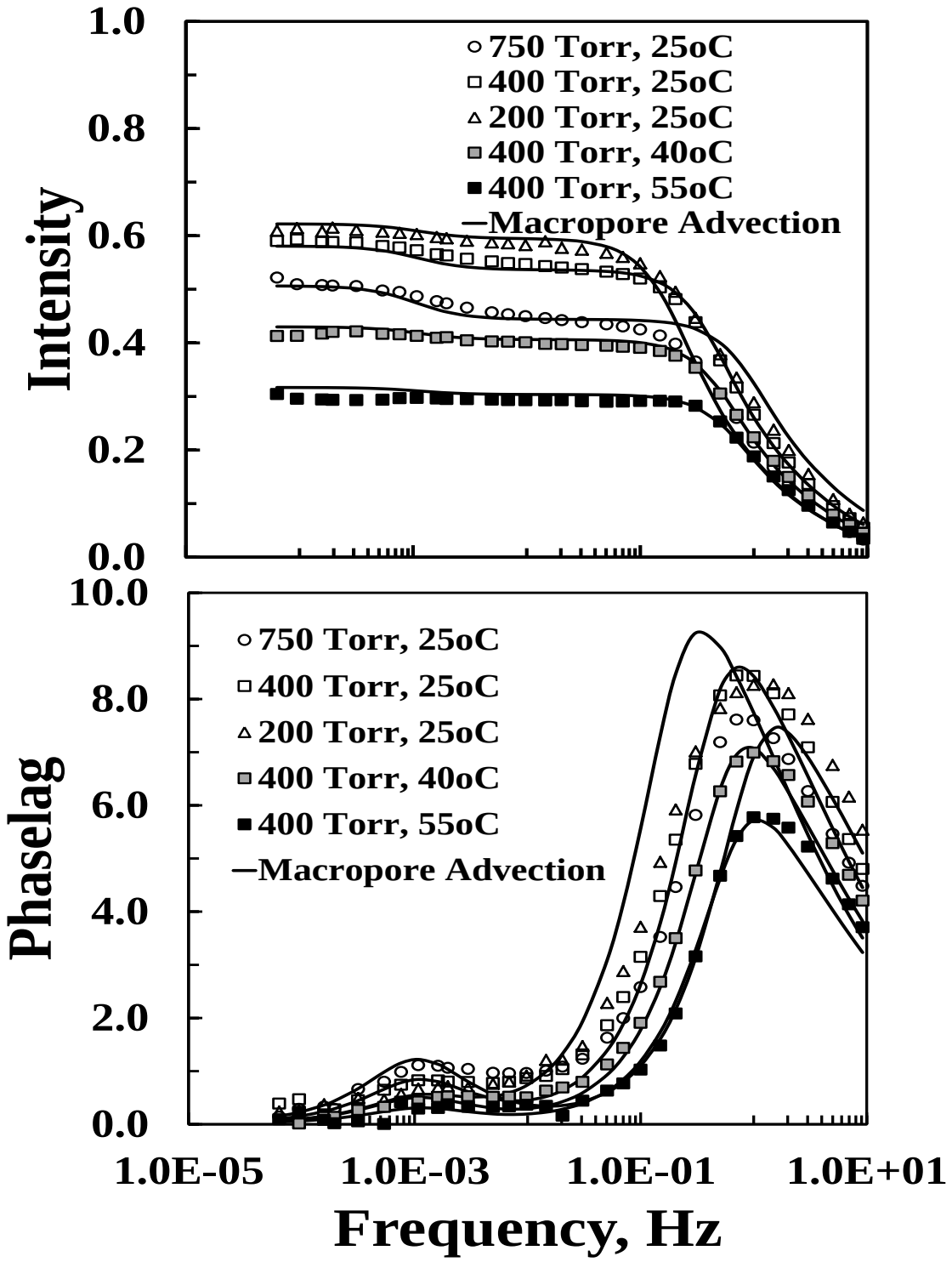

Figure 3.12 Intensity (top) and Phase lag (bottom) curves of N_2 on 13X beads at diffrerent conditions compared with nonisothermal macropore advection model with permeability κ = 1.25e-8 mm^2 and hA=0.051 J/K/s.

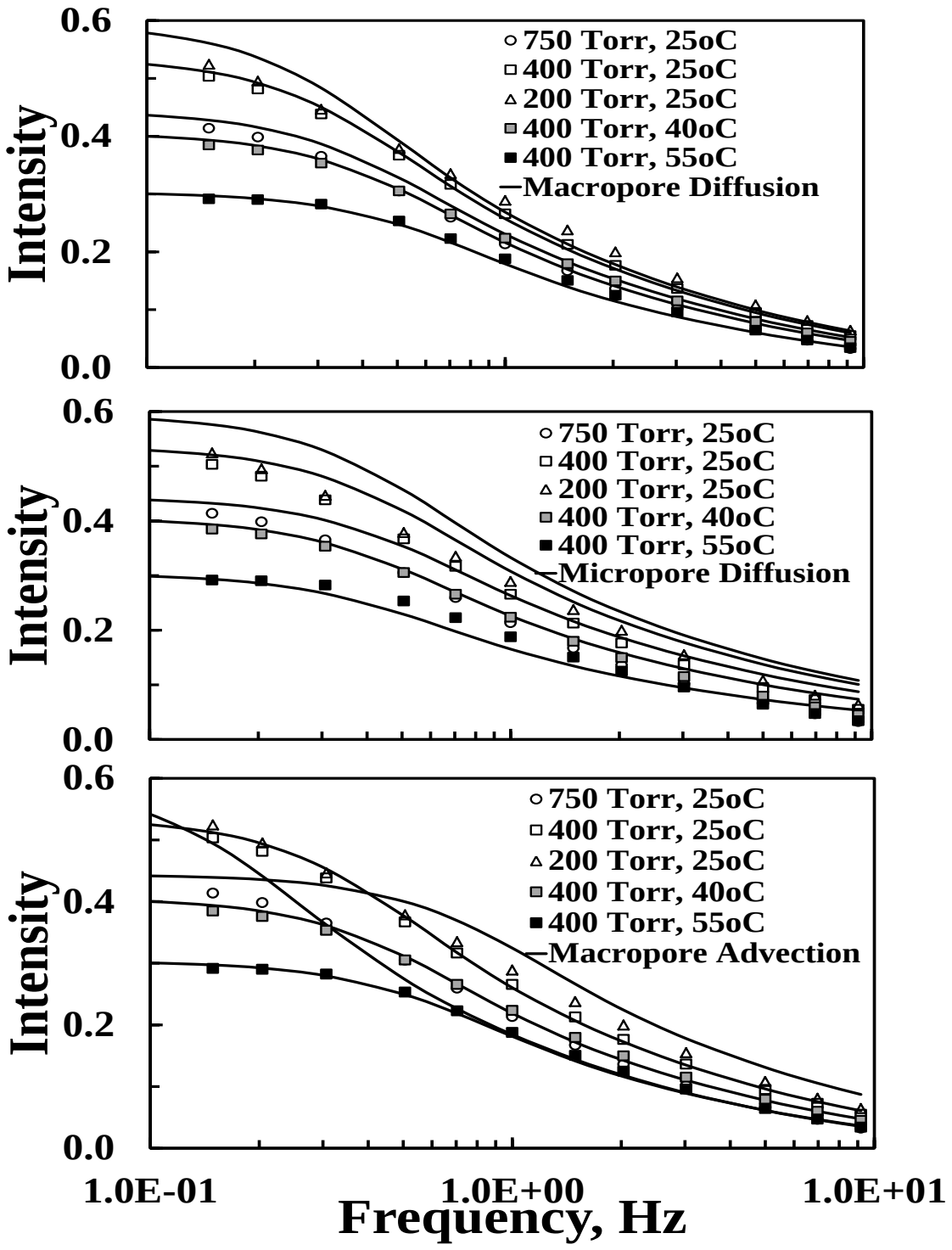

Figure 3.13 Comparison of fittings of three different mass transfer mechanisms with experimental intensity curve at five different conditions for the region where the process is dominated by its own characteristic mass transfer limitation to identify the governing mass transfer mechanism for the sorption process of N_2 in 13X. The best results observed with macropore diffusion model as compared to other two models.

CHAPTER 4

DETERMINATION OF THE MECHANISMS DOMINATING THE MASS TRANSFER PROCESSES OF O_2, N_2 AND ARGON ON A CARBON MOLECULAR SIEVE

Summary

Separation of air by PSA using porous adsorbents like zeolites or carbon molecular sieve to produce highly pure oxygen represents very important class of separation processes in industries these days. Understanding the mass transfer kinetics of gases in adsorbents is essential for designing, developing and efficient operation of PSA processes. Despite its significant applicability, very few studies have been conducted to understand the mass transfer behavior of O_2, N_2 and Ar in carbon molecular sieve adsorbents. A newly constructed volume swing frequency response system is used to study the mass transfer characteristics O_2, N_2 and Ar in Shirasagi MSC 3K 172 carbon molecular sieve materials. Experimental frequency response spectra at 750 Torr and and four different temperatures were fitted with different mass transfer models and found that the micropore diffusion with mouth resistance is the key governing mechanism for these gases in this particular CMS material. The values of corresponding mass transfer parameters are measured and the temperature dependences of the mass transfer parameters are investigated. It has been observed that O_2 exhibits much faster kinetics than N_2 and Ar in this CMS material.

4.1 Introduction

Production of highly pure oxygen from air is one of the major industrial separation processes in the chemical industry today. According to survey of industrial chemistry by Philip J. Chenier in 2004 O_2 is the third most widely used chemical in the world and it has an annual worldwide market over $9 billion that includes the demand of ultra-pure O_2 in both small scale and large scale industries. In latest few decades, separation of oxygen from air by adsorption based processes like pressure swing adsorption (PSA) has become an alternative method (Hayasi et al., 1996) instead of cryogenic distillation because of the large energy cost associated with the later. Understanding the mass transfer characteristics of major components of air like oxygen, nitrogen, argon, etc. in porous adsorbent is of fundamental interest of researchers due to its practically significance for improved design of gas separation processes. One particular adsorbent, carbon molecular sieve (CMS), exhibits substantial promise in air separation processes because of its ability to selectively discriminate on the basis of diffusion kinetics (Reid et al, 1998) and ability to separate oxygen (3.46 Å) over argon and nitrogen(3.64 Å) (Cabrera et al., 1993).

For porous adsorbent materials, the overall uptake and the performance of separation depends on the interplay of different controlling mechanisms within the particle (Rutherford and Do, 2000). The micropore and macropore diffusion processes, and the pore mouth barrier process of the micropore, could all play a significant role in the global uptake. The role they play in the dominating mechanism of global uptake varies from system to system. For most adsorbent materials the uptake is controlled by the first two mechanisms.(Ruthven, 1984) However, in small microporous adsorbent like

CMS, the mass exchange can be limited by the resistance into the micropore opening due to the large energy barrier at the pore mouth.(LaCava et al, 1989; Srinivasan et al, 1995).

Since CMS is a modified form of activated carbon along with its molecular sieving capability it has very high internal surface area which is believed to have a bidisperse pore structure along with a some kind of structural hindrance at micropore entrance. Researchers used various techniques both gravimetric and volumetric to identify the kind of controlling mechanisms in CMS. Kawazoe et al. (1974) and Chihara et al. (1978) measured the diffusion of N_2 and propylene in Takeda MSC 5A using pulse chromatographic method whereas Ruthven et al. (1986) and Chen et al. (1994) gravimetrically measured the diffusion of O_2 and N_2 in BF CMS and reported that the mass transfer is mainly govern by micropore diffusion. LaCava et al. (1989) used gravimetric and batch column adsorption methods to measure diffusion of O_2 and N_2, while Srinivasan et al. (1995) measured the diffusion of the same sorbates using the volumetric method and reported existence of non Fickian type barrier resistance in CMS. Reid et al, 1998 also found non-Fickian diffusion attributed to the pore mouth constriction and sometimes it's a combination of micropore diffusion and barrier resistance (mouth resistance) (Farooq et al., 2002, Loughlin et al., 1993). A dual Langmuir kinetic model with nonselective adsorption in mesosuper micropores followed by selective movement of adsorbed molecules into micropores through the pore mouth was proposed by Nguyen and Do (2000). Reid and Thomas (2001) observed that at different experimental and adsorptive condition with different probe molecule, CMS obeys different mechanism including a linear driving force, combined diffusion and mouth resistance and Fickian diffusion model. Therefore, previous studies on the

adsorption kinetics of CMS showed that the transport mechanism of gases like O_2, N_2 and Ar in CMS is yet to be understood unambiguously. Despite its unique ability to identify mass transfer mechanism effectively FR studies have not been conducted yet to understand the rate study of O_2, N_2 and Ar in CMS. Clearly, it is necessary to explore the strength of the FR technique to understand unambiguously the nature of governing mass transfer mechanism for this system. Moreover, despite a huge amount of study conducted relating air separation by CMS there is not enough work done on adsorption kinetics of Ar and only very few studies available in literature (Liu and Ruthven, 1996; Reid et al., 1998; Nguyen and Do, 2000) for Ar adsorption in CMS.

Frequency response (FR) methods have proven to be one of the efficient techniques and recently have been widely used to investigate kinetics behavior of gas-solid systems (Wang and LeVan, 2005, 2007, 2010; Geisy et al., , 2011; Jordi and Do, 1993) due to their ability to discriminate among different rate limiting mechanisms. In FR studies, a system initially in equilibrium is subjected to a continuous perturbation, typically in the form of a sinusoidal function, of one physical variable, i.e., pressure, volume or concentration to induce periodic response with the same frequency as the input but that differs in amplitude and displays a phase lag that uniquely reflects on the thermodynamic and kinetic characteristics of the system. The responses from a wide spectrum of frequencies could be analyzed to identify the controlling mechanism and determine the parameters associated with the kinetic processes occurring in the adsorbent.

In this work, a newly constructed and commissioned volumetric FR system at USC is used to identify the governing mass transfer mechanism for adsorption of O_2, N_2 and Ar in Shirasagi MSC 3K 172 supplied by Japan EnviroChemicals previously known

as Takeda Chemicals. A brief description of the apparatus is presented in corresponding section. The major advantage of this volumetric system over other frequency response system like flow through pressure swing or concentration swing system is its ability to measure response over a wide frequency spectra starting from 10^{-5} to near 10 Hz. This wide range is important specially for faster diffusing system like O_2 in CMS as well as slow diffusing gas like N_2 and Ar in CMS in order to characterize the dynamics of the system thoroughly and accurately. In order to verify the response feature observable only for fast diffusing gas like O_2, experiments with another faster diffusing gas i.e. CO_2 have also been conducted at similar experimental conditions.

Frequency response experiments have been conducted at 750 Torr at four different temperatures 20, 30, 40 and 50 ^{o}C for all gases. The experimental response curves are then fitted with different mass transfer model to identify the controlling mechanism of adsorption process as well as to estimate the corresponding mass transfer parameter. Investigating the response curves at different temperatures along with a wide frequency range will help to explore the strength and robustness of FR method in identifying the controlling mechanism of the rate processes associated with the adsorption process of probe gases in CMS pellet.

4.2 Theory

4.2.1 Material and Energy Balances

A schematic representation of the batch frequency response system is shown in Figure 4.1, where system volume is perturbed periodically around the equilibrium value

V_{b0}, and the system pressure P_b responds accordingly. Assuming that the entire system is at same pressure, the material balance over the entire volume is,

$$m\frac{\partial \overline{Q}}{\partial t}+\frac{\partial}{\partial t}\left(\frac{P_b V_b}{RT}\right)=0 \tag{4.1}$$

$$V_b = V_{b,o} + \Delta V \sin(2\pi f t) \tag{4.2}$$

$$\overline{Q} = \bar{\bar{q}} + \left(\varepsilon_p / \rho_p\right)\overline{C}_p \tag{4.3}$$

Energy balance is applied over the volume containing the adsorbent, assuming Temperature. T is only function of time; not of bed length or pellet radius

$$\frac{m}{\rho_p}\left[\frac{\varepsilon_b}{(1-\varepsilon_b)}+\varepsilon_p\right]\left[Cp_g\frac{P_b}{RT}\frac{\partial T}{\partial t}-\frac{\partial P_b}{\partial t}\right]+m\bar{q}Cp_a\frac{\partial T}{\partial t}$$
$$+mCp_s\frac{\partial T}{\partial t}+(-\Delta H_a)\frac{\partial \bar{\bar{q}}}{\partial t}=hA\left(T_{wall}-T\right) \tag{4.4}$$

The quantities $\bar{\bar{q}}$ and $\overline{C}_p$ are the volume average loading and gas phase concentration respectively over the pellet volume and defined as,

$$\bar{\bar{q}} \equiv \frac{3}{R_p^2}\int_0^{R_p}\bar{q}r_p^2 dr_p \tag{4.5}$$

$$\overline{C}_p \equiv \frac{3}{R_p^2}\int_0^{R_p} C_p r_p^2 dr_p \tag{4.6}$$

Where C_p is the gas phase concentration in side pore and $\bar{q}$ is the volume average loading over crystal and expressed as,

$$\bar{q} \equiv \frac{3}{R_c^2}\int_0^{R_c}\bar{q}r_c^2 dr_c \tag{4.7}$$

Depending on the kind of controlling mechanism $\bar{\bar{q}}$ and $\bar{q}$ can be correlated with the equilibrium loading in different manner which is explained in corresponding model description.

4.2.2 Macropore model

The macropore model used in this work only considered macropore gas diffusion as mass transfer mechanisms. The macropore mass balance equation is expressed in spherical coordinate in terms of dimensionless pellet radius with appropriate boundary and initial conditions,

$$\frac{\varepsilon_p}{RT}\frac{\partial P}{\partial t} - \frac{\varepsilon_p P}{RT^2}\frac{\partial T}{\partial t} + \rho_p \frac{\partial \bar{q}}{\partial t} = \frac{\varepsilon_p}{\xi_p^2}\frac{\partial}{\partial \xi_p}\left[\frac{\xi_p^2}{RT}\left(\frac{D_p}{R_p^2}\right)\right] \tag{4.8}$$

Where, $\xi_{\mathrm{p}} = \dfrac{r_p}{R_p}$

$$\frac{\partial P}{\partial \xi_{\mathrm{p}}} = 0 \qquad \text{at} \qquad \xi_{\mathrm{p}} = 0 \tag{4.9}$$

$$P = P_b \qquad \text{at} \qquad \xi_{\mathrm{p}} = 1 \tag{4.10}$$

$$P = P_{b,0} \text{ and } \mathrm{T} = \mathrm{T}_0 \qquad \text{at} \qquad t = 0 \tag{4.11}$$

For macropore controlled models there is no resistance in micropore/ crystal hence, the quantity $\bar{q}$ is in equilibrium with local gas phase concentration in macropore and estimated as,

$$\bar{q}(r_p) = q^*\left(P(r_p), T\right) \tag{4.12}$$

4.2.3 Micropore diffusion model

In micropore diffusion model the loading dependency of micropore diffusion is expressed by Darken correction factor for diffusivity and the mass balance is written in terms of dimensionless microporous crystal radius. If there is a mouth resistance present in micropore crystal the only difference will be in the boundary conditions.

$$\frac{\partial q}{\partial t} = \frac{1}{\xi_c^2}\frac{\partial}{\partial \xi_c}\left(\xi_c^2 \frac{D_c}{R_c^2}\right)\frac{\partial q}{\partial \xi_c} \tag{4.13}$$

Where, $\xi_c = \frac{r_c}{R_c}$

$$\frac{\partial q}{\partial \xi_c} = 0 \qquad \text{at} \qquad \xi_c = 0 \tag{4.14}$$

$$q = q^*(\mathrm{P},\mathrm{T}) \qquad \text{at} \qquad \xi_c = 1 \tag{4.15}$$

$$q = q_0^* \qquad \text{at} \qquad t = 0 \tag{4.16}$$

If mouth resistance is present at the crystal entrance, the boundary condition is given as-

$$-3\frac{D_c}{R_c^2}\frac{\partial q}{\partial \xi_c} = k_m(q^* - q|_{\xi_c=1}) \quad \text{at} \qquad \xi_c = 1 \tag{4.17}$$

with,

$$\frac{D_c}{R_c^2} = \frac{D_{co}}{R_c^2}\frac{1}{1-\left(\frac{q}{q_s}\right)^n} \tag{4.18}$$

4.2.4 Bimodal distributed micoporous crystal with or without mouth resistance

For various reasons there is possibility to have secondary crystal formation (cracks, etc) inside the pellet, which may introduce additional feature and may influence the mass transfer mechanism in the pellet. The existence of two transfer processes which occur independently can result in a bimodal form of frequency response curves. This can also be the result of a well-defined bimodal distribution of crystal sizes. In order to capture such effects a distributed micropors model has been developed where adsorption and diffusion through two different types of crystals are assumed to be occurred in parallel. The mass transfer in each crystal is governed by similar expression like the micropore diffusion model from equation 3.25 through 2.30 with diffusion parameters for each crystal as D_{c1}/R_{c1}^2 and D_{c2}/R_{c2}^2. The overall adsorption capacity is distributed between the two crystals.

4.2.5 LDF model

LDF model is a simplification of diffusion limited mass transfer to enhance the computational efficiency assuming that the average uptake rate is proportional to the driving force for adsorption and represented by-

$$\frac{\partial \bar{q}}{\partial t} = k_{LDF}(q^* - \bar{q}) \tag{4.19}$$

4.3 Experimental

The FR experiments have been conducted using the newly developed volume swing frequency response apparatus in university of South Carolina. The schematic of the automated batch volume swing FR system is shown in Figure 4.1. The system, which

uses total volume as input and pressure as output, has been constructed to operate at frequencies between 5×10-5 and 10 Hz, temperatures up to 80 oC, and vacuum pressures down to 0.2 atm. The system comprises of three different volume zones: a) the working volume in dark gray b) the reference volume in light gray, and c) the external volume in white connecting the system with the vacuum or gas feeds. The working volume includes a sample container to analyze between 10 and 100 g of sample and a metal bellows that contracts and expands via a shaft for volume modulation. During a run the sample container is immersed in a temperature controlled water jacketed bath that is connected to a chiller. During sample activation, the bath is removed and the container is heated via aluminum concentric sleeves and rigid electric band heaters. A closed sheath thermocouple is immersed in the sample for temperature determination. The shaft connected to the metal bellows is driven via an eccentric sheave for the working volume to vary sinusoidally. The position of the bellows is determined by a linear variable differential transformer (LVDT) along with a linear encoder and an angular encoder (US digital), which measures the input volume perturbation. A pressure transducer (MKS instruments Inc, USA). The Reference volume includes a two-liter ballast that is immersed within the bath of the chiller for temperature, and thus pressure, stabilization. The equilibrium pressure and the changes of pressure are respectively followed by an MKS pressure transducer located at the reference volume and a differential pressure transducer (Omegadyne, Inc) located between the reference and working volumes. Connectivity between the different zones is controlled via solenoid valves V1 through V4. Data acquisition from the LDVT, pressures transducers and thermocouple is accomplished via a LabVIEW program running on a Dell PC-AT 320. Microsoft excel

program is used to determine actual frequency, phase lags, amplitude of input and output variables, and characteristic response functions from pressure-volume experimental data.

In this work, volumetric frequency response experiments have been conducted over a wide range of frequencies starting from 7×10^{-5} Hz to 9.25 Hz for Shirasagi MSC 3K 172 beads from Japan EnviroChemicals with O_2 (UHP), N_2 (UHP300) and Ar (UHP300). Frequency response experiments have been performed at 750 Torr at four different temperatures, 20, 30, 40 and 50 oC for all gases. For this study, a system consisted of a 120 cc sample holder containing 75.6g of CMS beads had been used in volumetric frequency response apparatus.

Prior to the experiments, sample activation was conducted. For activation the system is evacuated by keeping valves V1, V2 and V4 open while valve V3 remains closed (Figure4.1). Aluminum sleeves and electric band heaters were used eventually reached at desired temperature which is 120^{o}C for CMS. The activation had been carried for 40 hours or until the pressure at the vacuum pump (adixen DRYTEL, 1025) is less than 1.5×10^{-5} Torr (Granville-Phillip 350 Ionization Gauge), which suggests satisfactory sample regeneration. Then, the system was let cool, the heaters and sleeves are removed and the container was fully immersed in the water jacketed bath which was set at desired temperature (20, 30, 40 or 50 oC for this study). Valve V4 is then closed and then the working gas is allowed in via valve V3 to pressurize the system to the target pressure. A needle valve is used (not shown) to control the flow of the working gas into the system. Once at a relatively stable target pressure, the shaft is moved to position where the bellows is at the mid-point. Valve V2 is then closed and the system is let equilibrate for 24-48 hours. Once at equilibrium, valve V1 connecting the reference and working

volumes is closed, the differential pressure ΔP between the two is at zero and the system is ready for a sample run.

Once the system is ready to start at equilibrium, the sample to subjected to volume modulation at a predefined set of frequencies between 7.0×10^{-5} and 9.25 Hz. Ten cycles are typically run at each particular frequency, before switching to the next. At the end of the run, the collected values of the shaft displacement and the differential pressure from the LDVT and the differential pressure transducer, respectively, are analyzed and fitted at the periodic behavior using the following functions:

$$\delta = \delta_o + \Delta\delta \sin(2\pi ft + \varphi_\delta) \tag{4.20}$$

$$P_d = P_{d,o} + \Delta P_d \sin(2\pi ft + \varphi_P) \tag{4.21}$$

where, f is the frequency, t is the time, δ and Pd are the shaft displacement and the differential pressure, respectively; δ_o and $P_{d,o}$ are the corresponding offsets, which at the periodic behavior are different from the zero value; φ_δ and φ_P, are the corresponding phase lags; and Δδ and ΔP_d are the corresponding amplitudes.

For each frequency the system can provide a response in the form of two variables. One of them is the phase lag response which is given by

$$\varphi = \varphi_P - \varphi_\delta \tag{4.22}$$

and the intensity response, which is conveniently expressed as:

$$I = \left(\frac{\Delta V}{V_{EXT}} \cdot \frac{P_o}{\Delta P_d} - 1 \right) \tag{4.23}$$

Where, Po is the absolute pressure at equilibrium, ΔV is the amplitude of the change of the working volume and V_{EXT} is the volume within the working volume external to the volume of the materials in the container (adsorbent, glass bead, etc). This ensures that **I** to approach zero at highest frequencies. The details of the activation procedure, experiment and method of analysis of experimental data to determine intensity and phase lag are described in details in chapter 2.

4.4 Results and Discussions

The empty volume and the maximum volume displacement have been determined using the procedure explained earlier elsewhere and values are shown in Table 4.1 along with other system properties used in this study. The experimental frequency response curves for all three gases in CMS at four different temperatures of 20oC, 30oC, 40oC and 50oC respectively are shown in figure 4.2. The primary Y axis represents the FR function and the secondary Y axis represents the phase lag of response curves. From the experimental response curve it has been observed that O_2 showing faster kinetics in CMS compared to N_2 and Ar indicated by the fact that the predominant change in the intensity curves and loci of the maxima in phase lag curves occurs at higher frequencies for O_2 than that of other two gases. This is very significant and promising from the view point of kinetic separation of O_2 from air using CMS as an adsorbent.

Figure 4.3 shows the experimental response spectra in terms of intensity function and phase lag for O_2 on the CMS beads at four temperatures at 750 Torr. Careful observation of each FR curve showed the existence of three distinct zones, A, B and C at

almost every temperature; though not much clear in the phase lag curves. Each zone has its own significance associated with the kinetics nature of the adsorption process.

Region A is identified by the initial plateau observed only at sufficiently slower frequencies. The time of cycling the pressure is sufficiently slow compared to the time constant of the diffusion process and mainly governed by the equilibrium. Thus the plateau actually indicates that the adsorbent is under isothermal local equilibrium conditions. This region is where the slope of the isotherm can be determined for that particular temperature and at that pressure.

Region B is represented by an intermediate plateau that reveals the existence of either an internal mass transfer resistance or a heat transfer limited local equilibrium process. For N_2 or Ar this intermediate characteristics feature is not significantly visible. Though all these three gases characterized by similar kind of isotherm associated with moderate heat of adsorption, but as observed from the experimental response curves and mentioned earlier O_2 has the fastest mass transfer dynamics among these gases in CMS. It is important to note that temperature oscillations in this region (not shown) are not necessarily significant for the effect to be observed (~ 0.1 oC). That zone is significantly visible for CO_2 response curves as shown in Figure 4.4 as CO_2 has a fast dynamics as well as high heat of adsorption.

Region C is where the process is dominated by its own characteristic mass transfer limitation. Frequencies at this point are so fast that the sample no longer experiences heat effects and thus remains isothermal. This distinguishable feature helps to identify the governing mass transfer mechanism. For N_2 and Ar this feature occurred at

comparatively slower frequencies indicating that the mass transfer kinetics of N_2 and Ar in CMS is slower compared to oxygen.

Figure 4.5 shows the theoretical model predictions using different model to fit the experimental response curve (black circle) for O_2 in CMS at 20 ^oC. Simple macropore diffusion model (black line) micropore diffusion model (black dot), LDF model (line with diamond), bimodal micropore model without mouth resistance (line with triangle) and with mouth resistance (broken line) and nonisothermal micropore with mouth resistance (line with black square) are used to predict the experimental response. The bimodal micropore model with mouth resistance showed a very good agreement to predict the response curve over the frequency spectrum. However, the fit with the nonisothermal micropore with mouth resistance also show somewhat better agreement, though not able to capture the feature at zone B perfectly. This might be due to the limitation of the energy balance model. As described earlier the energy balance over the adsorbent bed is simplified and represented by a point balance without considering the thermal conduction along radial or axial direction and the overall heat transfer process is represented by a single heat transfer coefficient from the solid to the surroundings which might not be adequate the complex thermal processes of the system. In Figure 4.6a and 4.6b the comparison between the experimental response curves and that predicted by both the bimodal micropore model with mouth resistance and nonisothermal micropore with mouth resistance are shown for all four temperatures for oxygen in CMS. At this point it is not fully clear that which of these two mechanism governing the transport kinetics of O_2 in CMS. The extracted parameters related to both models are tabulated in table 4.2 and 4.3 respectively. The parameters extracted are quite consistence.

Figure 4.7 and 4.9 show the theoretical model predictions using different model to fit the experimental response curve (black circle) for nitrogen and argon respectively in CMS at 20 ^{o}C. Simple macropore diffusion model (black line) micropore diffusion model (black dot), LDF model (line with diamond), micropore model with mouth resistance (broken line) and nonisothermal micropore with mouth resistance (line with black square) are used to predict the experimental response. It is noteworthy that the presence of secondary kinetics as visible for faster diffusing gases like O_2 and CO_2 is not observed in cases of these two gases. Both N_2 and Ar exhibit slower kinetics hence the heat transfer barrier was not significant for these two gases and predictions from both isothermal and nonisothermal micropore with mouth resistance models are almost identical for all four temperatures or the site with higher resistance as accessible in case of O_2 might not be accessible for comparatively larger molecules of N_2 and Ar. Figure 4.8a, 4.8b and 4.10a, 4.10b show the comparison between the experimental response curves and that predicted by both the isothermal and nonisothermal micropore models with mouth resistance for all four temperatures for N_2 and Ar respectively. The extracted parameters for N_2 and Ar are tabulated in table 4.4 and 4.5 respectively.

The presence of mouth resistance or barrier in entrance of micropore in CMS is also reported in several literatures as mentioned earlier. Karger and Ruthven (1992) explained the formation of pore barrier in micro porous carbonaceous material like CMS. CMS is a material which has controlled distribution of pore size and is designed to contain primarily narrow micropores on the order of molecular dimensions. The micropores are contained within a grain structure consisting of crystalline and amorphous carbon. These grains in CMS are treated via carbon deposition to produce a barrier for

mass transfer. The carbon deposited by this process is assumed to be located at the mouth of the micropores in the grains and hence form bottle neck shape micropores which have neck restrictions at the pore mouth. This pore mouth barrier, which is sized less than the micropore width, is believed to be responsible for the 'molecular sieving' or size selective nature of adsorption in CMS (Karger and Ruthven, 1992). Several other studies have also shown that the pore mouth formed by deposited carbon in CMS may create a barrier to penetration which generates a resistance in series with the micropore diffusion process through the micropore grains (LaCava et al., 1989; Loughlin et al., 1993).

Figure 4.11 shows the temperature dependence of mass transfer parameters for oxygen in CMS for the bimodal distributed micropore model with mouth resistance and nonisothermal micropore with mouth resistance model. The mass transfer coefficient is calculated using classical Gluekauf's LDF correlation, 15 D_c/R^2. It shows the activated transport processes in CMS. It is known in literature that the temperature dependence of the micropore diffusion process follows an Eyring equation represented as,

$$k = \mathrm{k}_0 e^{-E_a / RT} \tag{4.24}$$

Where, E_a is the activation energy. Using the data presented in Table 4.2, Activation energy for all transport parameter are calculated and they are 25.64 kJ/mol, 37.67 kJ/mol and 7.67 kJ/mol for k1(mass transfer coefficient for crystal1), k2 (mass transfer coefficient for crystal2) and km respectively. And for nonisothermal model, they are 23.78 kJ/mol for k(mass transfer coefficient for microporos crystal) and 10.27 kJ/mol for km., Figure 4.12 and 4.13 show similar kind of plots for N_2 and Ar respectively.

4.5 Conclusions

The newly constructed and commissioned volumetric FR system at USC has been used for study the mass transfer characteristics of commercially important gases like O_2 N_2 and Ar in CMS adsorbent. The FR apparatus has the ability to characterize more thoroughly over wide frequency spectra which is suitable for both slow and fast moving gas-adsorbent systems. Moreover, representing the FR data in terms of a function of amplitude ratio and phase lag not only simplify the treatment of data but also enhance the understanding of multiple simultaneous dynamic processes. The sorption kinetics of pure O_2, N_2 and Ar in CMS beads were mainly controlled by micropore diffusion with mouth resistance. However, there are certain issues that have not been clearly investigate and understand in this work specially for faster diffusing gas O_2 a secondary kinetics have been observed which could be explained by both an internal mass transfer resistance associated with presence of a slower diffusing crystal site and heat transfer limited local equilibrium process. That clearly, shows that more investigation along with further refinements of the models specially the heat transfer model for the interpretation of the volumetric system more adequately is needed to better characterize such faster transport mechanism like O_2 in CMS system. Despite of few disagreements between the model and experiment, it has been showed that barrier resistance or mouth resistance in micropore entrance is mainly controlling the mass transfer of above mentioned gases in CMS which is also consistent with previous studies over CMS adsorbent.

4.6 Tables

Table 4.1 Properties of the system used in frequencies response study

Parameter	Value	Unit
Empty volume(V_E)	210.79	cm^3
Stroke Half Volume (ΔV)	1.10	cm^3
Mass of CMS	75.6	min^{-1}
Skelital density (ρ_s)	1.89	g/cm^3
Pellet Density (ρ_p)	0.90	g/ cm^3
Heat Capacity	1.30	kJ/kg/K
Heat Capacity of Gas Phase	0.0295	kJ/mol/K

Table 4.2 Extracted parameters for bimodal micropore with mouth resistance models for O_2

Temperature (oC)	**Mass fraction of crystal 1**	**D_{c1}/R_{c1}^2 (1/s)**	**D_{c2}/R_{c2}^2 (1/s)**	**k_m (1/s)**
20	0.751	0.025	0.0006	0.132
30		0.039	0.0009	0.141
40		0.052	0.0015	0.158
59		0.067	0.0025	0.176

Table 4.3 Extracted parameters for nonisothermal micropore with mouth resistance models for O_2

Temperature (oC)	**Heat transfer parameter hA (kJ/K/s)**	**D_c/R_c^2 (1/s)**	**k_m (1/s)**
20	0.0042	0.016	0.118
30		0.022	0.143
40		0.031	0.158
59		0.039	0.176

Table 4.4 Extracted parameters for micropore with mouth resistance models for N_2

Temperature (oC)	**D_c/R_c^2 (1/s)**	**k_m (1/s)**
20	0.00049	0.0033
30	0.00061	0.0045
40	0.00096	0.0060
59	0.00130	0.0070

Table 4.5 Extracted parameters for micropore with mouth resistance models for Ar

Temperature (oC)	**D_c/R_c^2 (1/s)**	**k_m (1/s)**
20	0.00027	0.0022
30	0.00050	0.0026
40	0.00094	0.0030
59	0.00120	0.0043

4.7 Figures

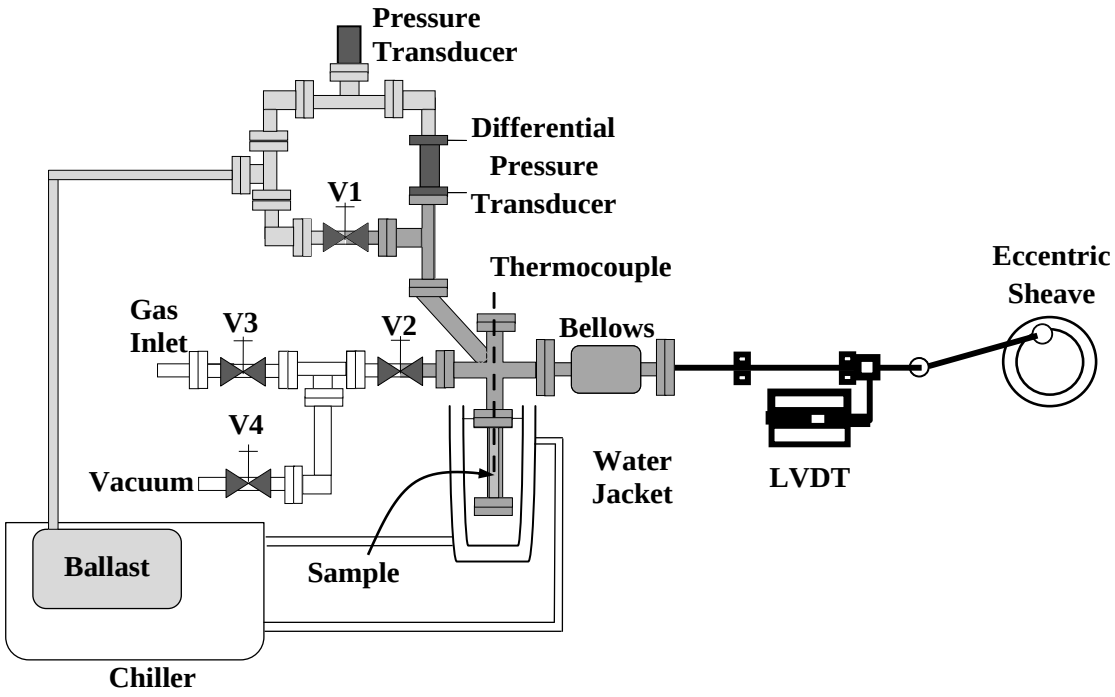

Figure 4.1 Schematic of Volumetric Frequency Response instrument used to identify the mass transfer mechanisms in CMS material.

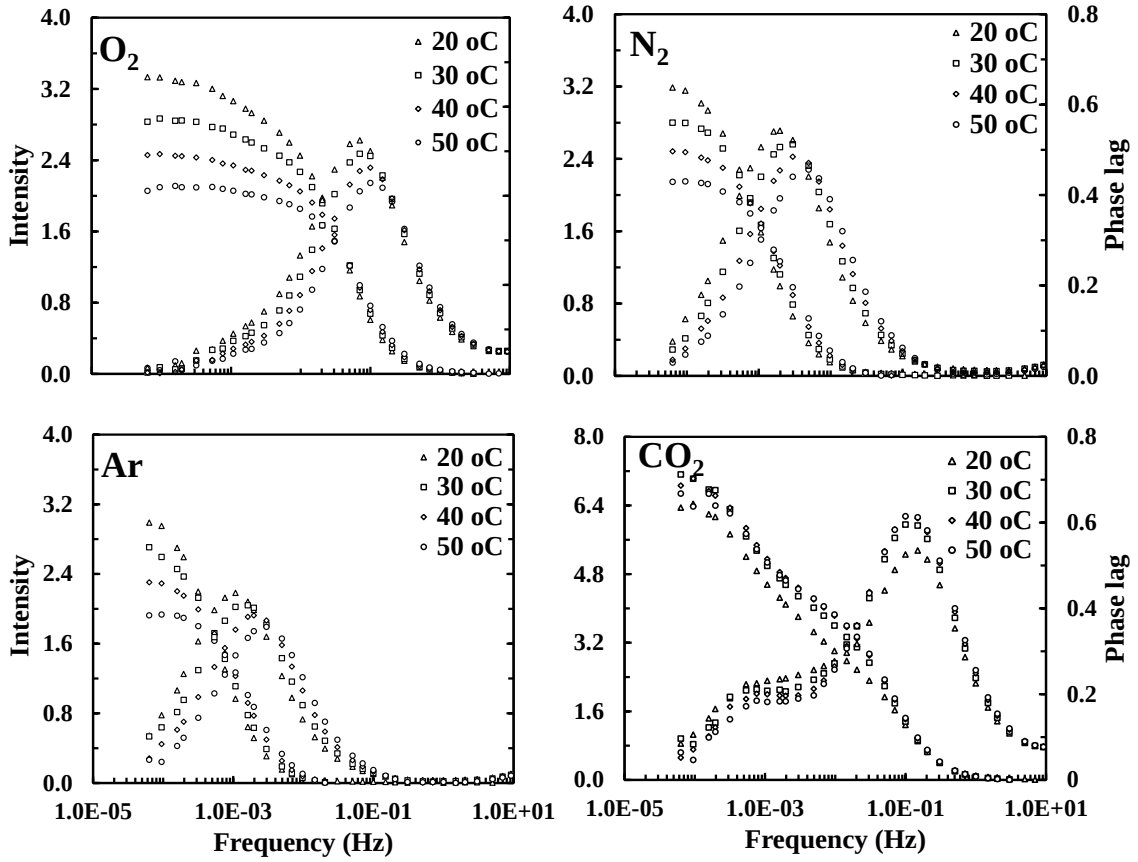

Figure 4.2 Experimental Intensity and Phase lag functions of O_2, N_2, Ar and CO_2 on Shirasagi CMS 3K 172 at four different temperatures (20, 30, 40 and 50 ^{o}C) at 750 Torr.

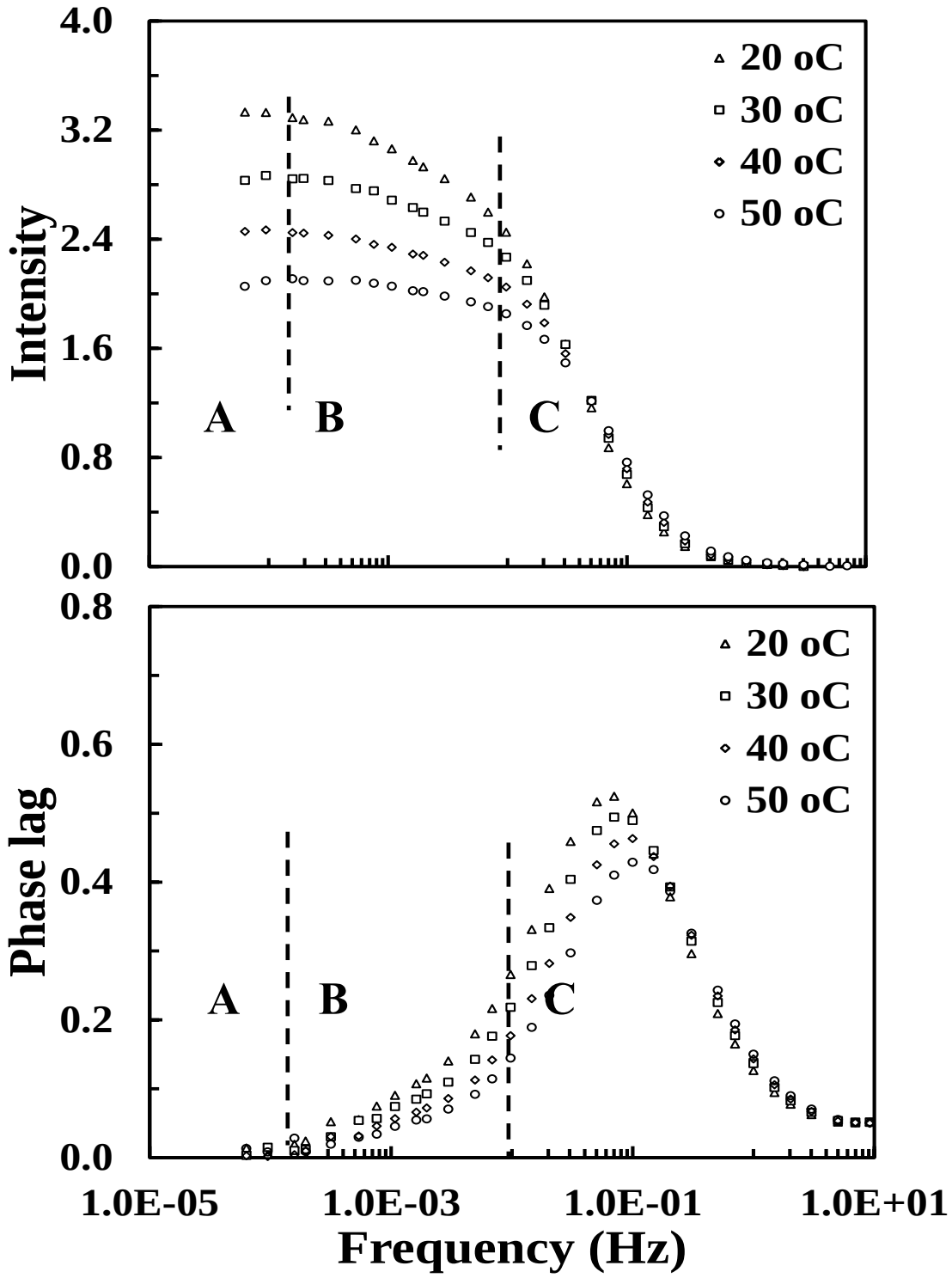

Figure 4.3 Experimental Intensity and Phase lag functions of O_2 on Shirasagi CMS 3K 172 at four different temperatures (20, 30, 40 and 50 ^{o}C) at 750 Torr. showing three distinct zones, A, B and C, each depicting the kinetic nature of the adsorption process.

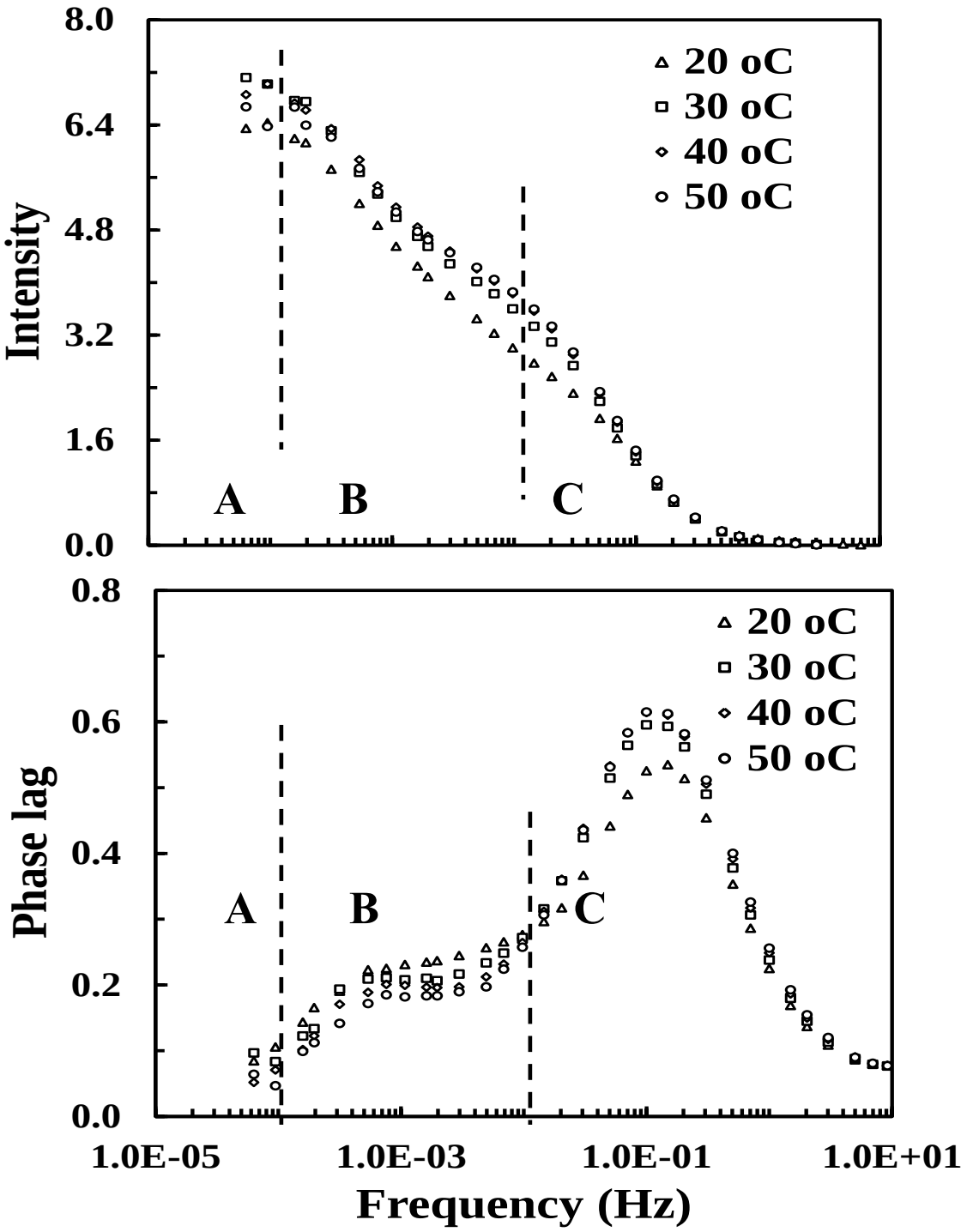

Figure 4.4 Experimental Intensity and Phase lag functions of CO_2 on Shirasagi CMS 3K 172 at four different temperatures (20, 30, 40 and 50 ^{o}C) at 750 Torr. showing three distinct zones, A, B and C, each depicting the kinetic nature of the adsorption process.

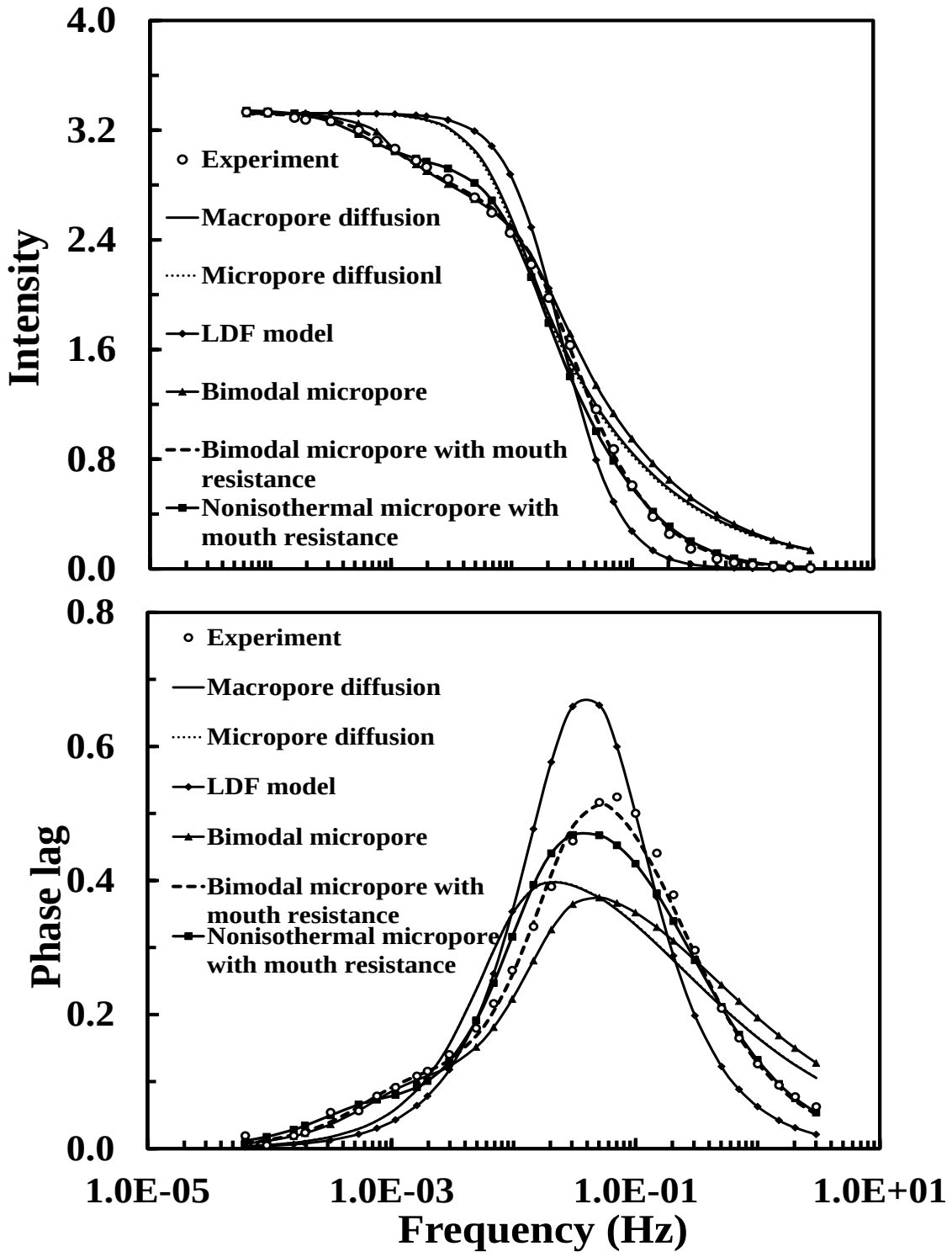

Figure 4.5 Experimental Intensity (top) and Phase lag (bottom) curves of O_2 on Shirasagi CMS 3K 172 at 20 ^{o}C fitted with different mass transfer model to identify the governing mechanism of mass transfer.

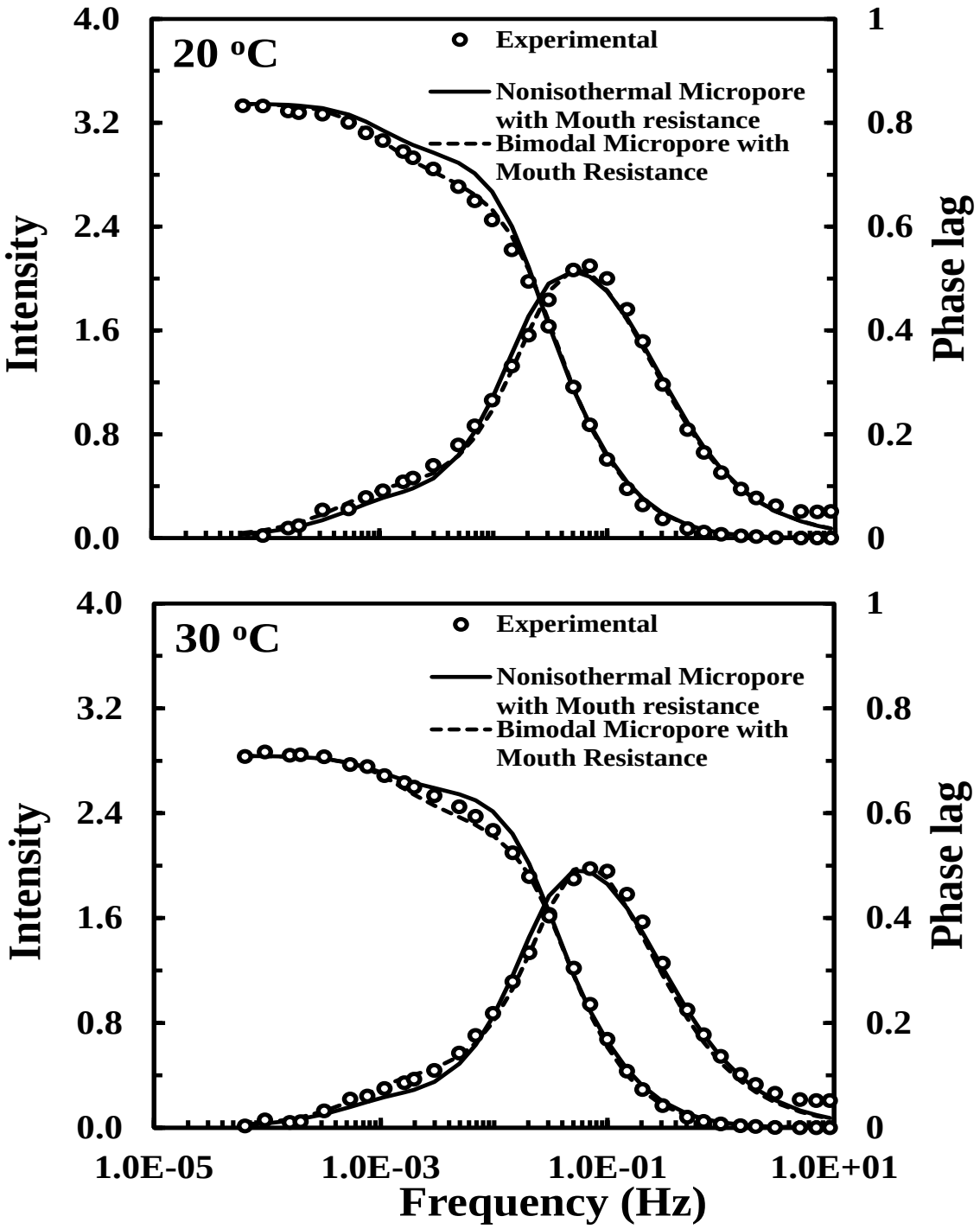
20 °C
Experimental
Nonisothermal Micropore with Mouth resistance
Bimodal Micropore with Mouth Resistance
30 °C
Experimental
Nonisothermal Micropore with Mouth resistance
Bimodal Micropore with Mouth Resistance
Intensity
Phase lag
4.0
3.2
2.4
1.6
0.8
0.0
1
0.8
0.6
0.4
0.2
0
1.0E-05
1.0E-03
1.0E-01
1.0E+01
Frequency (Hz)

(a)

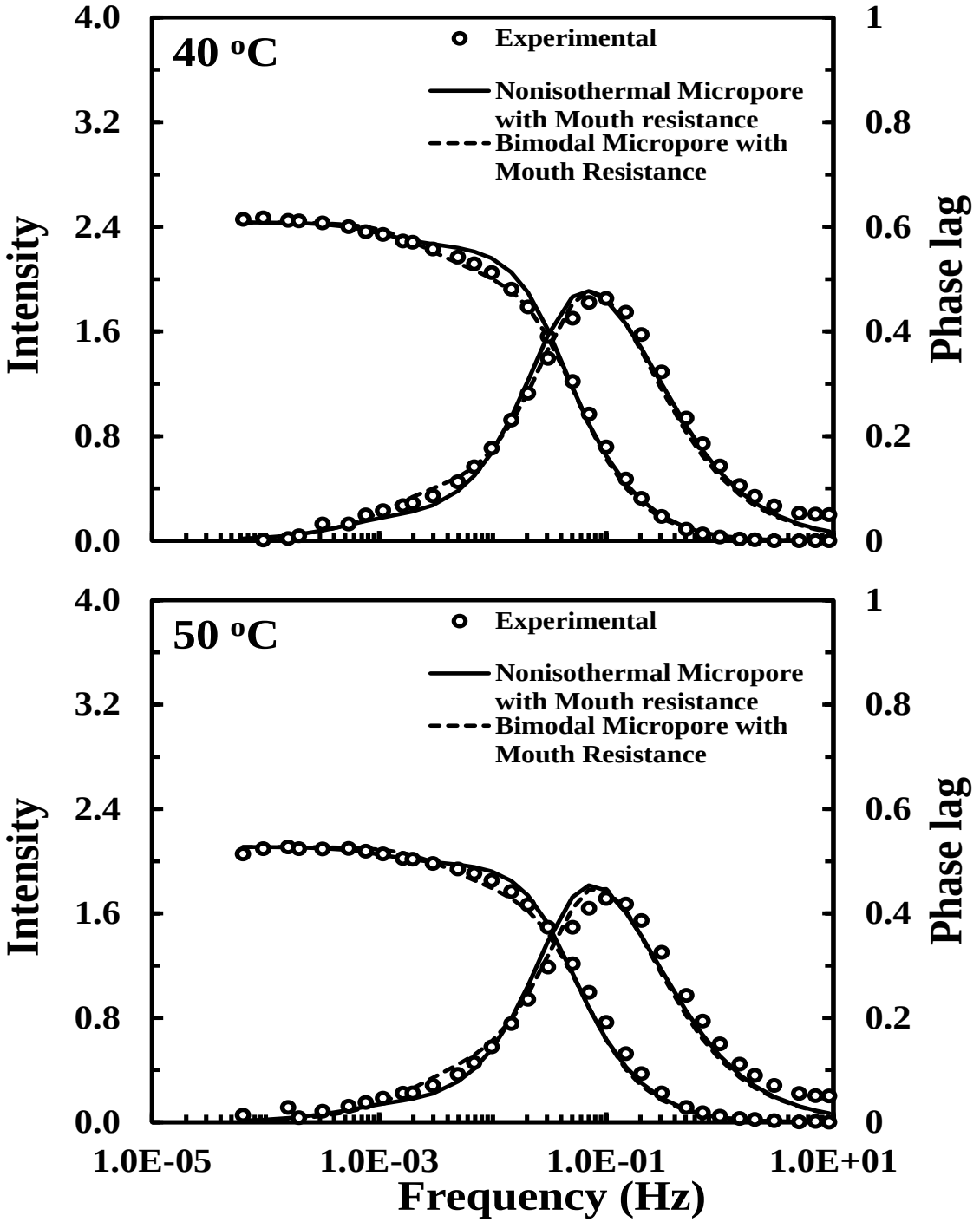

(b)

Figure 4.6 Intensity and Phase lag curves of O_2 on Shirasagi CMS 3K 172 at 750 torr at (a) 20 ^{o}C, 30 ^{o}C and (b)40 ^{o}C, 50^{o}C temperatures compared with bimodal micropore diffusion with mouth resistance model and nonisothermal micropore with mouth resistance model. The loci of the maxima for the experimental phase lag that from the model exhibit fairly good agreement.

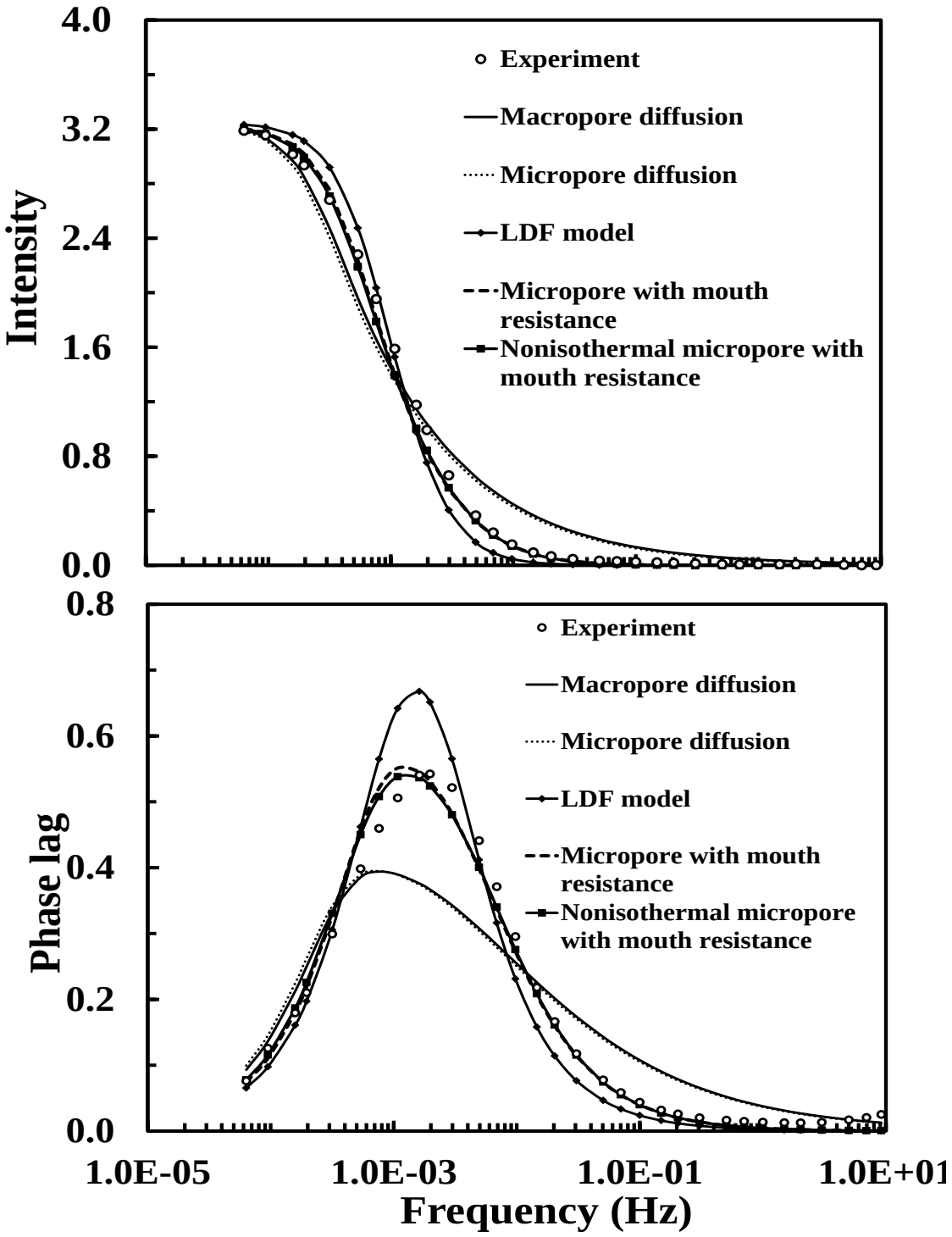

Figure 4.7 Experimental Intensity (top) and Phase lag (bottom) curves of N_2 on Shirasagi CMS 3K 172 at 20 ^{o}C fitted with different mass transfer model to identify the governing mechanism of mass transfer.

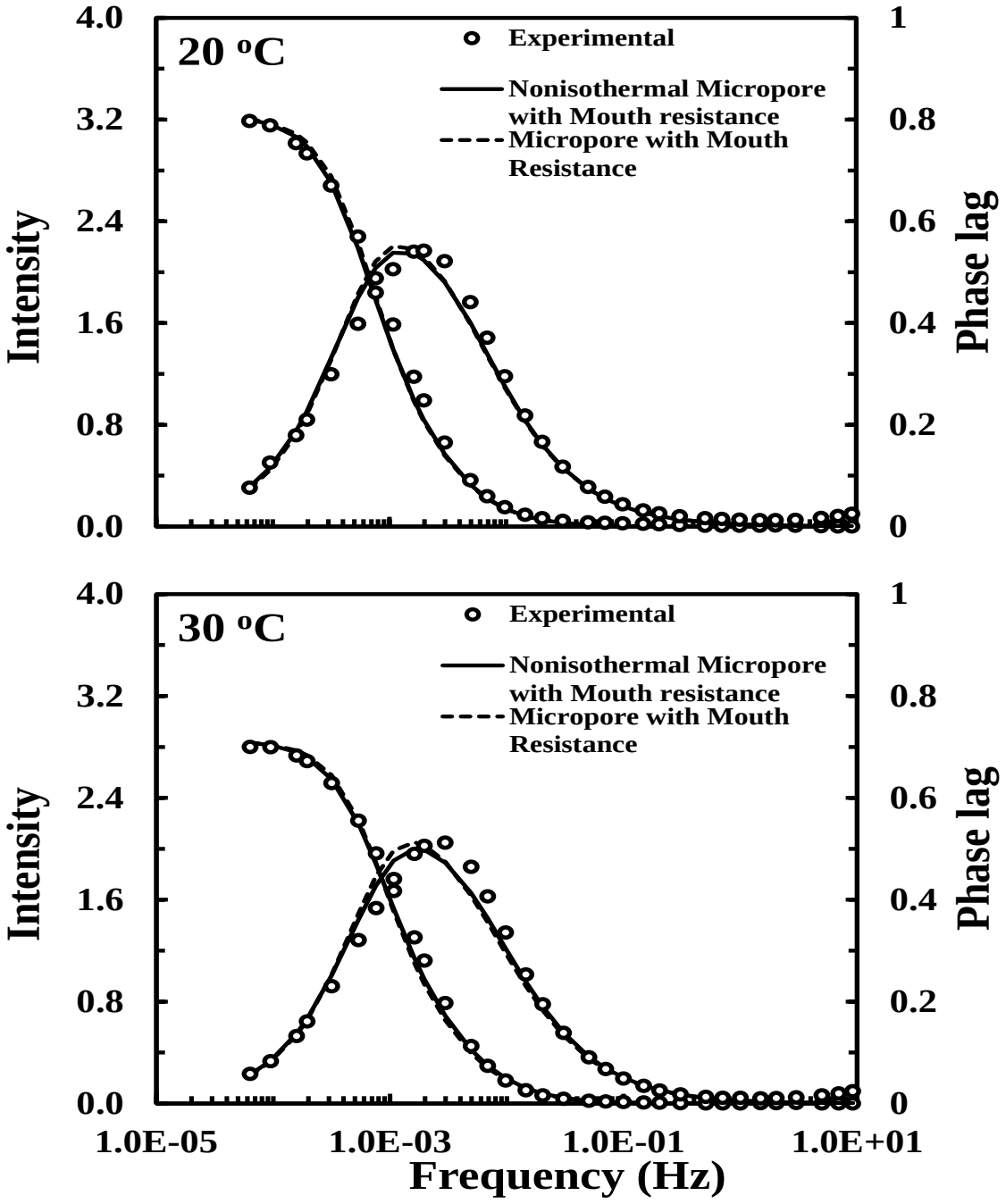
20 °C
Experimental
Nonisothermal Micropore with Mouth resistance
Micropore with Mouth Resistance
30 °C
Experimental
Nonisothermal Micropore with Mouth resistance
Micropore with Mouth Resistance
Intensity
Phase lag
4.0
3.2
2.4
1.6
0.8
0.0
1
0.8
0.6
0.4
0.2
0
1.0E-05
1.0E-03
1.0E-01
1.0E+01
Frequency (Hz)

(a)

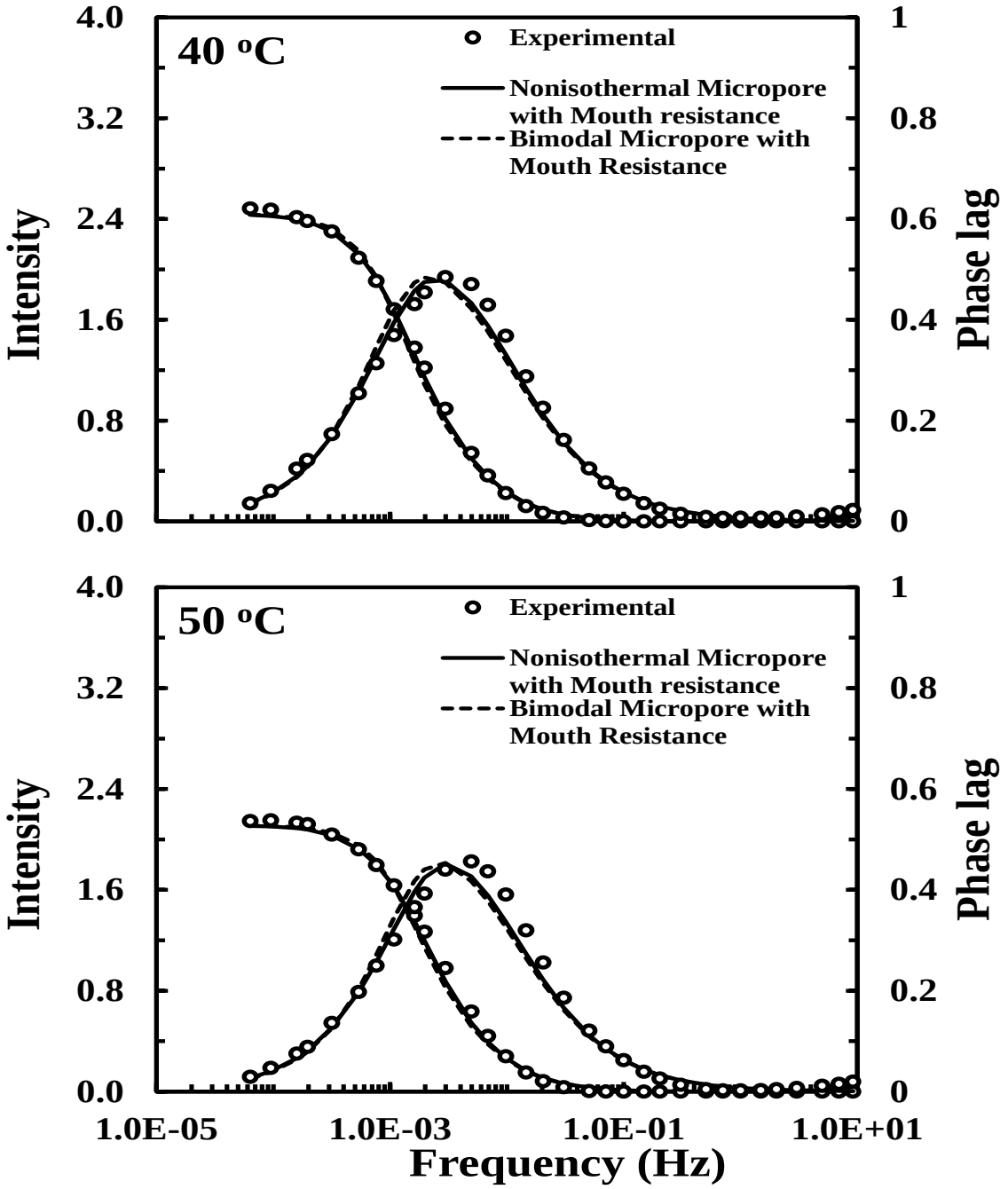

(b)

Figure 4.8 Intensity and Phase lag curves of N_2 on Shirasagi CMS 3K 172 at 750 torr at (a) 20 ^oC, 30^oC and (b)40 ^oC, 50^oC temperatures compared with micropore diffusion with mouth resistance model and nonisothermal micropore with mouth resistance model. The loci of the maxima for the experimental phase lag that from the model exhibit fairly good agreement.

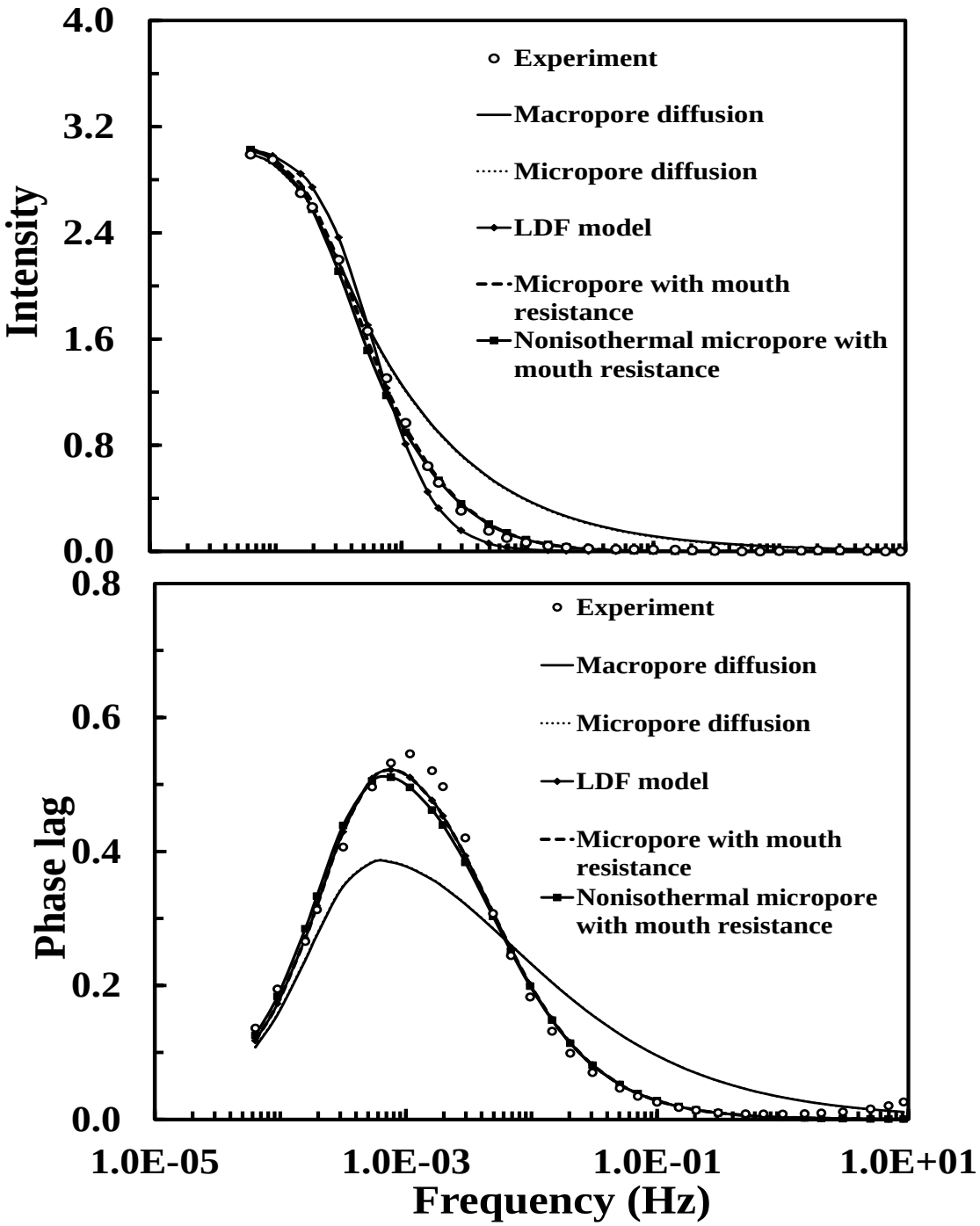

Figure 4.9 Experimental Intensity (top) and Phase lag (bottom) curves of Ar on Shirasagi CMS 3K 172 at 20 ^{o}C fitted with different mass transfer model to identify the governing mechanism of mass transfer.

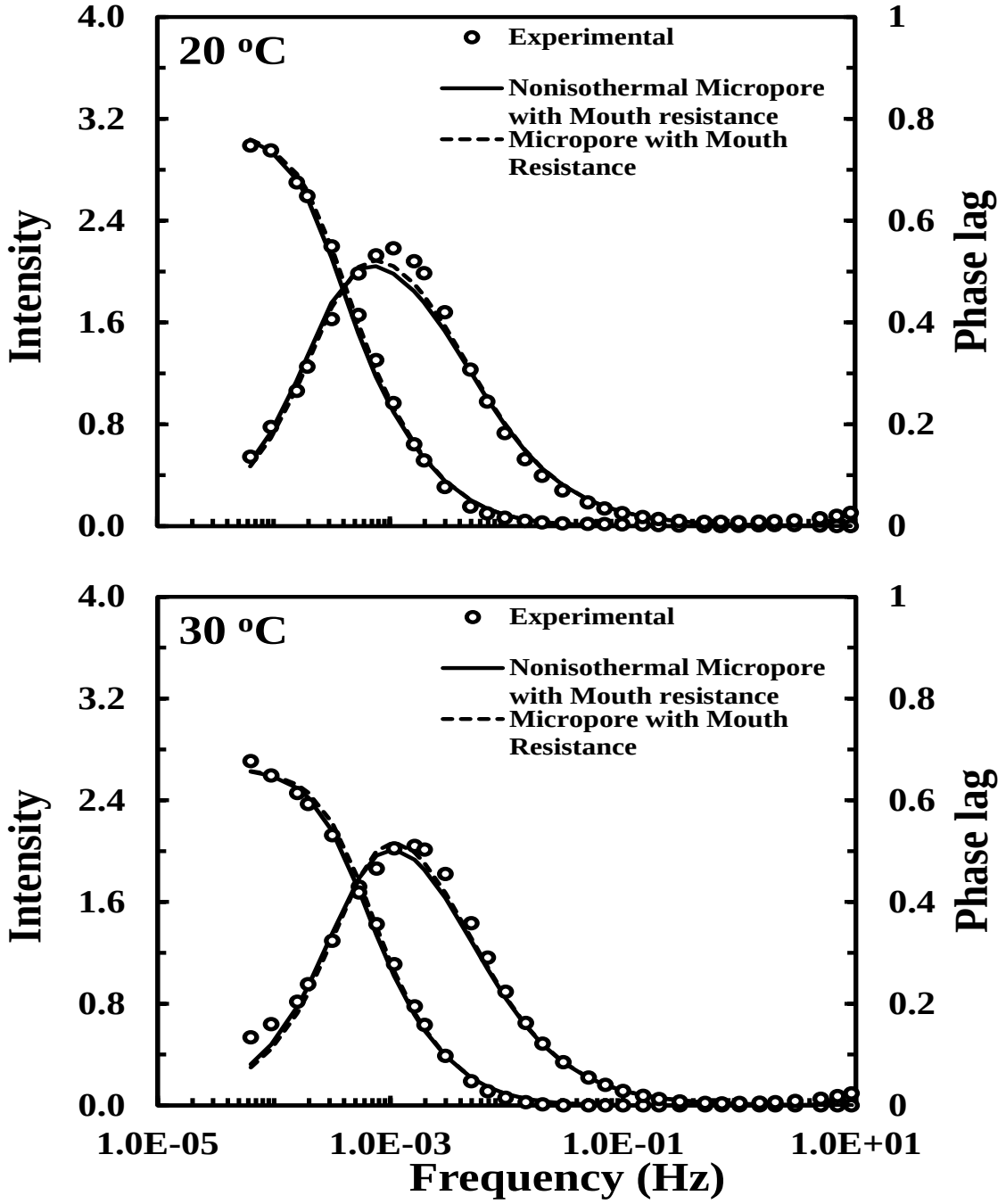
20 °C
Experimental
Nonisothermal Micropore with Mouth resistance
Micropore with Mouth Resistance
30 °C
Experimental
Nonisothermal Micropore with Mouth resistance
Micropore with Mouth Resistance
Intensity
Phase lag
4.0
3.2
2.4
1.6
0.8
0.0
1
0.8
0.6
0.4
0.2
0
1.0E-05
1.0E-03
1.0E-01
1.0E+01
Frequency (Hz)

(a)

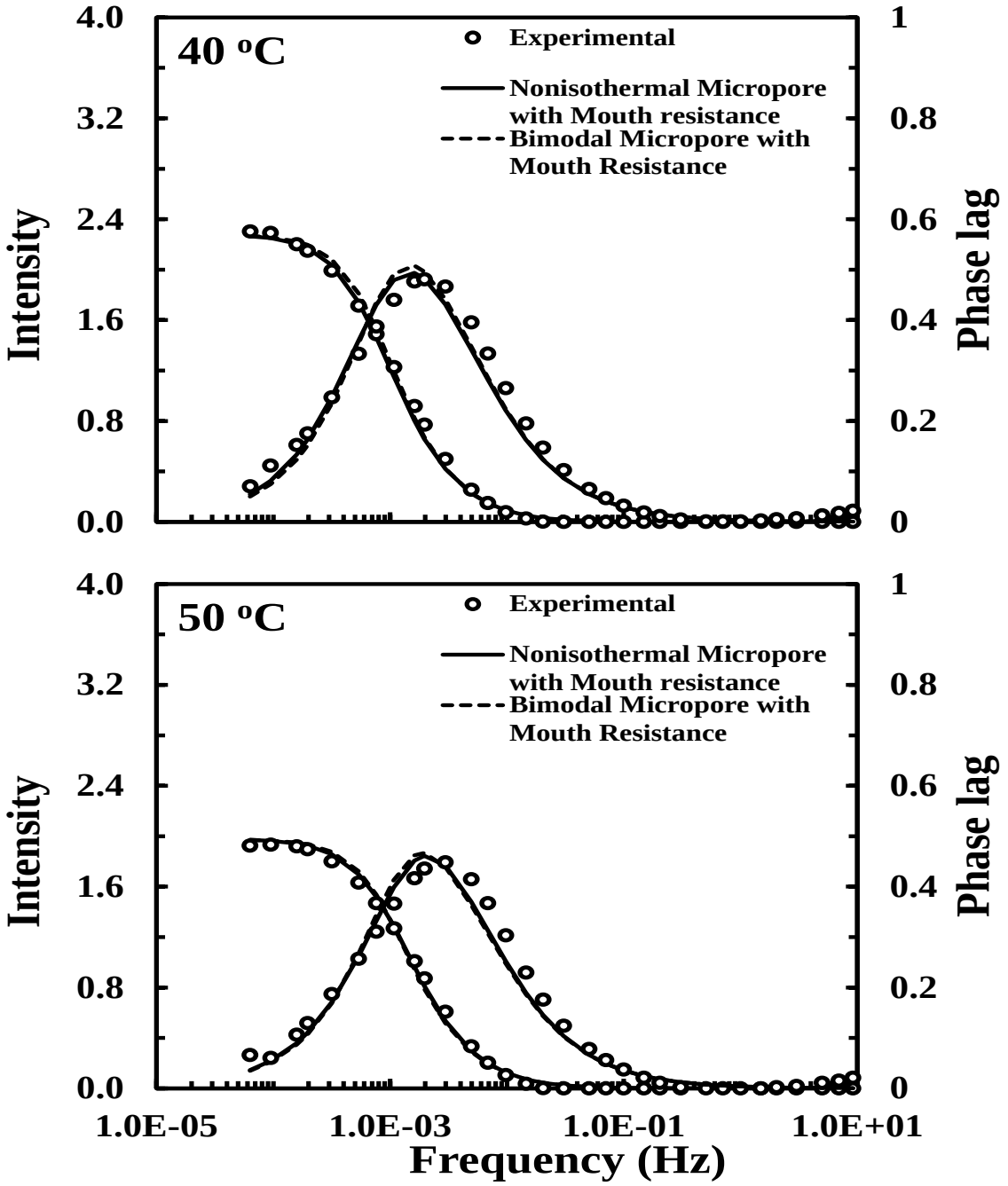

(b)

Figure 4.10 Intensity and Phase lag curves of Ar on Shirasagi CMS 3K 172 at 750 torr (a) 20 ^{o}C, 30^{o}C and (b)40 ^{o}C, 50^{o}C temperatures compared with micropore diffusion with mouth resistance model and nonisothermal micropore with mouth resistance model. The loci of the maxima for the experimental phase lag that from the model exhibit fairly good agreement.

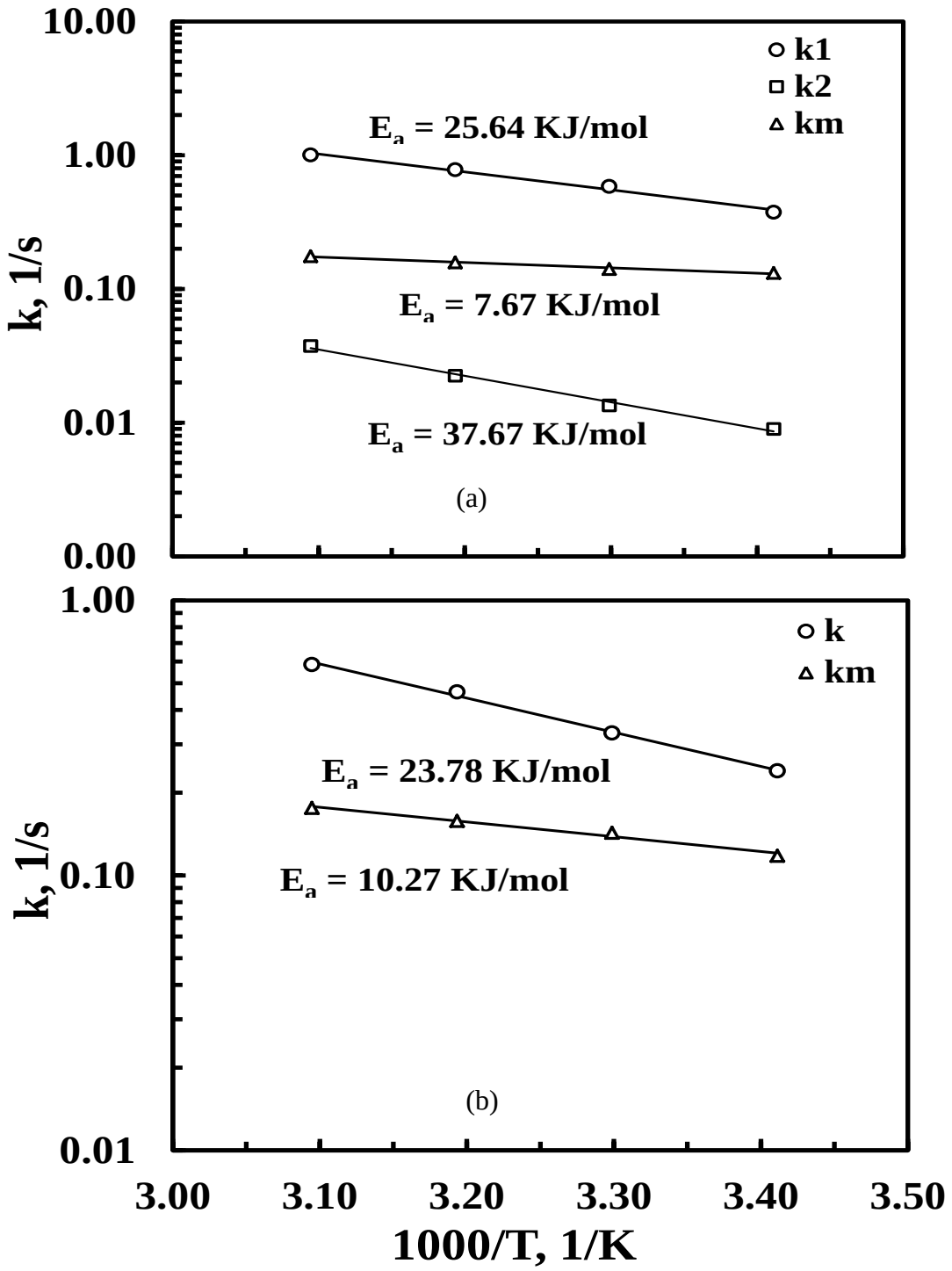

Figure 4.11 Erying plot for the mass transfer parameters for bimodal micropore with mouth resistance (a) and nonisothermal micropore with mouth resistance model (b) for O_2 in CMS.

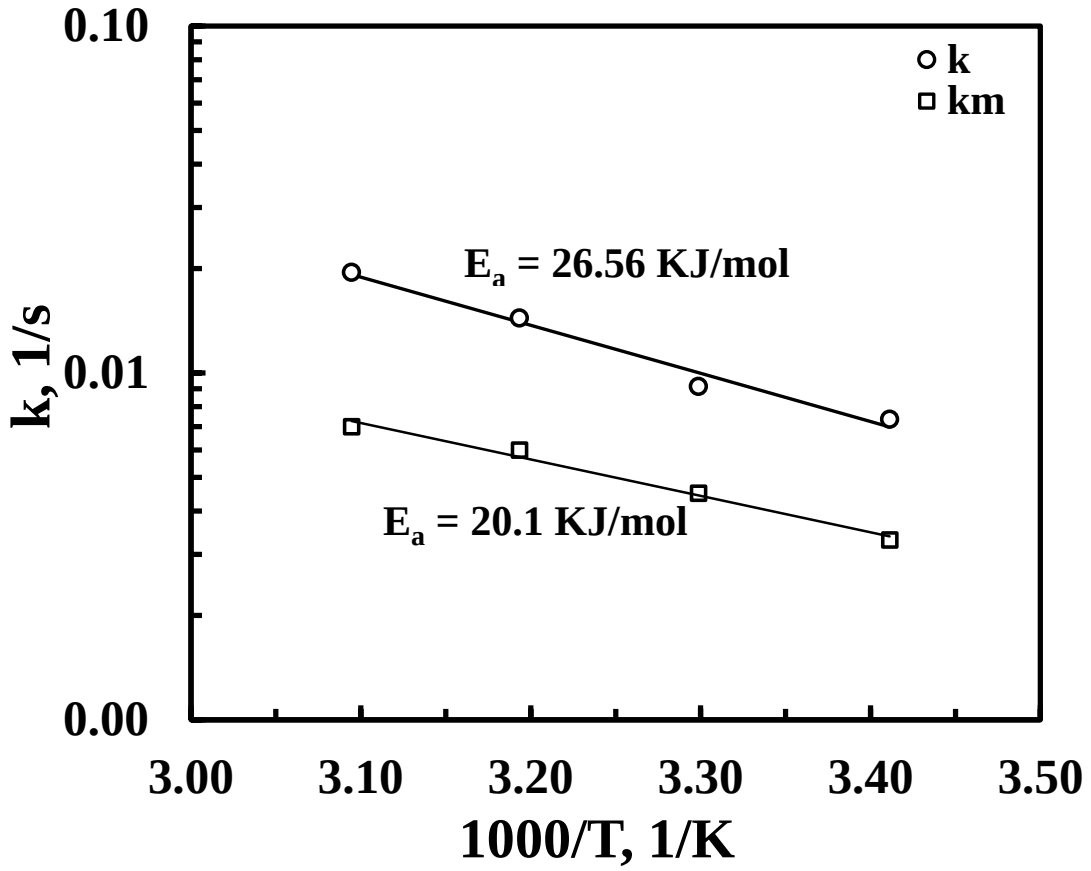

Figure 4.12 Erying plot for the mass transfer parameters for micropore with mouth resistance model for N_2 in CMS.

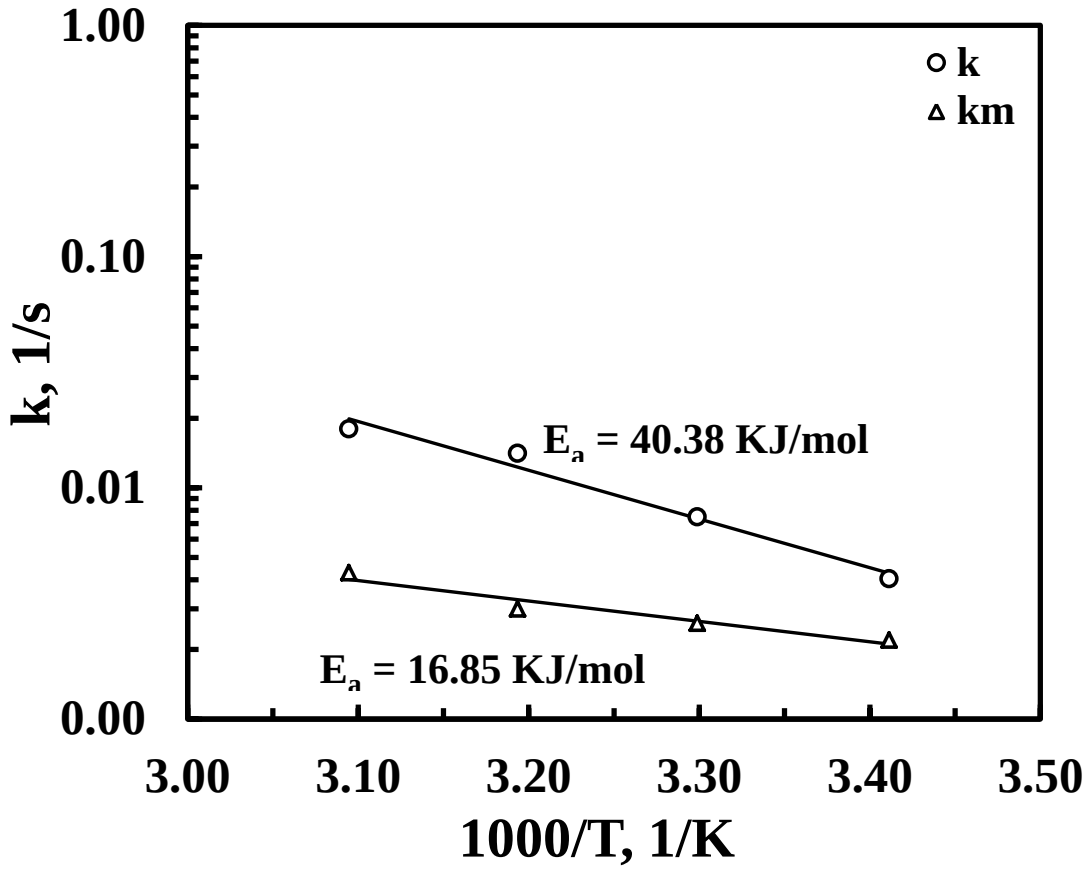

Figure 4.13 Erying plot for the mass transfer parameters for micropore with mouth resistance model for Ar in CMS.

CHAPTER 5

CORRELATION FOR LDF MASS TRANSFER COEFFICIENTS IN DIFFUSION LIMITED SPHERICAL ADSORBENT PARTICLES

Summary

The kinetics of adsorption and desorption in adsorbents is often described in a simplified manner using the linear driving force (LDF) approximation using a mass transfer coefficient that is conventionally estimated using the expression suggested by Glueckauf, namely, $k_{LDF} = 15\ D/R^2$. However, it has been observed that for faster cycling processes this expression is inapt to describe the said kinetics properly. Moreover, a strong dependency of loading on the intrapartcle diffusivity has been reported by researchers which could affect the concentration distribution of adsorbate along the particle as well as the mass transfer processes. To investigate the effect of cycle time and loading dependency of the mass transfer dynamics cyclic adsorption and desorption is simulated by changing the fluid-phase concentration in a sinusoidal fashion in the boundary of a spherical adsorbent particle for a adsorbent –adsorbate system represented by a single process Langmuir isotherm that resembles that of 13X zeolite – CO_2. Both the diffusion equation and LDF mass transfer model is solved numerically using COMSOL Multiphysics. The value of LDF mass transfer coefficient (k) has been

extracted by matching $\frac{\partial \bar{q}}{\partial t}$ and $k(q^* - \bar{q})$ from the numerical solution of the diffusion model. The procedure has been repeated for a wide range of cycle time as well as with three different concentration of fluid phase. A modified and refined form of analytical expression suggested by Alpay and Scott to estimate cycle time dependent mass transfer coefficient k' has been implemented to account for the loading dependency of mass transfer coefficient. Finally a generalized correlation between correction factor defined as the ratio of the extracted mass transfer coefficient to that estimated by modified analytical expression, k/k' and dimensionless half cycle time θ_c has been established, which can be used to predict the LDF mass transfer coefficient for cycling processes irrespective to any loading and any limitation on the θ_c value.

5.1 Introduction

The dynamics adsorption and desorption of molecules in porous adsorbents are often, if not mostly limited by the diffusion process within the adsorbent particles (Yang, 1987). The mathematical model of the diffusional transport in a porous particle is usually expressed by a partial differential equation originated from the differential mass balance of the adsorbate on the particle. It is not always possible to have an exact analytical solution of such model due to the mathematical complexities associated with the process model and its operation. Typically, numerical analyses are used to solve such kind of complex problem. However, numerical calculations are often complicated, tedious and computationally intensive (Hsuen, 2000). So, various simplified mass transfer models are usually applied to represent the adsorption rates of sorbents. Due to its simplicity, the

linear driving force (LDF) method is the one most commonly used requiring only knowledge of the isotherm and the use of a single parameter known as the LDF mass transfer coefficient (Liaw et al., 1979; Nakao and Suzuki, 1983). The LDF model was first proposed by Glueckauf and Coates (1947) and the expression for the LDF mass transfer coefficient, i.e., $k = 15\ D/R^2$, was soon after determined (Glueckauf, 1955). It was later showed that this expression can be derived by assuming a parabolic concentration profile within the sorbent (Liaw et al., 1979) and valid only for processes with half cycle times tc that satisfy the condition $Dt_c/R^2 > 0.1$ (Nakao and Suzuki, 1983). Research efforts followed to improve Glueckauf LDF approximation by a good number of investigators (Vermeulen, 1953; Vermeulen and Quilici, 1970; Do and Rice, 1986; Doong & Yang, 1986; Hills, 1986; Do and Mayfield, 1987; Buzanowski & Yang, 1989; Zhang and Ritter, 1997; Carta & Cincotti, 1998; Hsuen, 2000; Gadre, and Ritter, 2002).

All of the above mentioned models were developed, however, for the stepwise adsorption processes, and developed further upon expressions that either use a non-linear driving force, or require mass transfer coefficients that are time dependent. Further, these models are limited to adsorption-desorption cyclic processes with time scales larger than those of the diffusion dynamics inside particle, with their predictive ability breaking down as the concentration profiles within the particle evolve into very complex shapes. Nakao and Suzuki (1983), Buzanowski and Yang (1989, 1991), and Kikkinides and Yang, 1993 addressed the issue by determining alternative cycle time or frequency dependent mass transfer coefficient for the LDF model using numerical methods. About the same time, Alpay and Scott (1992) followed by Carta (1993) utilized different approaches to penetration theory and reached identical analytical expressions for the

mass transfer coefficient. Both studies showed strong agreement with the graphical correlation provided by Nakao and Suzuki for short cycle time.

The purpose of the present study is to numerical methods under isothermal conditions to investigate and confirm the formula developed by both Glueckauf and that via penetration theory (Alpay and Scott, 1992; Carta, 1993) and provide a simple generalized approach to estimate LDF mass transfer coefficient as function of the half cycle time covering both conditions and the transition from to the other. A spherical adsorbent particle exposed to a binary gaseous mixture with one adsorbable and one non-adsorbable gas has been considered for this. Rapid cyclic adsorption and desorption is simulated by changing the fluid-phase concentration in a sinusoidal fashion. The diffusion equation is solved numerically using COMSOL Multiphysics 3.5a. The study will also include the role of adsorbate loading on the diffusivity that occurs with systems operating with strongly non-linear isotherms (Goddard and Ruthven, 1986) with a dependence on concentration consistent with a transport process controlled by either micropore or macropore diffusion.

5.2 Modeling

Adsorptive separations are mainly controlled by the diffusional resistance with in the adsorbent particle and for the transport of adsorbate in a spherical particle, the mass balance within the particle usually described by the diffusion equation as:

$$\frac{\partial q}{\partial t} = \frac{1}{a(q)r^2}\frac{\partial}{\partial r}\left(r^2 Db(q)\frac{\partial q}{\partial r}\right) \tag{5.1}$$

with boundary conditions

$$r = R : q = q^*(P_o, T) \tag{5.2}$$

$$r = 0 : \frac{\partial q}{\partial r} = 0 \tag{5.3}$$

and initial condition

$$t = 0 : q = q_i = q^*(P_{o,i}, T) \tag{5.4}$$

where, D is the intraparticle diffusivity, R is the particle radius, q is the amount absorbed in the particle, q* is the amount absorbed in equilibrium with the concentration of surrounding fluid phase, qi is the initial loading of the particle, T is the temperature, Po is partial pressure of the adsorbate outside the particle and a(q) and b(q) are functions of loading q that depend of the type diffusion resistance and are evaluated from the isotherm. For a macropore controlled diffusion the particle radius R is that of the spherical pellet, R_p; D is the is the macropore gas diffusivity $D_{M,g}$ and,

$$\boldsymbol{a(q)} = \frac{1}{\rho_p + \dfrac{\varepsilon_p}{\boldsymbol{R_g T}} \left| \dfrac{\boldsymbol{dP}}{\boldsymbol{dq}} \right|^*} \tag{5.5}$$

$$\boldsymbol{b(q)} = \alpha \rho_p \gamma + \frac{\varepsilon_p}{\boldsymbol{R_g T}} \left| \frac{\boldsymbol{dP}}{\boldsymbol{dq}} \right|^* \tag{5.6}$$

Where, ρ_p and ε_p are the pellet density and porosity, respectively, α represents the fraction of adsorption sites participating in surface diffusion at the macropore, and γ is the ratio between surface diffusion and gas diffusion in the macropore. i.e.,

$$\gamma = \frac{D_{M,s}}{D_{M,g}} \tag{5.7}$$

For a micropore controlled diffusion the particle radius R is that of the spherical crystal or micropore domain, R_c, D is the is the micropore surface diffusivity under dilute adsorb phase concentrations $D_{m,s}$ and the expressions a(q) and (b) are consistent with Darken's relationship:

$$a(q) = 1 \tag{5.8}$$

$$b(q) = \left.\frac{d \ln P}{d \ln q}\right|^{*} \tag{5.9}$$

For simplicity, the equilibrium loading, q* in this work, will be related to the partial pressure of the adsorbate P through the Langmuir isotherm:

$$q^{*} = \frac{q_s b P}{1 + bP} \tag{5.10}$$

Thus, the loading dependent terms of equations (5.6) and (5.9) are given by:

$$\left.\frac{dP}{dq}\right|^{*} = \frac{1}{\left(1 - \frac{q}{q_s}\right)^2 b q_s} \tag{5.11}$$

$$\left.\frac{d \ln P}{d \ln q}\right|^{*} = \frac{1}{\left(1 - \frac{q}{q_s}\right)} \tag{5.12}$$

where, q_s and b are the saturation capacity and affinity of the adsorbate, respectively. Usually the mass transfer process described by equation (5.1) is represented by LDF approximation given by:

$$\frac{\partial \bar{q}}{\partial t} = k(q^{*}(P_o, T) - \bar{q}) \tag{5.13}$$

where k is the LDF mass-transfer coefficient, and $\bar{q}$ is the average loading in the spherical particle, i.e.,

$$\bar{q} \equiv \frac{3}{R^2}\int_0^R qr^2 dr \tag{5.14}$$

To evaluate the magnitude of the LDF mass transfer coefficient, equation (5.1) is solved numerically subject to sinusoidal perturbation of the partial pressure P_o according to the expression

$$P_o = P_{o,i} + \Delta P \cdot \sin\left(\frac{\pi t}{t_c}\right) \tag{5.15}$$

where ΔP is the amplitude of the perturbation and t_c is half cycle time. The value of the LDF mass transfer coefficient k is then determined by using the solution of equation (5.1) and then matching the difference between maximum and minimum values for both left hand side the right hand side of equation (5.11).

The value k will be compared to the known expressions determined by Glueckauf (1955) and fast cycling penetration theory (Alpay and Scott, 1992; Carta, 1993). The Glueckauf formula is given by:

$$k' = 15\frac{D\vartheta(q)}{R^2} \tag{5.16}$$

and is valid for a dimensionless half cycle times θ_c restricted to

$$\theta_c \equiv \vartheta(q)\cdot\theta_{c,o} > 0.1 \tag{5.17}$$

Where,

$$\theta_{c,o} \equiv \frac{Dt_c}{R^2} \tag{5.18}$$

The formulation for the fast cycling penetration theory is given by:

$$k'' = \frac{5.14}{\sqrt{\frac{R^2 t_c}{D\vartheta(q)}}} \tag{5.19}$$

which is valid for

$$\theta_c \equiv \vartheta(q) \cdot \theta_{c,o} < 0.1 \tag{5.20}$$

The function $\vartheta(q)$ is equivalent to the ratio b(q)/a(q). For the macropore controlled and micropore controlled models $\vartheta(q)$ is respectively given by

$$\vartheta(\boldsymbol{q}) = \frac{1 + \alpha\gamma \frac{\rho_p \boldsymbol{R}_g \boldsymbol{T}}{\varepsilon_p} \left(1 - \frac{\boldsymbol{q}}{\boldsymbol{q}_s}\right)^2 \boldsymbol{b}\boldsymbol{q}_s}{1 + \frac{\rho_p \boldsymbol{R}_g \boldsymbol{T}}{\varepsilon_p} \left(1 - \frac{\boldsymbol{q}}{\boldsymbol{q}_s}\right)^2 \boldsymbol{b}\boldsymbol{q}_s} \tag{5.21}$$

and

$$\vartheta(q) = \frac{1}{\left(1 - \frac{q}{q_s}\right)} \tag{5.22}$$

In addition to solving equation (5.1), equation (5.11) is also solved numerically using either expressions (5.16) or (5.19) for the mass transfer coefficient and then the solution is compared to the solution of equation (5.1).

5.3 Results and Discussions

For this study, it will be assumed that the adsorbate-adsorbent systems studied here will have identical thermodynamics to that between CO_2 and 13X zeolite at 300 K

and that the physical properties of the adsorbent are that of 13X zeolite. However, the studied systems will have differing diffusing mechanisms controlling the transport of the adsorbate. The system properties and the parameters single process Langmuir isotherm at 300K are listed in Table 5.1. All initial partial pressure $P_{o,i}$ of the adsorbate is selected according to the expression

$$P_{o,i} = \frac{1}{b}\frac{\frac{q_i}{q_s}}{\left(1-\frac{q_i}{q_s}\right)} \tag{5.23}$$

such that q_i/q_s is either 0.001, 0.5 or 0.95. In all runs the amplitude ΔP is equivalent to one hundredth of P_i . All simulation results for equation (5.1) are shown in Table 5.2. The three first rows show simulations results of the micropore limited model at all three different values of q_i/q_s, whereas the last row shows simulations results of the macropore limited model at q_i/q_s = 0.95. The mass transfer coefficient k was obtained by running the simulation at a half cycle time t_c determined from the corresponding value of θ_c and equations (5.17) and (5.18):

$$t_c \equiv \frac{\theta_c R^2}{D\vartheta(q)} \tag{5.24}$$

whereas value of k" is obtained directly from equation (5.19).

Figures 5.1 and 5.2 shows comparison results between simulations from the diffusion equation (5.1) and LDF equation (5.11) using a mass transfer coefficient predicted from Gluekauf equation (5.16), for a q_i/q_s = 0.001 and for four different values of the dimensionless half cycle time, i.e., θ_c = 1.0, 0.1, 0.01 and 0.001 and a micropore controlled diffusion system. Figure 5.1 shows the average loading $q_{avg}\left(\equiv \bar{q}\right)$ relative to q_i

while Figure 5.2 shows the time derivative of q_{avg}. The response using the conventional value of $15D_c/R^2$ for the LDF mass transfer coefficient apparently shows pretty good agreement with the response from the diffusion model for longer cycles, $\theta_c = 1.0$ and $\theta_c = 0.1$. However, for the case of faster cycles ($\theta_c = 0.01$ and $\theta_c = 0.001$) the simulations of both models show important disagreements as expected. The response from the LDF model with Gluekauf's LDF mass transfer coefficient becomes smaller than the response from the diffusion equation as the θ_c is smaller than 0.1 consistent with findings elsewhere (Nakao and Suzuki, 1983). For comparison purposes, the scale for the axis representing dimensionless loading has been kept same for all four cases. At relatively large time scales ($\theta_c = 1.0$), the diffusion kinetics are irrelevant as controlling element in the transport of the adsorbate and hence, q_{avg} is expected to remain close to $q^*(P_o, T)$. For a condition that is well within the Henry's law regions, i.e., $q_i/q_s = 0.001$, this condition is clearly verified by observing that the amplitude of q_{avg} is about one hundreds the value of q_i (Figure 5.1.a) which is identical to the ratio $\Delta P / P_{o,i}$ established for the partial pressure. As the time scale of the cycle become smaller than the diffusional time scale ($\theta_c < 1.0$), the amplitude of the responses become smaller in both models because the adsorption and desorption become now controlled by the diffusion kinetics. However as times scale become further small ($\theta_c < 0.1$), discrepancy becomes apparent now between the amplitudes of the two models. As shown by Liew et al. (1979) the Glueckauf's LDF approximation of mass transfer coefficient can do good job when concentration profiles within the particle can be described fairly well in terms of a

parabolic concentration distribution in the particle. However, this is not true at faster cycle times as the concentration distributions are complicated.

Contrastingly different results are obtained comparing the diffusion equation (5.1) and LDF equation (5.11) using a mass transfer coefficient predicted from the fast cycling penetration theory expression in equation (5.19) as shown in figures 5.3 and 5.4. Conditions are the same as before, i.e., a micropore controlled diffusion model with q_i/q_s = 0.001 at all four different values of the dimensionless half cycle time, i.e., θ_c = 1.0, 0.1, 0.01 and 0.001. The figure shows the validity of the analytical expression suggested by Alpay and Scott for θ_c <0.1, showing good agreement between the two models at the two lowest half cycle times, i.e., θ_c = 0.01, 0.001, and a very small discrepancy of the amplitudes at θ_c = 0.1. At longer cycle times θ_c = 1.0) the difference between both models become more conspicuous though not significantly, with the predictions from the LDF model displaying smaller amplitudes.

Figure 5.5 shows the predicted mass transfer coefficient k of out equation (5.1) for a micropore controlled diffusion for a q_i/q_s = 0.001 and wider range of half cycle times ($0.001 \leq \theta_c < 5$) along with the value of mass transfer coefficient estimated from the expressions determined by Glueckauf (eq. 5.16) and Alpay and Scott (Eq. 5.19). The predicted mass transfer coefficients k are listed in Table 5.2. The figure show three distinct zones, A, B and C from the shorter cycle with short half cycle times at the left hand side to the longer slower half cycle times at the right hand side. In Zone A (θ_c < 0.01) the expression by Alpay and Scott very closely matches the extracted mass transfer coefficient, and significantly lower than the previous established limit (θ_c < 0.1). Zone C ($\theta_c \geq 0.3$) is for the slower half cycle times wherein mass transfer coincides with

conventional Glueckauf LDF approximation and also is off the previously established limit ($\theta_c > 0.1$). Finally, Zone B ($0.1 \leq \theta_c < 0.3$) is a transition zone between zones A and C, where both models both disagree and underestimate the correct mass transfer coefficient. This is where the assumptions for both models break down.

The results shown so far were carried out for a micropore controlled diffusion model under conditions ($q_i/q_s = 0.001$) where there is no loading dependence by the diffusion coefficient, i.e., a(q) = 1, b(q) ~1 $\vartheta(q) \sim 1$ (from Eqs, (5.8), (5.9), (5.11) and (5.22)) Figure 5.6 shows a comparison between equation (5.1) and the LDF model using Alpay and Scott's expression equation (5.19) for a micropore diffusion controlled system, for $\theta_c = 0.1$ and for conditions wherein concentration has a strong impact on the diffusivity coefficient, i.e., $q_i/q_s = 0.5$ (a and c) and $q_i/q_s = 0.95$ (b and d),. The quite good agreements between both predicting behavior indicate that the correcting factor $\vartheta(q)$ is correctly used in equations (5.19) and (5.20) to predict the right value for k" for the LDF model and the half cycle time t_c, respectively.

Results are not that different for the macropore diffusion controlled model, which has not been touched so far. Figure 5.7 shows all the results displayed in Table 5.2, including both conditions for the micropore diffusion controlled model for which q_i/q_s = 0.001, 0.5 and 0.95 and the macropore diffusion controlled model for which $q_i/q_s = 0.95$ without surface diffusion ($\alpha = 0.0$ and $\gamma = 0.0$). The figure expresses the results in terms of the ratio k/k" against $\theta_c^{0.5}$. The straight line corresponds to the ratio k'/k" which according to equations (5.16) through (5.19) is given by:

$$\frac{k'}{k''} = \frac{15}{5.14}\sqrt{\theta_c} \qquad (5.25).$$

The results for the predicted k, show an excellent overlap into one curve, regardless of the mechanism and the value of q_i/q_s. Further, at long half cycle time the curve merges perfectly well with equation (5.25), suggesting that the Gluekauf are being satisfied. Similarly, at short half cycle times and approaching towards zero, the curve becomes closer to a value of one, which is consistent with Alpay and Carta's formulation for fast cycle conditions. This excellent curve could be used to determine a function that could help the value of k given the value of $\sqrt{\theta_c}$, namely:

$$\frac{k}{k''} = \psi(\sqrt{\theta_c}) \tag{5.26}$$

The function $\psi(\sqrt{\theta_c})$ can be best represented by:

$$\psi(\sqrt{\theta_c}) = \frac{15}{5.14}\sqrt{\theta_c} + \phi(\sqrt{\theta_c}) \tag{5.27}$$

Where $\phi(\sqrt{\theta_c})$ is a function such that it is equal to 1.0 at $\theta_c = 0.0$ and equal to 0.0 when $\theta_c \to \infty$. The best function for this is the Fermi Dirac function which is given by:

$$\phi(\sqrt{\theta_c}) = 2\left(1 - \frac{1}{1+\exp\left(-\beta \cdot \frac{15}{5.14}\sqrt{\theta_c}\right)}\right) \tag{5.28}$$

Where β is twice the value of the slope of $\phi(\sqrt{\theta_c})$ against $\sqrt{\theta_c}$ at $\theta_c = 0.0$. The curve $\psi(\sqrt{\theta_c})$ is shown in the figure, which fits the data for a β of 1.42, which coincidently matches closely the value of $\sqrt{2}$. Hence k, could be predicted from equation (5.26) with $\psi(\sqrt{\theta_c})$ given by

$$\psi(\sqrt{\theta_c}) = \frac{15}{5.14}\sqrt{\theta_c} + 2\left(1 - \frac{1}{1+\exp\left(-\frac{15}{5.14}\sqrt{2\theta_c}\right)}\right) \tag{5.29}$$

5.4 Conclusion

A series of rapid cyclic adsorption and desorption simulations were performed by changing the fluid-phase concentration of the adsorbate around a spherical adsorbent particle in a sinusoidal fashion with a magnitude of 1% of its initial value operating isothermally at 300 K and 1atm for three different loadings. Both diffusion equation and the LDF equation were solved numerically. It has been observed that the conventional value of mass transfer coefficient as suggested by Gluekauf is inapt to use in analysis of rapid cycling process with shorter cycle time. For cyclic adsorption desorption processes with dimensionless half cycle time, θ_c <0.1 the analytical expression for estimating LDF mass transfer coefficient suggested by Alpay and Scott and Carta could be used, however, it would be more appropriate to use the modified equation as suggested in this communication where the loading dependency has been introduced. Finally, a generalized graphical method were presented which along with the modified analytical expression (equation 5.29) could be used to estimate LDF mass transfer coefficient irrespective to any loadings and without any limitations imposed on the θ_c value.

5.5 Tables

Table 5.1 Parameters used in the study

Adsorbent characteristics		
	Adsorbate	CO_2
	Adsorbent	13X
	Pellet density (ρ_p)	1100 kg/m^3
	Pellet porosity (ε_p)	0.4
Equilibrium and kinetic properties (at 300 K)*		
	q_s for CO_2	3.96 mol/kg
	b for CO_2	0.209 kPa^{-1}
Micropore	D_m/R_c^2	0.1 s^{-1}
Macropore	$D_{M,g}/R_p^2$	30.0 s^{-1}
	γ	0.0
	α	0.0

***Determined from experimental data by Wang and LeVan (2009) for CO_2 on 13X.**

Table 5.2 Extracted and estimated LDF mass transfer coefficients and correction factors

	Micropore									Macropore	
	$\frac{q_i^*}{q_s} = 0.001$			$\frac{q_i^*}{q_s} = 0.5$			$\frac{q_i^*}{q_s} = 0.95$			$\frac{q_i^*}{q_s} = 0.95$	
θ_c	**k s^{-1}**	**k" s^{-1}**	**k/k"**	**k s^{-1}**	**k" s^{-1}**	**k/k"**	**k s^{-1}**	**k" s^{-1}**	**k/k"**	**k s^{-1}**	**k/k"**
0.0010	17.20	16.26	1.06	---	---	---	---	---	---	---	---
0.0017	13.52	12.59	1.07	---	---	---	---	---	---	---	---
0.0020	---	---	---	24.64	22.99	1.07	---	---	---	---	---
0.0025	11.07	10.28	1.08	---	---	---	---	---	---	---	---
0.0033	9.68	8.91	1.09	19.28	17.81	1.08	---	---	---	---	---
0.0050	7.97	7.27	1.20	15.91	14.54	1.09	---	---	---	---	---
0.0067	---	---	---	13.90	12.59	1.10	---	---	---	---	---
0.0100	5.76	5.14	1.12	11.52	10.28	1.12	115.32	102.82	1.12	115.32	1.12
0.0125	---	---	---	---	---	---	104.01	91.97	1.13	104.08	1.13
0.0143	---	---	---	---	---	---	97.94	86.03	1.14	97.86	1.13
0.0167	---	---	---	---	---	---	91.40	79.64	1.15	91.47	1.15
0.0200	---	---	---	8.42	7.27	1.16	84.24	72.71	1.16	84.34	1.16
0.0250	3.83	3.25	1.18	---	---	---	---	---	---	---	---
0.0333	---	---	---	---	---	---	67.44	56.32	1.20	67.53	1.20
0.0500	2.86	2.3	1.24	5.69	4.60	1.24	56.95	45.98	1.24	57.00	1.24
0.0667	---	---	---	---	---	---	50.71	39.82	1.27	50.77	1.28
0.1000	2.18	1.63	1.34	4.35	3.25	1.34	43.45	32.52	1.34	43.51	1.34
0.1667	1.84	1.26	1.47	---	---	---	---	---	---	---	---
0.2000	---	---	---	3.51	2.3	1.53	35.09	22.99	1.53	35.14	1.53
0.2500	1.67	1.03	1.63	---	---	---	---	---	---	---	---
0.3333	---	---	---	3.21	1.78	1.80	---	---	---	---	---
0.5000	1.56	0.73	2.15	3.10	1.45	2.13	30.98	14.54	2.13	31.04	2.14
0.6667	1.52	0.63	2.42	---	---	---	---	---	---	---	---
1.0000	1.52	0.52	2.95	3.02	1.03	2.94	30.26	10.28	2.94	30.31	2.95
1.2500	1.51	0.46	3.28	---	---	---	---	---	---	---	---
1.3333	---	---	---	3.02	0.89	2.29	---	---	---	---	---
1.4286	1.51	0.43	3.50	---	---	---	---	---	---	---	---
1.6667	1.50	0.39	3.78	---	---	---	---	---	---	---	---
2.0000	1.50	0.36	4.13	3.01	0.73	3.39	30.07	7.27	4.14	30.13	4.14
2.5000	1.50	0.33	4.61	3.01	0.65	4.14	---	---	---	---	---
2.8571	1.50	0.31	4.93	---	---	---	---	---	---	---	---
3.3333	1.50	0.28	5.33	---	---	---	30.02	5.63	5.33	30.08	5.34
4.0000	1.50	0.26	5.84	---	---	---	---	---	---	---	---
5.0000	1.50	0.23	6.52	2.99	0.46	6.50	30.01	4.60	6.53	30.04	6.53

5.6 Figures

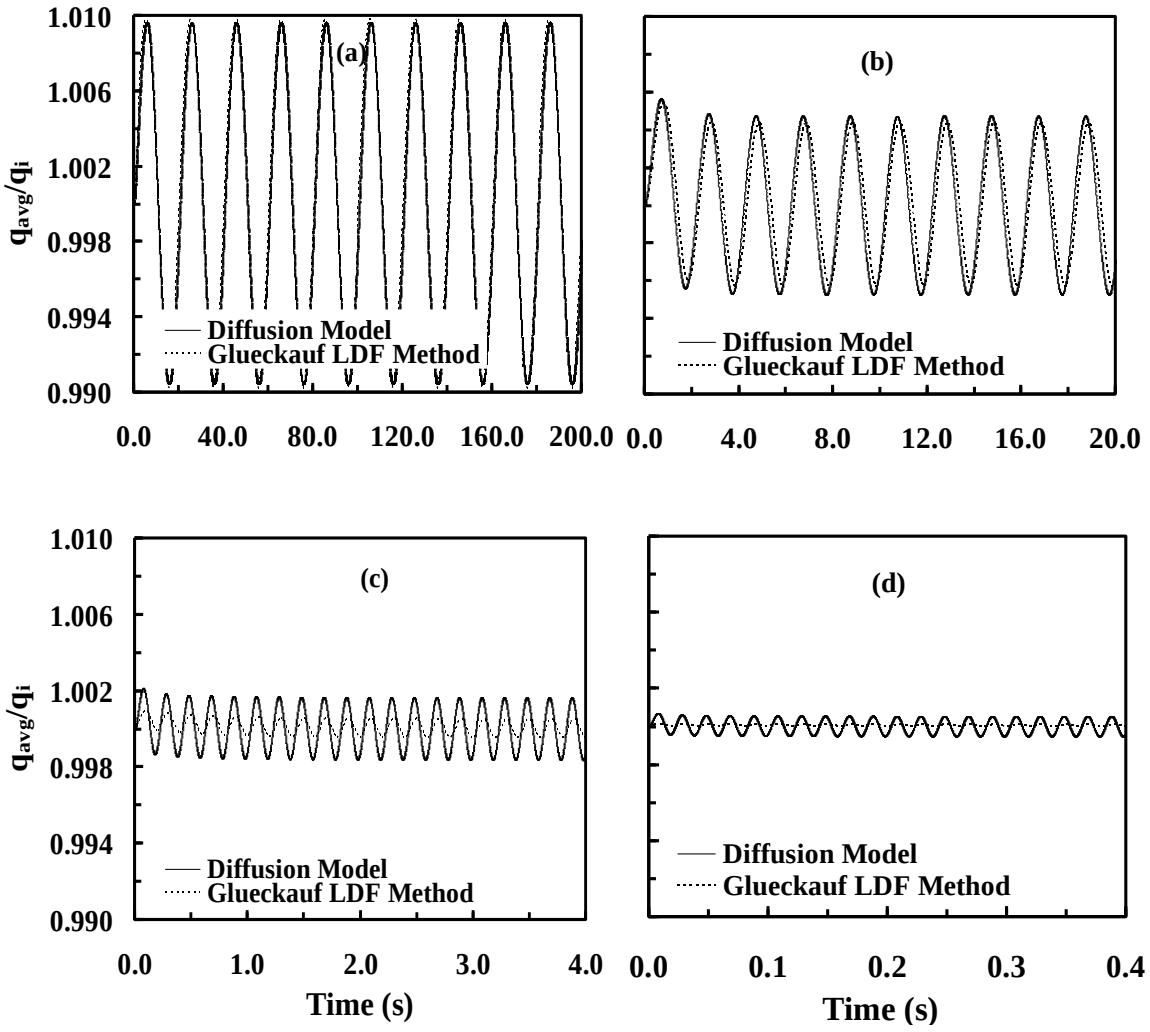

Figure 5.1 Response in terms of dimensionless loading of the adsorbent particle with time from the numerical solution of diffusion model and LDF model for (a) θ_c=1, (b) θ_c=0.1, (c) θ_c=0.01 and (d) θ_c=0.001. Glueckauf's LDF model shows close agreements with the numerical solution of diffusion model for slower cycle with large cycle time (θ_c=1 and 0.1) however for smaller value of θ_c i.e. for very fast cycling process Gluckauf's LDF model shows large discrepancy and apparently failed.

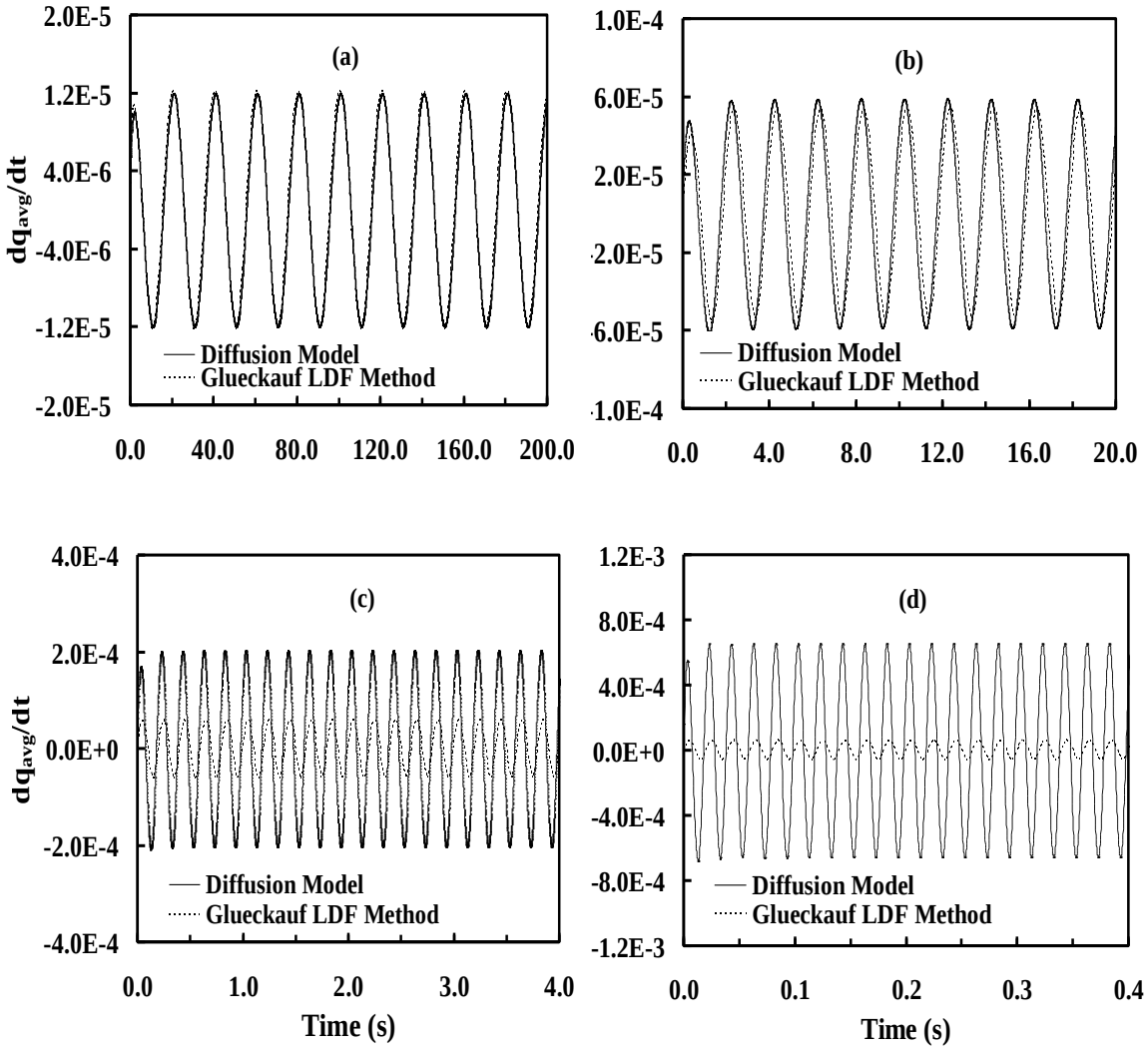

Figure 5.2 Response in terms of average adsorption-desorption rate with time from the numerical solution of diffusion model and LDF model for (a) θ_c=1, (b) θ_c=0.1, (c) θ_c=0.01 and (d) θ_c=0.001. Glueckauf's LDF model shows close agreements with the numerical solution of diffusion model for slower cycle with large cycle time (θ_c=1 and 0.1) however for smaller value of θ_c i.e. for very fast cycling process Gluckauf's LDF model shows large discrepancy and apparently failed.

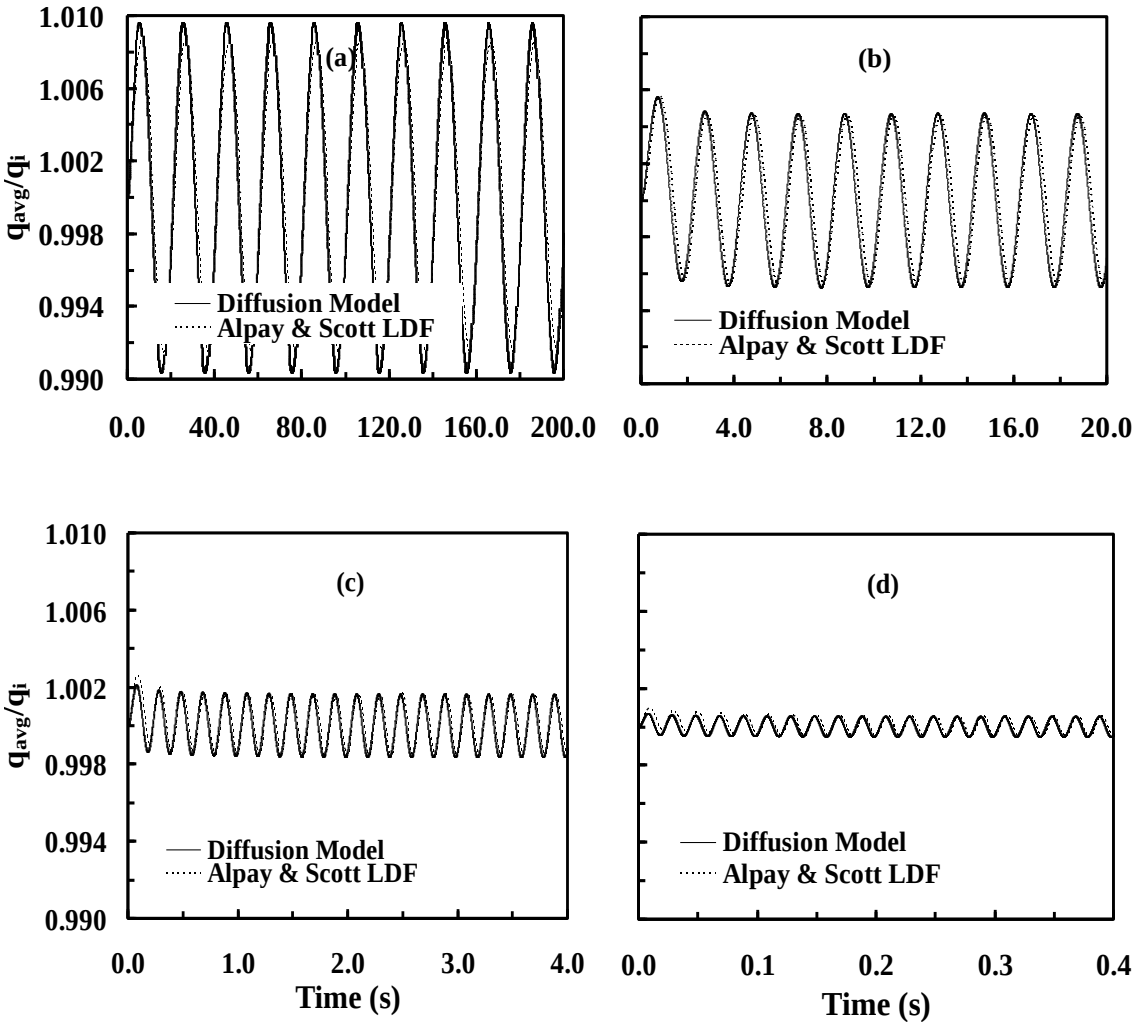

Figure 5.3 Response in terms of dimensionless loading of the adsorbent particle with time from the numerical solution of diffusion model and LDF model for for (a) θ_c=1, (b) θ_c=0.1, (c) θ_c=0.01 and (d) θ_c=0.001. LDF model with mass transfer coefficient estimated by Alpay and Scott shows close agreements with the numerical solution of diffusion at faster cycles but failed at slower cycle with θ_c=1.

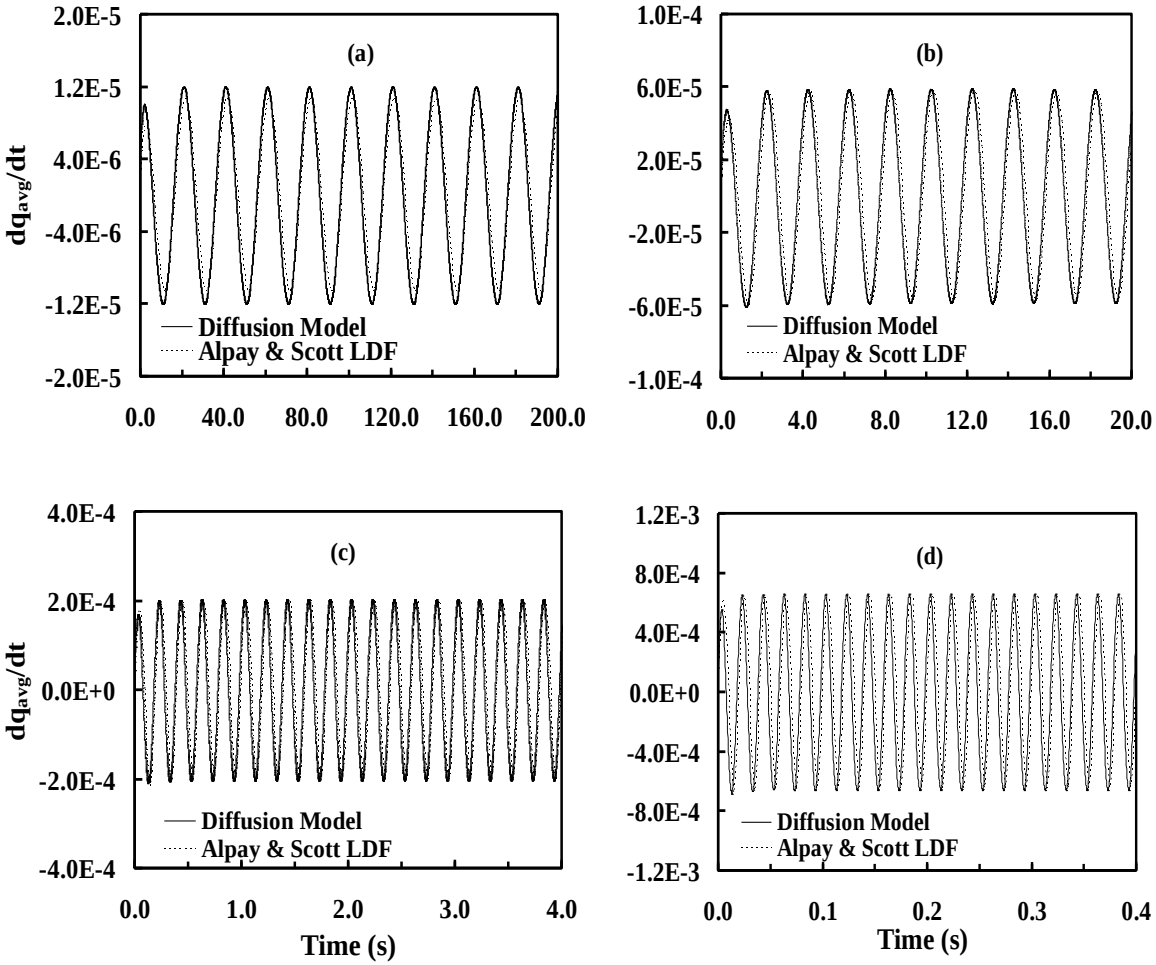

Figure 5.4 Response in terms of in terms of average adsorption-desorption rate from the numerical solution of diffusion model and LDF model for (a) θ_c=1, (b) θ_c=0.1, (c) θ_c=0.01 and (d) θ_c=0.001. LDF model with mass transfer coefficient estimated by Alpay and Scott shows close agreements with the numerical solution of diffusion at faster cycles but failed at slower cycle with θ_c=1.

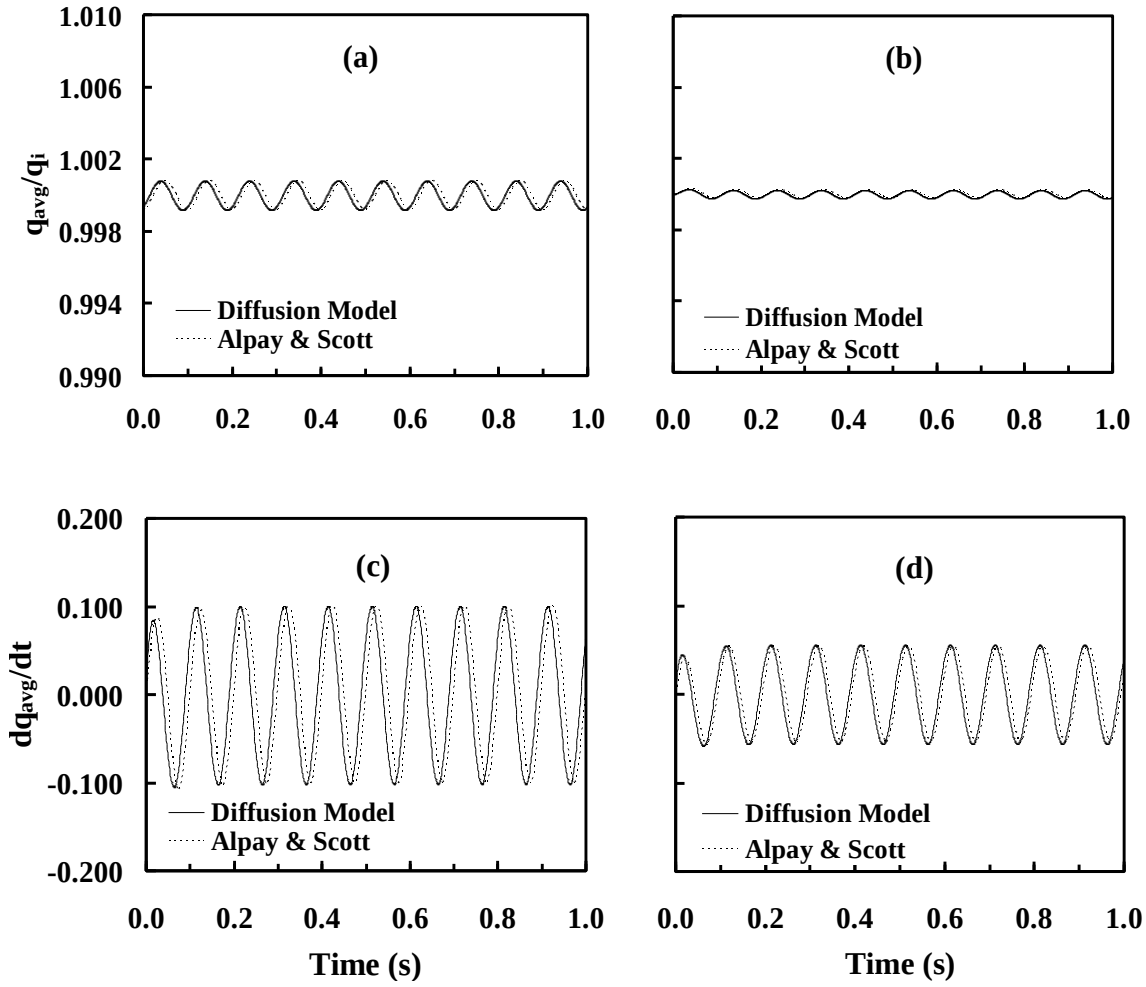

Figure 5.5 Loading dependency of LDF mass transfer coefficient. The analytical expression by Alapy and Scott for particle mass transfer coefficient able to predict the response from the diffusion model reasonably good for $q/q_s = 0.5$ (a and c) and $q/q_s = 0.95$ (b and d) for $\theta_c=0.1$. Results are shown in terms of dimensionless average loading (top) and average adsorption-desorption rate (bottom).

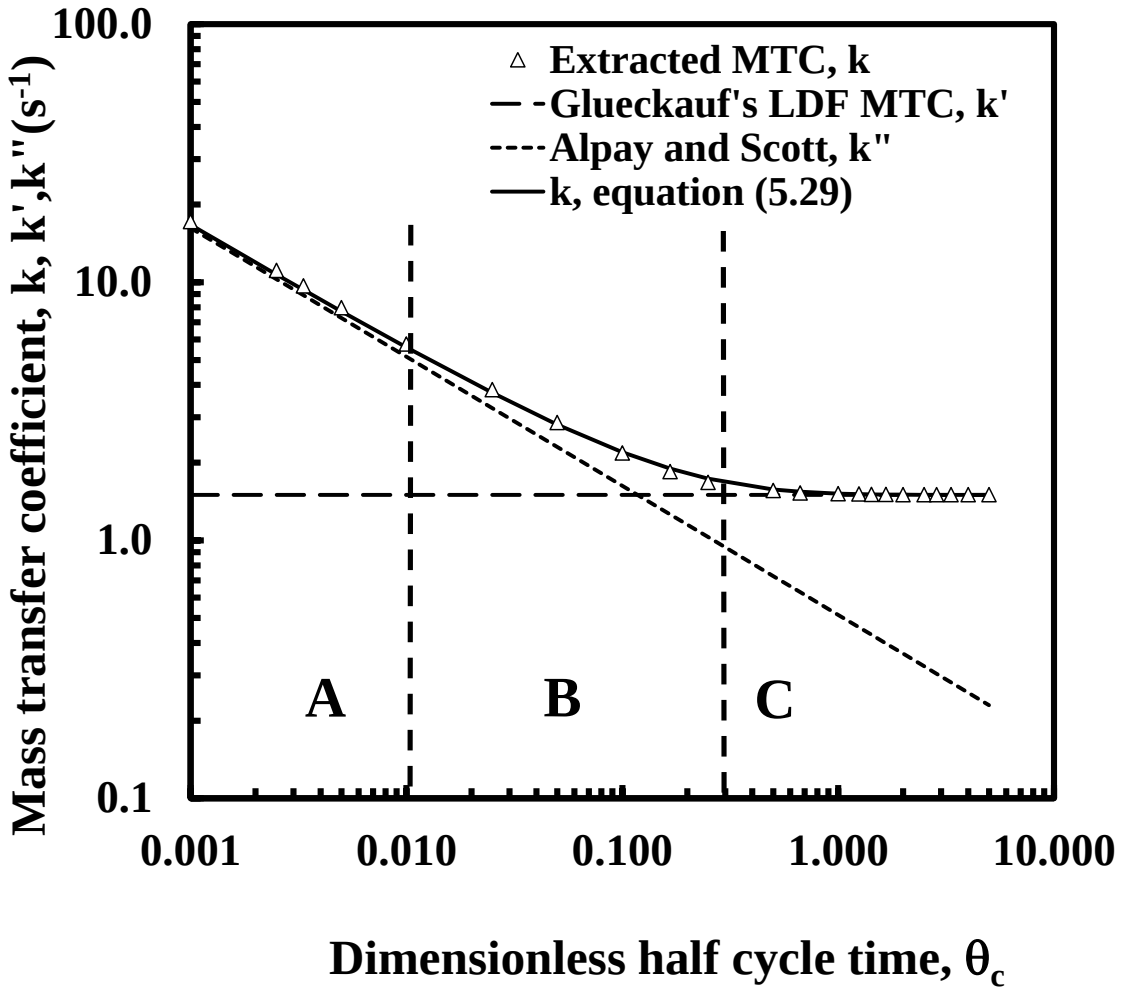

Figure 5.6 Effects of rapid cycling on Mass Transfer Coefficient (MTC) for dilute system. Mass transfer coefficient decreases with increase of the cycle time. For faster cycle (dimensionless half cycle time, $\theta_c << 0.01$) and dilute system the particle mass transfer coefficient shows very close agreement with the analytical expression given by Alpay and Scott (1992) and Carta (1993) (Zone **A**). But as the cycle time increases and approaches value 0.1 (Zone **B**)the mass transfer coefficient as calculated from the analytical expression starts deviating from the actual mass transfer coefficient and eventually for longer cycle ($\theta_c > 0.2$) coincide with the Gluckauf's LDF mass transfer coefficient (Zone **C**).

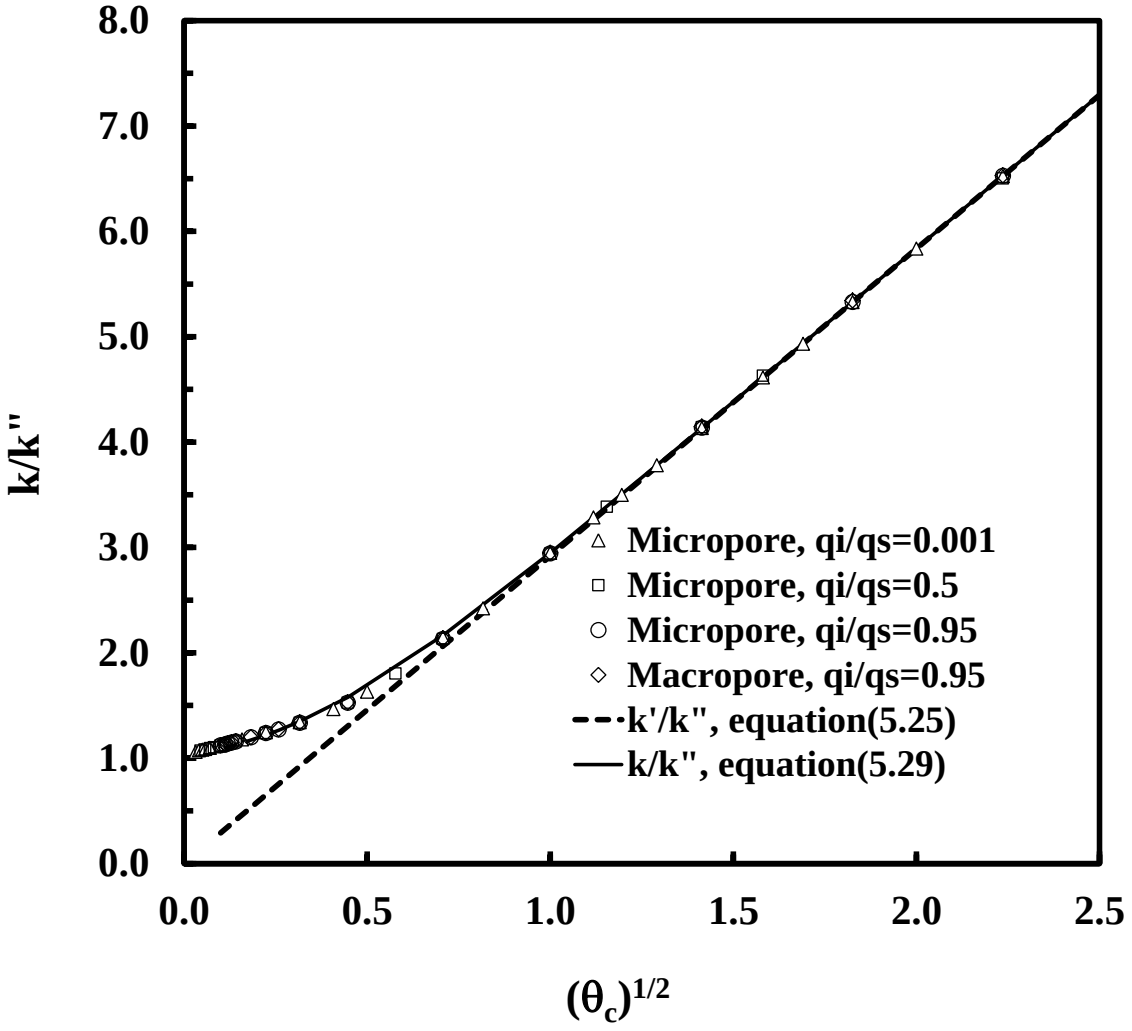

Figure 5.7 Correction factor for LDF mass transfer coefficient as a function of dimensionless half cycle time.

REFERENCES

1. Ruthven, D. M. *Principles of Adsorption and Adsorption Processes*. **1984**, Wiley, New York.
2. Sircar, S. Basic Research Needs for Design of Adsorptive Gas Separation Processes. *Ind. Eng. Chem. Res*., **2006**, 45, 5435.
3. Rutherford, S. W.; Do, D. D. Characterization of Carbon Molecular Sieve 3A. *Langmuir*, **2000**, 16, 7245.
4. Karger, J.; Ruthven, D. M. *Diffusion in Zeolites and Other Microporous Solids*. **1992**, John Wiley and sons, Inc. New York.
5. Wang, Y.; LeVan, M. D. Master Curves for Mass Transfer in Bidisperse Adsorbents for Pressure-swing and Volume-swing Frequency Response Methods. *AiChE J.*, **2011**, 57(8), 2054.
6. Sircar, S. Recent Developments in Macroscopic Measurement of Multicomponent Gas Adsorption Equilibria, Kinetics, and Heats. *Ind. Eng. Chem. Res*., **2007**, 46, 2917.
7. Wang, Yu.; Sward, B. K.; LeVan, M. D. Frequency Response Method for Measuring Adsorption Rates Via Pressure Modulation: Application to Oxygen and Nitrogen in a Molecular Sieve. *Ind. Eng. Chem. Res*., **2003**, 42, 4213.

8. Do, D. D.; Do, H. D.; Prasetyo, I. Constant Molar Flow Semibatch Adsorber as a Tool to Study Adsorption Kinetics of Pure Gases and Vapors. *Chem. Eng. Sci*., **2000**, 55, 1717.
9. Yasuda Y. Frequency Response Method for Study of the Kinetic Behavior of a Gas-surface System. 1. Theoretical Treatment. *J. Phys. Chem.*, **1976**, 80, 1867.
10. Brandani, S. Effects of Nonlinear Equilibrium on Zero Length Column Experiments. *Chem. Eng. Sci*., **1998**, 53, 2791.
11. Brandani, S.; Cavalcante, C.; Guimaraes, A.; Ruthven, D. M. Heat Effects in ZLC Experiments. *Adsorption*, **1998**, 4, 275.
12. Brandani, F.; Ruthven, D. M.; Coe, C. G. Measurement of Adsorption Equilibrium by the Zero Length Column (ZLC) Technique Part1: Single-Component Systems. *Ind. Eng. Chem. Res*., **2003**, 42, 1451.
13. Hu, X.; Do, D. D.; Rao, G. N. Experimental Concentration Dependence of Surface Diffusivity of Hydrocarbons in Activated Carbon. *Chem. Eng. Sci*., **1994**, 49, 2145.
14. King, B.; Do, D. D. Measurement of Multicpmponent Adsorption Kinetics of Gases in Activated Carbon by a Batch Adsorber FT-IR Technique. *Chem. Eng. Sci*., **1996**, 51, 423.
15. Qinglin, H.; Farooq, S.; Karimi, I. A. Binary and Ternary Adsorption Kinetics of Gases in Carbon Molecular Sieves. *Langmuir*, **2003**, 19, 5722.
16. Naphtali, L. M.; Polinski, L. M. A Novel Technique for Characterization of Adsorption Rates on Heterogeneous Surfaces. *J. Phys. Chem.*, **1963**, 67 (2), 369.

17. Jordi, R. G.; Do, D. D. Analysis of the Frequency Response Method for Sorption Kinetics in Bidispersed Structured Sorbents. *Chem. Eng. Sci.*, **1993**, 48, 1103.
18. Yasuda, Y.; Sugasawa, G. A Frequency Response Technique to Study Zeolitic Diffusion of Gases. *J Catal.*, **1984**, 88, 530.
19. Yasuda, Y.; Mizusawa, H.; Kamimura, T. Frequency Response Method for Investigation of Kinetic Details of a Heterogeneous Catalyzed Reaction of Gases. *J. Phys. Chem. B*, **2002**, 106, 6706.
20. Sun, L. M.; Meunier, F.; Grenier, P. Frequency Response for Nonisothermal Adsorption in Biporous Pellets. *Chem. Eng. Sci.*, **1994**, 49, 373.
21. Reyes, S. C.; Iglesia, E. Frequency Response Techniques for the Characterization of Porous Catalytic Solids. *Catalysis*, **1994**, 11, 51.
22. Reyes, S. C.; Sinfelt, J. H.; DeMartin, G. J.; Ernst, R. H. Frequency Modulation Methods for Diffusion and Adsorption Measurements in Porous Solids. *J. Phys. Chem. B*, **1997**, 101, 614.
23. Sward, B. K.; LeVan, M. D. Frequency Response Method for Measuring Mass Transfer Rates in Adsorbents Via Pressure Perturbation. *Adsorption*, **2003**, 9, 37.
24. Wang, Y.; LeVan, M. D. Nanopore Diffusion Rates for Adsorption Determined by Pressure-swing and Concentration-swing Frequency Response and Comparison with Darken's Equation. *Ind. Eng. Chem. Res.*, **2008**, 47, 3121.
25. Coughanowr, D. R.; Koppel, L. B. *Process System Analysis and Control*, **1965**, McGraw-Hill, New York.
26. Stephanopoulos, G. *Chemical Process Control*, **1984**, Prentice Hall, Englewood, New Jersey.

27. Evnochides, S. K.; Henley, E. J. Simultaneous Measurement of Vapor Diffusion and Solubility Coefficients in Polymers by Frequency Response Techniques. *J. Poly. Sci. Part A2 : Polymer Physics*, **1970**, 8(11), 1987.
28. Yasuda, Y.; Yamamoto, A. Zeolitic Diffusivities of Hydrocarbons by the Frequency Response Method. *J. Catal.*, **1985**, 93, 176.
29. Yasuda, Y. Kinetic Details of a Gas/Porous Adsorbent System by the Frequency Response Method. *J. Phys. Chem*., **1991**, 95, 2486.
30. Yasuda, Y. Determination of Vapor Diffusion Coefficients in Zeolite by the Frequency Response Method. *J. Phys. Chem*. **1982**, 86, 1913.
31. Shen, D.; Rees, L. V. C. Diffusivities of Benzene in HZSM-5, Silicalite-I, and NaX Determined by Frequency-response Techniques. *Zeolites*, **1991**, 11(7), 666.
32. Song, L. J.; Rees, L. V. C. Adsorption and Diffusion of Cyclic Hydrocarbon in MFI-type Zeolites Studied by Gravimetric and Frequency-response Techniques. *Microporous Mesoporous Mater*., **2000**, 35, 301.
33. Jordi, R. G.; Do, D. D. Analysis of the Frequency Response Method Applied to Non-isothermal Sorption Studies. *Chem. Eng. Sci.*, **1994**, 49, 957.
34. Wang, Y.; LeVan, M. D. Investigation of Mixture Diffusion in Nanoporous Adsorbents Via the Pressure-swing Frequency Response Method. 2. Oxygen and Nitrogen in a Carbon Molecular Sieve. *Ind. Eng. Chem. Res*., **2005**, 44, 4745.
35. Wang, Y.; LeVan, M. D. Mixture Diffusion in Nanoporous Adsorbents: Development of Fickian Flux Relationship and Concentration-swing Frequency Response Method. *Ind. Eng. Chem. Res*., **2007**, 46, 2141.

36. Xiao, P.; Zhang, J.; Webley, P.; Li, G.; Singh, ZR.; Todd, R. Capture of CO_2 from Flue Gas Streams with Zeolite 13X by Vacuum-pressure Swing Adsorption. *Adsorption*, **2008**, 14, 572.

37. Ebner, A.D.; Ritter, J.A. State-of-the-art Adsorption and Membrane Separation Processes for Carbon Dioxide Production from Carbon Dioxide Emitting Industries. *Sep. Sci. technol.*, **2009**, 44, 1273.

38. Kikkinides, E.S.; Yang, R.T; Cho, S.H. Concentration and Recovery of CO_2 from Flue Gas by Pressure Swing Adsorption. *Ind. eng. Chem. Res*., **1993**, 32, 2714.

39. Zhang, J.; Webley, P. A. CO_2 Capture from Flue Gas by Vacuum Swing Adsorption: Cycle Development and Design. *Environ. Sci. Technol.,* **2008**, 42, 563.

40. Chue, K. T.; Kim, J. N.; Yoo, Y. J.; Cho, S. H.; Yang, R. T. Comparison of Activated Carbon and Zeolite 13X for CO_2 Recovery from Flue Gas by Pressure Swing Adsorption. *Ind. Eng. Chem. Res.*, **1995** 34(2), 591.

41. Siriwardane, R. V.; Shen, M. S.; Fisher, E. P. Adsorption of CO_2, N_2, and O_2 on Natural Zeolites. *Energy Fuels*, **2003**, 17, 571.

42. Harlick, P. J. E.; Tezel, F. H. An Experimental Adsorbent Screening Study for CO_2 Removal from N_2. *Microporous Mesoporous Mater*., **2004**, 76, 71.

43. Ruthven, D.M.; Lee, L.K. Kinetics of Nonisothermal Sorption: System with Bed Diffusion Control. *AIChE J*., **1981**, 27, 654.

44. Hu, X.; Mangano, E.; Friedrich, D.; Ahn, H.; Brandani, S. Diffusion Mechanism of CO_2 in 13X Zeolite Beads. *Adsorption*, **2013**, 19, 1.

45. Silva, J.A.C.; Schumann, K.; Rodrigues, A.E. Sorption and Kinetics of CO_2 and CH_4 in Binderless Beads of 13X Zeolite. *Microporous Mesoporous Mater*., **2012**, 158, 219.

46. Onyestyák, G.; Shen, D.; Rees, L.V.C. Frequency-response Study of Micro- and Macro-pore Diffusion in Manufactured Zeolite Pellets. *J. Chem. Soc. Faraday Trans*., **1995**, 91, 1399.

47. Onyestyák, G.; Rees, L.V.C. Frequency Response Study of Adsorbate Mobilities of Different Character in Various Commercial Adsorbents. *J. Phys. Chem. B*, **1999**, 103, 7469.

48. Onyestyák, G. Comparison of Dinitrogen, Methane, Carbon Monoxide, and Carbon Dioxide Mass-transport Dynamics in Carbon and Zeolite Molecular Sieves. *Helv. Chim. Acta.*, **2011**, 94, 206.

49. Giesy, T.J.; Wang, Y.; LeVan, M.D. Measurements of Mass Transfer Rates in Adsorbents: New Combined-techniques Frequency Response Apparatus and Application to CO_2 in 13X Zeolite. *Ind. Eng. Chem. Res*., **2012**, 51, 11509.

50. Dunne, J.A.; Rao, M.; Sircar, S.; Gorte, R.J.; Myers, A.L. Ar, CO_2, CH_4, C_2H_6, and SF_6 on NaX, H-ZSM-5, and Na-ZSM-5 Zeolites. *Langmuir*, **1996**, 12, 5896.

51. Ruthven, D.M.; Xu, Z. ; Farooq, S. Sorption Kinetics in PSA Systems. *Gas Sep. Purif.*, **1993**, 7, 75.

52. Sircar, S.; Rao, M. B.; Golden, T.C. Fractionation of Air by Zeolites. *Studies in Surface Science and Catalysis*, **1999**, 120, 395.

53. Dantas, T.L.P.; Luna, F.M.T.; Silva Jr., I.J.; Torres, A.E.B.; de Azevedo, D.C.S.; Rodrigues, A.E.; Moreira, R.F.P.M. Modeling of the Fixed-bed Adsorption of

Carbon dioxide and Carbon dioxide-Nitrogen Mixture on Zeolite 13X. *Braz. J. Chem. Eng.*, **2011**, 28(3), 533.

54. Chenier, P. J. *Survey of Industrial Chemistry*. **2004**, Kluwer Academic Publishers, New York.
55. Hayashi, S.; Kawai, M.; Kaneko, T. Dynamics of High Purity Oxygen PSA. *Gas Sep. Purif.*, **1996**, 10, 19.
56. Reid, C. R.; O'koye, I. P.; Thomas, K. M. Adsorption of Gases on Carbon Molecular Sieves Used for Air Separation. Spherical Adsorptives as Probes for Kinetic Selectivity. *Langmuir*, **1998**, 14, 2415.
57. Cabrera, A. L.; Zehner, J. E.; Coe, C. G.; Gaffney, T. R.; Farris, T. S. Armor, J. N. Preparation of Carbon Molecular Sieves, I. Two-step Hydrocarbon Deposition with Single Hydrocarbon. *Carbon*, **1993**, 31(6), 969.
58. LaCava, A. I.; Koss, V. A.; Wickens, D. Non-Fickian Adsorption Rate Behavior of Some Cabon Molecular Sieves. *Gas Sep. Purif*., **1989**, 3, 180.
59. Srinivasan, R.; Auvil, S. R.; Schork, J. M. Mass Transfer in Carbon Molecular Sieves: An Interpretation of Langmuir Kinetics. *Chem. Eng. J*., **1995**, 57, 137.
60. Kawazoe, K.; Suzuki, M.; Chihara, K. Chromatographic Study of Diffusion in Molecular Sieve Carbon, *J. Chem. Eng. Jpn*., **1974**, 7, 151.
61. Chihara, K.; Suzuki, M.; Kawazoe, K. Adsorption Rate on Molecular Sieving Carbon by Chromatography. *AIChE J*., **1978**, 24, 237.
62. Ruthven, D. M.; Raghavan, N. S.; Hassan, M. M. Adsorption and Diffusion of Nitrogen and Oxygen in a Carbon Molecular Sieve. *Chem. Eng. Sci*., **1986**, 41, 1325.

63. Chen, Y. D.; Yang, R. T.; Uawithya, P. Diffusion of Oxygen, Nitrogen and Their Mixtures in Carbon Molecular Sieve. *AIChE J*., **1994**, 40, 577.

64. Farooq, S.; Huang, Q. L.; Karimi, I. A. Identification of Transport Mechanism in Adsorbent Micropores from Column Dynamics. *Ind. Eng. Chem. Res*., **2002**, 41, 1098.

65. Loughlin, K. F.; Hassan, M. M.; Fatehi, A. I.; Zahur, M. Rate and Equilibrium Sorption Parameters for Nitrogen and Methane on Carbon Molecular Sieve, *Gas Sep. Purif.*, **1993**, 7(4), 264.

66. Nguyen, C.; Do, D. D. Dual Langmuir Kinetic Model for Adsorption in Carbon Molecular Sieve Materials. *Langmuir*, **2000**, 16, 1868.

67. Reid, C. R.; Thomas, K. M. Adsorption Kinetics and Size Exclusion Properties of Probe Molecules for the Selective Porosity in a Carbon Molecular Sieve Used for Air Separation *J. Phys. Chem. B,* **2001**, 105, 10619.

68. Liu, H.; Ruthven, D. M. *Diffusion in Carbon Molecular Sieve, In Fundamentals of Adsorption*, ed., by Levan, M. D. **1996**, Kluwer Academic Publishers, Boston.

69. Alpay, E. ; Scott, D. M. The Linear Driving Force Model for Fast-cycle Adsorption and Desorption in a Spherical Particle. *Chem. Eng. Sci.,* **1992**, 47, 499.

70. Buzanowski, M. A.; Yang, R. T. Extended Llinear Driving-force Approximation for Intraparticle Diffusion Rates Including Short Times. *Chem. Eng. Sci.*, **1989**, 44, 2683.

71. Carta, G. The Linear Driving Force Approximation for Cyclic Mass Transfer in Spherical Particles. *Chem. Eng. Sci.*, **1993**, 48, 622.

72. Carta, G.; Cincotti, A. Film Model Approximation for Non-linear Adsorption and Diffusion in Spherical Particles. *Chem. Eng. Sci.,* **1998**, 53, 3483.

73. Do, D. D.; Mayfield, P. L. J. A New Simplified Model for Adsorption in a Single Particle. *A.I.Ch.E. J.*, **1987**, 33, 1397.

74. Do, D. D.; Rice, R. G. Validity of the Parabolic Assumption in Adsorption Studies. *A.I.Ch.E. J.*, **1986**, 32, 149.

75. Doong, S. J.; Yang, R. T. Bulk Separation of Multicomponent Gas mixtures by Pressure Swing Adsorption: Pore/Surface Diffusion and Equilibrium Models. *AIChE J.*, **1986**, 32, 397.

76. Gadre, S. A.; Ritter, J. A. New Analytical Solution for Nonlinear Adsorption and Diffusion in a Single Particle. *Chem. Eng. Sci.,* **2002**, 57, 1197.

77. Glueckauf, E.; Coates, J. J. Theory of Chromatography. Part IV. The Influence of Iincomplete Equilibrium on the Front Boundary of Chromatogram and on the Effectiveness of Separation. *J. Chem. Soc.*, **1947**, 1315.

78. Glueckauf, E. Theory of Chromatography. Part X. Formulae for Diffusion into Spheres and Their Application to Chromatography. *Trans. Faraday Soc.*, **1955**, 51, 1540.

79. Goddard, M.; Ruthven, D. M. Sorption and Diffusion of C8 Aromatic Hydrocarbons in Faujasite Type Zeolites. II Sorption Kinetics and Intracrystalline Diffusivities. *Zeolites*, **1986**, 6, 275.

80. Hills, J. H. An Investigation of the Llinear Driving Force Approximation to Diffusion in Spherical Particles. *Chem. Eng. Sci.,* **1986**, 11, 2279.

81. Hsuen, H. -K. An Improved Linear Driving Force Approximation for Intraparticle Adsorption. *Chem. Eng. Sci.,* **2000**, 55, 3475.

82. Kikkinides, E.S.; Yang, R. T. Further Work on Approximations for Intraparticle Diffusion Rates in Cyclic Adsorption and Desorption. *Chem. Eng. Sci.*, **1993**, 48, 1169.

83. Liaw, C.; Wang, J. S. P.; Greenkorn, R. A.; Chao, K. C. Kinetics of Fixed-bed Adsorption: A New Solution. *AIChE J.*, **1979**, 25, 376.

84. Nakao, S-I.; Suzuki, M. Mass Transfer Coefficient in Cyclic Adsorption and Desorption. *J. Chem. Eng. Jpn.*, **1983**, 16, 114.

85. Vermeulen, T. Theory for Irreversible and Constant-pattern Solid Diffusion. *Ind. Eng. Chem.*, **1953**, 45(1), 1664.

86. Vermeulen, T.; Quilici, R. E. Analytic Driving-force Relation for Pore-diffusion Kinetics in Fixed-bed Adsorption. *Ind. Eng. Chem. Fundam.*, **1970**, 9, 179.

87. Zhang, R.; Ritter, J. A. New Approximate Model for Nonlinear Adsorption and Diffusion in a Single Particle. *Chem. Eng. Sci.,* **1997**, 52, 3161.

88. Wang, Y.; LeVan, D. M. Adsorption Equilibrium of Carbon Dioxide and Water Vapor on Zeolites 5A and 13X and Silica gel: Pure Components. *J. Chem. Eng. Data*, **2009**, 54, 2839.